UiT The Arctic University of Norway

The Faculty of Science and Technology - Department of Geosciences

Structurally controlled hydrothermal mineralization

A case study from Vanna island, northern Norway

Hanne-Kristin Paulsen

A dissertation for the degree of Philosophiae Doctor – December 2019

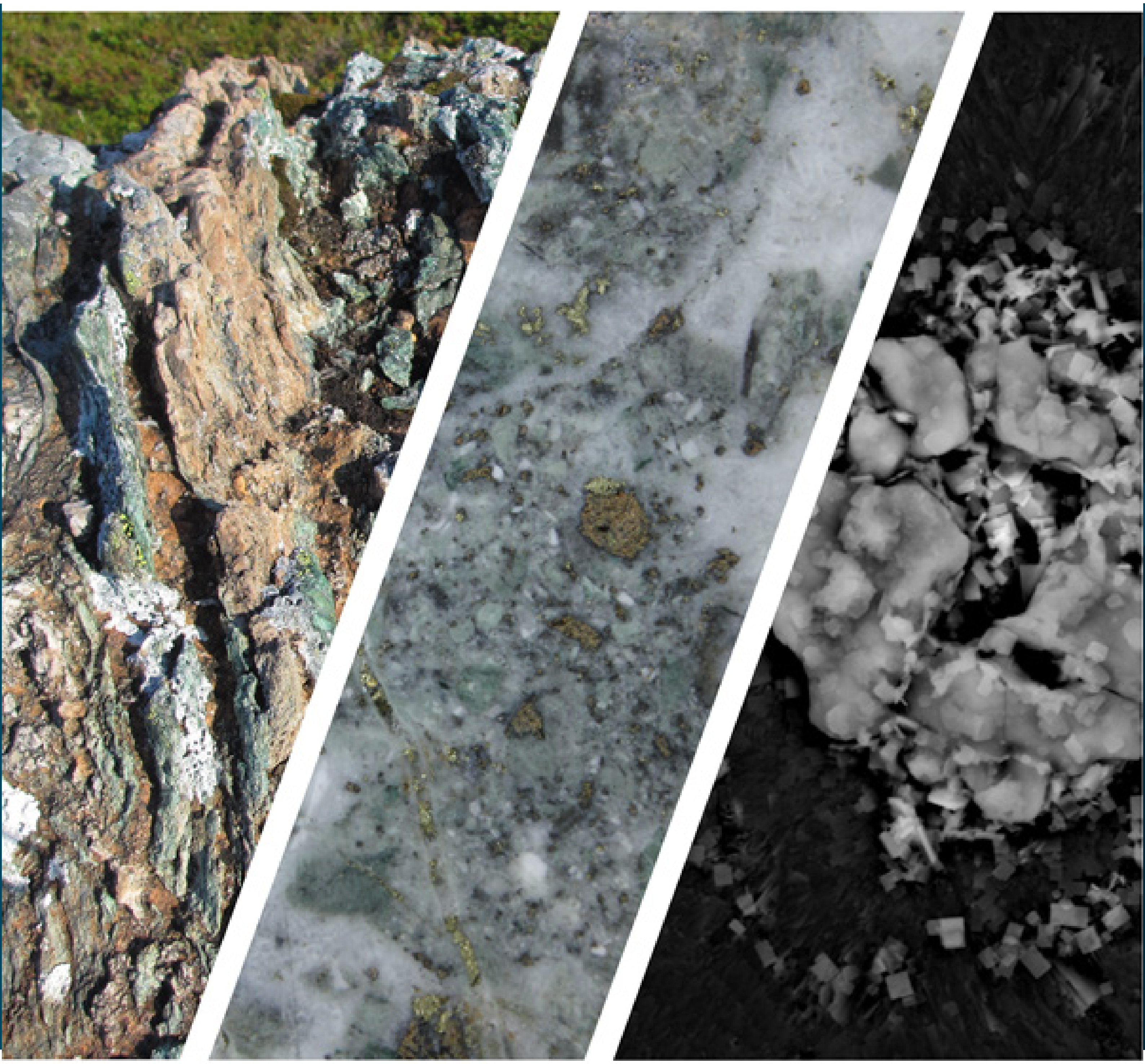

"Å eg veit meg eit land langt der oppe mot nord, med ei lysande strand
mellom høgfjell og fjord"
–Elias Blix

Abstract

The formation of mineral deposits is closely related to the tectonic setting in which they form. Structures create avenues of net permeability that allow ore-bearing fluids to transport and deposit mineralization. In a deeper crustal setting these structures can be ductile shear zones, while brittle faults and fractures are the dominant fluid pathways in the upper continental crust. The formation of local structures are strongly related to the regional tectonic setting. This work focusses on the metallogeny of Vanna, an island located in the northern part of the Archaean to Palaeoproterozoic West Troms Basement Complex. The complex is a part of the north-western margin of the Fennoscandian Shield, which is the most prolific mining area in Europe. Vanna has been subjected to a prolonged multiphased deformation history with several episodes of extension and compression. Paper I focusses on the geotectonic history of Vanna; normal faulting during the 2.2-2.4 Ga extension created rift basins that subsequently became inverted during the accretionary Svecofennian orogeny (c. 1.8-1.7 Ga), and possibly younger events. Inversion tectonics during crustal shortening resulted in the formation of low-grade fold and thrust belt structures in the basement rocks and metasedimentary cover sequence. This event also involved reactivation of the basin-bounding normal faults in the basement. Further, the youngest recorded tectonic event on Vanna is late-Paleozoic post-Caledonian extensional normal faults. This geological and structural framework outlined in Paper I forms the basis for understanding the metallogenic evolution of Vanna. Paper II and III each discuss a different style of hydrothermal mineralization. In paper II we show that emerald mineralization formed by hydrothermal fluids circulating in the Olkeeidet tectonic shear zone; a large, crustal scale dextral shear zone active during the contractile deformation that resulted in the formation of fold and thrust belt structures. Emerald mineralization is associated with extensive metasomatic alteration of the host rocks within the shear zone. This highly saline hydrothermal fluid likely originated as a magmatic fluid and strongly Na/K metasomatised the host rocks, and deposited quartz-tourmaline veins, dolomite and emerald. Emeralds were formed by Be sourced from the hydrothermal fluids, and Cr was likely sourced locally from chromite in an assumed metasedimentary unit. Paper III investigates hydrothermal Cu-Zn mineralization hosted by the Palaeozoic brittle Vannareid-Burøysund fault. Here, highly saline fluids composed of $CaCl_2$ and NaCl transported Cu and Zn as chloride complexes using the brittle fault as a fluid conduit. The subsequent deposition of Zn in the form of sphalerite first, and Cu in the form of chalcopyrite second also shows that the fault progressively evolved and widened with time. Considered together, the three papers in this thesis show that mineralization on Vanna is structurally controlled, and the results can be used to discuss the mineralization potential and the key geological controls on mineralization more broadly.

Acknowledgements

First and foremost I would like to thank my two supervisors, Sabina Strmić Palinkaš and Steffen G Berg who have guided and supported me throughout these four years. Without your help, patience and inspiration I would never have made it this far. Thank you for allowing me to make mistakes, and for supporting me when trying to mend them. I am grateful for the opportunity to work with two scientists that each show passion and knowledge in each of your scientific fields. I have truly learned a lot from you.

I would like to thank my colleagues, who helped me develop and mature the work and my co-authors for scientific discussions and contributions to the papers. Paul Armitage - thanks for your company in the field and valuable discussions. In particular I am grateful to Siri Karlsen, Sofie Kolsum and Ida Rønningen for lively debates and constructive conversations. I would like to thank Trond Slagstad, Morgan Ganerød, and Asis Nasuti at NGU for Ar-Ar analyses and geophysics processing. Many thanks to Andrea Čobić for XRD analyses.

I would like to say thanks to the lab-staff - Trine, Karina, Ingvild and Matheus - for high-quality thin-sections, isotope analyses and help with SEM data. Kai - thanks for your enthusiasm and support with the SEM. Many thanks also goes to the administrative staff at IG, Matthias, John-Arne, Anders, Inger, Margrete, Cecilie and Andre - you always found time to offer a helping hand.

To my friends and fellow peers at IG, this could not have been accomplished without you. I would like to thank JB, Fredrik, Erland, Holger, Jiri, and Melanie for scientific discussions. To all the people whom I at one point have shared an office with - Harald, Yulia, Kai, Jack, Louise, Paul, Marina, and Stephan - thanks for listening when I inadvertently decided to explain something in great detail. In particular I would like to thank Carly Faber for patient proofreading and for always having time to explain the intricacies of metamorphic geology to me. Sina Marti - never stop asking those questions that seem so simple, but that in reality are the important ones. To Carly, Sina, Mariana, Calvin, Henry, Andrea, Lis and Torbjørn - what better way is there ponder the meaning of life than out and about climbing, hiking and skiing in the mountains. This journey would have been way too bland without you.

Thanks to my big, loud and ever expanding family, mamma og pappa, Marianne, Britt, Sissel-Marie, Sven-Are, and Liza. To all of you - thank you for never letting me forget that there are new adventures waiting everywhere. All of your support, encouragement and love has been essential throughout this journey.

Figure 1: View of Vanna from the top of Vanntinden (1031 m.a.s.l.)

Preface

This thesis is the outcome of a 4-year PhD project starting in September 2015. The work was mainly funded by the UiT–The Arctic University of Norway, with additional financial support from Dynamics and Evolution of Earth and Planets (DEEP) at the University of Oslo. UiT The Arctic University of Norway is the degree-awarding institution. Associate professor Sabina Strmić Palinkaš and Professor Steffen G. Berg were my supervisors.

The PhD program requires that 25% of the four-year period is duty work. This was fulfilled through practical teaching of field courses, and assisting with exercises in general geology, mineralogy, structural geology, and regional geology. I also assisted MSc students with their thesis work and took part in outreach events including Forskningsdagene at UiT and UiO.

The following ECTS-accredited courses were completed as part of my PhD: Philosophy of science and ethics (UiT); Gold from bedrock to bullion: sustainable mining (University of Oulu); Communicating science: Scientific writing (UiT); Hydrothermal processes and mineral resources (University of Oulu); Solid Earth - fluid Earth interactions (DEEP PhD school at University of Oslo); Seafloor mineral resources and prospects of deep-sea mining: geological, environmental and technological challenges ahead (University of Bergen); and Deformation processes (UiT).

The thesis presented herein aims to discuss metallogeny of Vanna, an island located in the northern part of the West Troms Basement Complex in northern Norway. Fieldwork was carried out over four field seasons with the aim of understanding the structural and tectonic evolution of Vanna and its controls on hydrothermal mineralization.

This thesis consists of an introduction, a brief synthesis and three manuscripts. Parts of the work in this thesis has been presented at national and international conferences, and workshops.

The three papers are presented in this thesis are:

Paper I: Hanne-Kristin Paulsen, Steffen G. Bergh, Sabina Strmić Palinkaš, Siri Elén Karlsen, Sofie Kolsum, Ida U. Rønningen and Aziz Nasuti, **Fold-thrust structures and oblique faults on Vanna island, West Troms Basement Complex, and their relation to inverted metasedimentary sequences**, Manuscript

Paper II: Hanne-Kristin Paulsen, Steffen G. Bergh and Sabina Strmić Palinkaš **Hydrothermal emeralds: a shear zone hosted mineralization on Vanna Island, northern Norway** Manuscript

Paper III: Hanne-Kristin Paulsen, Steffen G. Bergh and Sabina Strmić Palinkaš . **Late Palaeozoic fault controlled hydrothermal Cu-Zn mineralization on Vanna Island, West Troms Basement Complex, northern Norway,** Manuscript submitted to Norwegian Journal of Geology

Conferences, workshops and meetings

2019 EGU General Assembly, Vienna Austria. PICO presentation

NGF Winter Meeting, Bergen Norway. Oral and poster presentation.

3_{rd} general assembly Norwegian research school for Dynamics and Evolution of Earth and Planets, Sommarøy Norway. Poster presentation

2018 2_{nd} general assembly Norwegian research school for Dynamics and Evolution of Earth and Planets, Bergen Norway. Poster presentation

AMGG annual meeting, Tromsø Norway. Oral presentation

Mineral Resources in the Arctic Workshop. Tromsø Norway. Oral presentation

2017 1_{st} general assembly Norwegian research school for Dynamics and Evolution of Earth and Planets, Geilo Norway. Poster presentation

AMGG annual meeting, Tromsø Norway. Oral presentation

NGF Arctic days conference, Svolvær Norway. Oral presentation

Fennoscandian Exploration and Mining Conference. Levi Finland.

Geonor Conference. Mo i Rana Norway.

Broken Hill Deposit field trip. New South Wales Australia.

2016 32_{nd} Nordic Geological Wintermeeting, Helsinki Finland. Poster presentation.

2015 Mineralklynge Norge workshop. Mo i Rana Norway.

Contents

List of Figures

1

Introduction

Ore deposits can form in a variety of geological and tectonic settings. However, their formation depend on the interaction between several key geological mechanisms. In particular, geological structures and mineral deposits are closely linked; for a significant ore-deposit to form, ore-forming fluids need to migrate though the crust in avenues of net permeability from its place of origin to a place where it can be deposited. This permeability can be faults, ductile shear zones, brittle fractures and fracture systems. The latter is particularly important as fluid pathways in the brittle upper continental crust (Gabrielsen and Braathen, 2014; Sibson et al., 1975). In addition to a fluid conduit, favourable physiochemical fluid properties are needed for transport and deposition of ore. The solubility, also expressed as the metal-bearing capacity of a fluid, is dependent on several factors. Fluid chemistry/salinity, temperature, pressure, pH and oxidation state all affect the fluid solubility to varying degrees. A fluid under favourable physiochemical conditions can therefore transport significant amounts of metal, and likewise deposit these metals in the solid state if the solubility decreases. The origin of such an ore-bearing fluid can be diverse; it can be magmatic, formed from metamorphic dehydration reactions or expulsion of pore fluids from compaction of sediments, or meteoric. A combination of one or more of these sources is also common. Regardless of origin, the fluid properties may also be modified by the interaction with host rock through which they migrate. Identifying these key geological mechanisms that results in the formation of ore deposits is essential to ensure continued supply of metals and minerals for further socio-economic development and for making the green shift.

Vanna island, with its excellent exposure and protracted geological history is an ideal place to investigate ore-forming processes. A suite of felsic and mafic intrusive rocks overlain by metasedimentary rocks have recorded a lengthy geotectonic history, from Archaean to late Palaeozoic, including multiple tectonic events of extension and compression. The island is located in the northern part of the West Troms Basement Complex, a basement horst interpreted to be the western continuation of the Archaean to Palaeoproterozoic Fennoscandian Shield - the most prolific mining district in Europe (Eilu, 2012).

On Vanna, two distinctly different mineral-occurrences are investigated, emerald mineralization at Olkeeidet and the Vannareid-Burøysund Cu-Zn occurrence. Detailed structural mapping done on each of these occurrences reveal a strong structural control, however they formed in different geotectonic settings; the former is hosted by a ductile shear zone formed in a contractile event that resulted in fold and thrust belt structures, while the latter is hosted by a brittle fault related to continental rifting. In addition, we analyse the hydrothermal ore-bearing fluid in each of these deposits by fluid inclusion investigations. Further, we indirectly investigate the fluid properties by analysing ore-minerals and minerals associated with hydrothermal fluid alteration by scanning electron microscope analyses, Raman spectroscopy, and X-ray diffraction. Although neither mineral occurrence currently has any economic value or exploitation potential, they do provide excellent examples of structurally controlled hydrothermal ore mineralization. By studying them in detail we gain not only information about how each of these occurrences formed but also where to search for new ore bodies.

1.1 Geological background

1.1.1 Northern Fennoscandian Shield

The Fennoscandian Shield is the largest exposed area of Archaean and Proterozoic rocks in Europe, and extends from the north-western part of Russia though Finland, Sweden and Norway (Fig. 1.1). The rocks get progressively younger towards the south-west. It is the most important metal mining district in Europe, and most known ore deposit types are present in this region. These ore deposits are distributed within several metallogenic areas, and their spatial and temporal distribution are related to different geotectonic events (Eilu et al., 2003; Eilu, 2012).

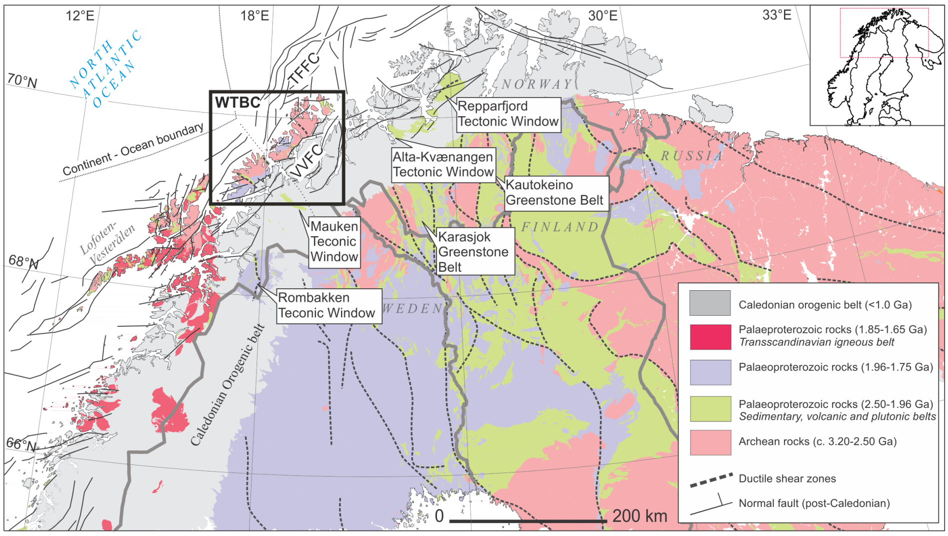

Figure 1.1: Northern Fennoscandian Shield after Koistinen et al., (2001). The West Troms Basement Complex is separated from the main Fennoscandian Shield by a c. 100 km wide section of Caledonian rocks. Post-Caledonian extensional faults are present along most of the North-Norwegian margin (Olesen et al., 2002; Indrevær et al., 2013; Davids et al., 2013; Koehl, 2013). TFFC - Troms-Finnmark Fault Complex, VVFC - Vestfjorden-Vanna Fault Complex

Archaean rocks are located in the northern and eastern part of the shield and are mainly partly migmatitic TTG-gneisses (tonalite, trondhjemite and granodiorite) and volcano-sedimentary supracrustal rocks deposited in rift-basins (Hölttä et al., 2008; Lahtinen et al., 2011). With the exception of banded iron formations like Bjørnevatn and Kostomuksha, the Archaean rocks are relatively unmineralized (Eilu, 2012).

The Archaean rocks are unconformably overlain by a number of **Palaeopro-**

terozoic sedimentary-volcanic successions and associated mafic sills and dikes ranging in age from c. 2505 to 1930 Ma, with a general decrease in age to the north-west (Hanski et al., 2001; Lahtinen et al., 2011; Eilu, 2012; Bingen et al., 2015). This tectonic rifting event in the Fennoscandian Shield has been correlated to a global record of Palaeoproterozoic breakup of an/several Archaean super-craton(s) (Bleeker, 2003).

The two main Palaeoproterozoic tectonic events in the Fennoscandian Shield are the **Lapland-Kola** (1.94-1.86 Ga) and the **Svecofennian** (1.92-1.79 Ga) orogenies. The Lapland-Kola event is a collisional belt containing both Archaean terrains, felsic granulites and juvenile Palaeoproterozoic crust (Daly et al., 2006). The Svecofennian Orogeny was the most important tectonic event in the Northern Fennoscandian Shield (Koistinen et al., 2001). It is an accretionary orogen that involved large-scale formation of new continental crust. Palaeoproterozoic passive margin sediments, juvenile arcs, and microcontinents were accreted on to the continent along an array of major north-west to north striking crustal scale shear zones which progressively developed across the Archaean and Palaeoproterozoic continents (Gaál and Gorbatschev, 1987; Nironen, 1997; Bark and Weihed, 2007; Angvik, 2014). This deformation was also the last major ductile event to shape the currently exposed penetrative structural grain of the rocks (Koistinen et al., 2001; Henderson et al., 2015). Emplacement of the Transscandinavian igneous batholith occurred along the south western margin of the Svecofennian protocraton (1.80-1.78 Ga) (Gaál and Gorbatschev, 1987; Högdahl et al., 2004). This NE to SW trending belt stretches from southern Sweden to Lofoten in Norway. It is composed of granitoid rocks with associated mafic intrusions.

The Svecofennian Orogeny is the most prolific metallogenic event in northern Fennoscandia (Weihed et al., 2005). It includes the formation of VMS deposits in intra-arc extensional settings prior to basin inversion. A number of economically important iron skarn-iron ores and Fe-apatite ores were also formed at this time, as well as porphyry copper and iron oxide copper gold (IOCG) deposits. Numerous orogenic gold deposits formed throughout the Proterozoic greenstone belts during syn- to post collisional stages (Eilu et al., 2003; Lahtinen et al., 2012).

In northern Norway, the Fennoscandian Shield with Palaeoproterozoic meta-supracrustal belts is found as the Kautokeino and Karasjok Greenstone Belts, as basement windows exposed in the Caledonides - the Alta-Kvænangen, Repparfjord, Mauken, and Rombakken tectonic windows, and the West Troms Basement Complex horst exposed to the west of the Caledonian orogenic rocks (Fig. 1.1).

1.1.2 Caledonian orogenic rocks in northern Norway

In northern Scandinavia, Caledonian orogenic rocks are found in a c. 100 km wide belt mainly in eastern Norway and western Sweden (Fig. 1.2). The Caledonian Orogeny is a continent-continent collision between the continents Laurentia and Baltica that closed the Iapetus Ocean during the Ordovician and Silurian. Terrains that are exotic to Baltica were placed on top of a wedge of Neoproterozoic to early Palaeozoic passive margin sediments during the collision (Augland et al., 2014). This resulted in a nappe sequence of allochthons that are generally increasingly distal from the continental margin westward and upwards in the nappe-stack. These nappes cover large parts of northern Norway and the western part of Sweden, and the underlying Archaean and Proterozoic basement has been reworked to different degrees.

The Kalak Nappe Complex is the structurally lowest nappe, and it is separated from the basement by a thin Neoproterozoic to Cambrian autochthonous cover. It is comprised of Precambrian basement rocks and metapsammites with local mafic intrusive rocks. It also includes the Seiland igneous province - a large igneous province that intruded intracontinental rift zones prior to the opening of the Iapetus Ocean, around 610-550 Ma (Larsen et al., 2018). The Caledonian metamorphic grade increases upwards, with greenschist facies at its base and amphibolite facies metamorphism in the middle and upper units (Faber et al., 2019). The overlying Vaddas and Kåfjord Nappes are composed of high grade metasedimentary rocks with felsic and mafic intrusive rocks that records amphibolite to granulite facies metamorphism (Faber et al., 2019). A mylonitic high strain zone marks the boundary between the Kåfjord Nappe and the overlying Normannvik Nappe. The Normannvik Nappe is composed of migmatized garnet-mica schists and gneisses. A greenschist-facies shear zone marks the transition from the Nordmannvik Nappe to the overlying Lyngsfjell Nappe, which is composed of two distinctly different units; the Lyngen Magmatic Complex and the unconformably overlying Late Ordovician/Early Silurian Balsfjord Group. The Nakkedal and Tromsø Nappes are the stratigraphically uppermost nappes.

1.1.3 Collapse of the Caledonian orogenic rocks and opening of the Atlantic Ocean

During the collapse of the Caledonian orogeny, many of the nappe-bounding thrust faults were reactivated as normal faults. Continued extension and incipient rifting resulted in a series of NE-SE striking brittle normal faults in rhombic, zigzag-shaped fault trends that evolved to major fault zones like the Vestfjorden-Vanna fault complex and the Troms Finnmark fault complex. (Lippard and Prestvik, 1997; Olesen et al., 1997; Roberts and Lippard, 2005;

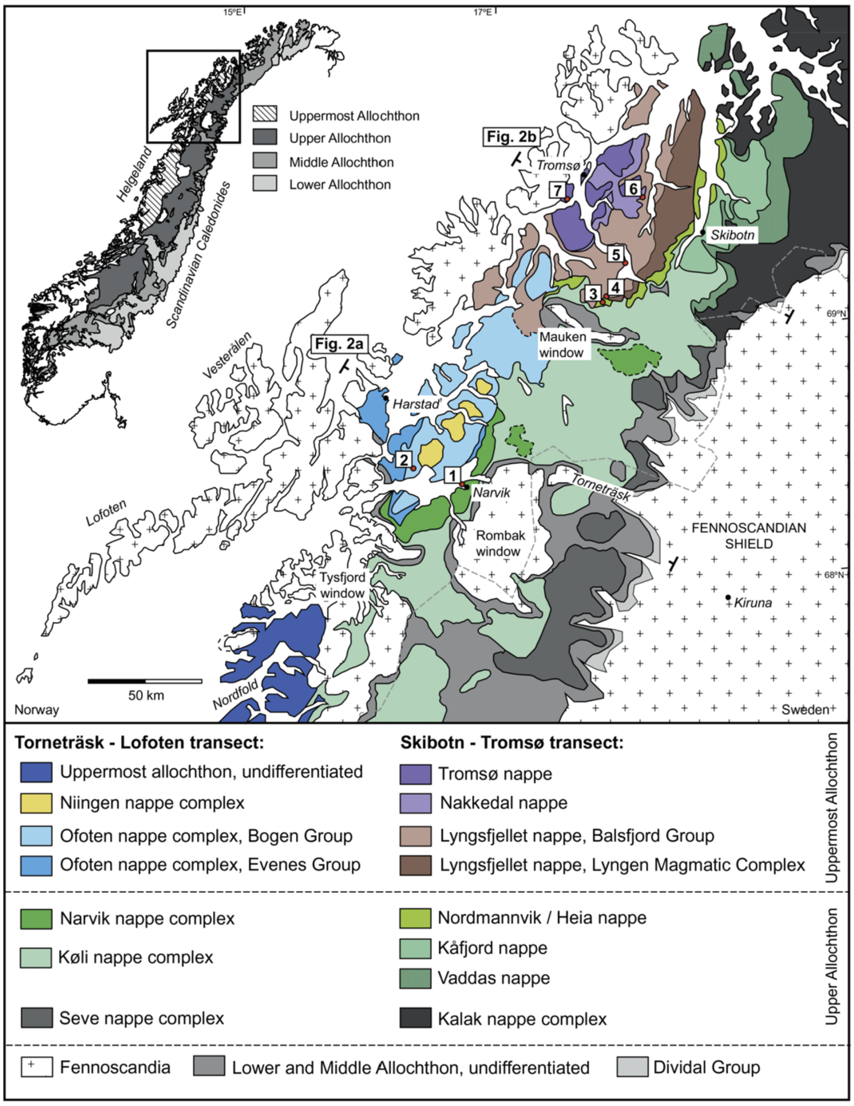

Figure 1.2: Caledonian orogenic rocks exposed in nothern Norway Figure from Augland et al., 2014.

Hansen et al., 2012; Davids et al., 2013; Indrevær et al., 2013; Koehl et al., 2018). The Vestfjorden-Vanna Fault Zone separates the West Troms Basement Complex horst, and the Vannareid-Burøysund fault that hosts Cu-Zn mineralization described in paper III, is a part of this fault zone. The Troms-Finnmark fault complex is an offshore fault zone that runs parallel to it. As rifting continued from incipient continental faulting, the wide part of the margin of the coast of Vanna became passive as faulting moved westward and further south to the Lofoten area (Fig. 1.1; Mosar, 2003; Davids et al., 2012; Indrevær et al., 2013). As a result, the continental margin along the Norwegian coast narrows northward towards Lofoten, and then abruptly widens again to the north of the Senja fracture zone that acted as a transfer zone.

1.1.4 The geology of West Troms Basement Complex

The Archaean/Palaeoproterozoic West Troms Basement Complex horst is situated west of the Caledonian orogenic rocks (Fig. 1.2). It is interpreted to be a part of the Fennoscandian Shield (Henderson et al., 2015; Bergh et al., 2010), although a link with the Lewisian in Scotland has also been suggested (Bergh et al., 2012).

The West Troms Basement Complex is (Fig. 1.3) a basement window composed of TTG gneisses (2.9-2.6 Ga) (Bergh et al., 2010; Myhre et al., 2013). The basement rocks are all strongly deformed, partly migmatized by Neoarchaean orogenies (c. 2.8-2.6 Ga: Myhre et al., 2013) and intruded by mafic dyke swarms dated at c. 2.4 Ga (Kullerud et al., 2006). Numerous supracrustal cover units (greenstone belts) with variable ages, composition and metamorphic grade (Zwaan, 1989; Armitage and Bergh, 2005; Bergh et al., 2010) overlie the basement gneisses. The Archaean volcano-sedimentary Ringvassøya greenstone belt was deposited at c. 2.8 Ga (Zwaan, 1989; Motuza, 2000), while the metasedimentary Vanna Group was deposited between 2.2 and 2.4 Ga (Bergh et al., 2007). Peak metamorphism reached high-grade granulite and amphibolite facies in Senja and Lofoten/Vesterålen parts of the transect during the D1-D2 events (Zwaan, 1995). Ringvassøya was subjected to medium grade amphibolite facies, while medium- to low grade greenschist facies dominated in the north-east (Vanna island, this work, Opheim and Andresen, 1989). This presumed metamorphic gradient implies that the studied transect evolved from a hinterland (deep crust) in the south-west to a foreland (upper crust) in the north-east (Bergh et al., 2010).

A suite of granites (Ersfjord Granite) and mafic igneous rocks (Hamn Gabbro) formed synchronous with a major suite of 1.8–1.7 Ga plutonic rocks in Lofoten and Vesterålen (Griffin et al., 1978; Corfu et al., 2003; Corfu, 2004). The Ersfjord Granite may have formed by partial melting of the TTG crust (Haaland, 2018; Laurent et al., 2019) and emplaced during the waning stages of the Svecofennian Orogeny (1.92-1.78 Ga), as defined in the Fennoscandian Shield (Lahtinen et al., 2011). This Svecofennian deformation in West Troms Basement Complex affected the entire province. Early deformation generated a main ductile gneiss-foliation (S1), SW- and NE-dipping thrusts (S1), and NV-SØ trending tight (F1). Continued deformation folded these early fabrics into upright (F2) fold systems. During the late-stage, partly orogen-parallel event (D3) steeply NW-SE plunging folds (F3) and subvertical ductile shear zones (strike-slip faults) formed in the Senja Shear Belt, whereas SE-directed orogen-normal thrusts and steep NW-SE striking lateral shear zones formed in the northeast, i.e. on Ringvassøya and Vanna. This D3 deformation is dated at c. 1.77-1.65 Ga in the Senja Shear Belt, a major ductile deformation zone (Fig. 1.3) (Bergh et al., 2015; Laurent et al., 2019), which involved polyphase crustal contraction and accretion (D1) and partitioned thrust and strike-slip deformation (D3-transpression) (Bergh et al., 2010).

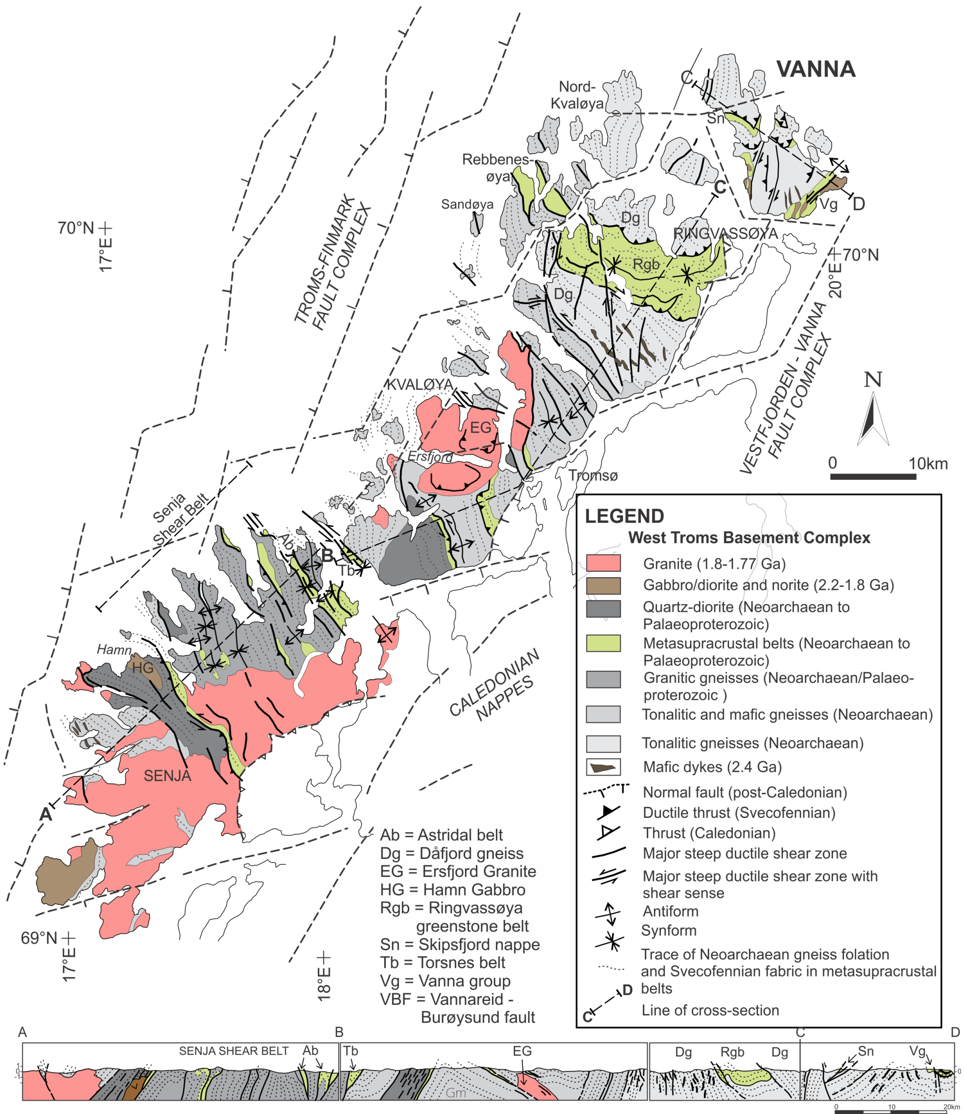

Figure 1.3: Geologic and tectonic map of the Archaean/Palaeoproterozoic West Troms Basement Complex (Bergh et al., 2010; Thorstensen, 2011; Haaland, 2018; Davids et al., 2013; Bergh et al., 2007). Archaean and Palaeoproterozoic basement blocks and Vanna Island is located at the northern end of the complex.

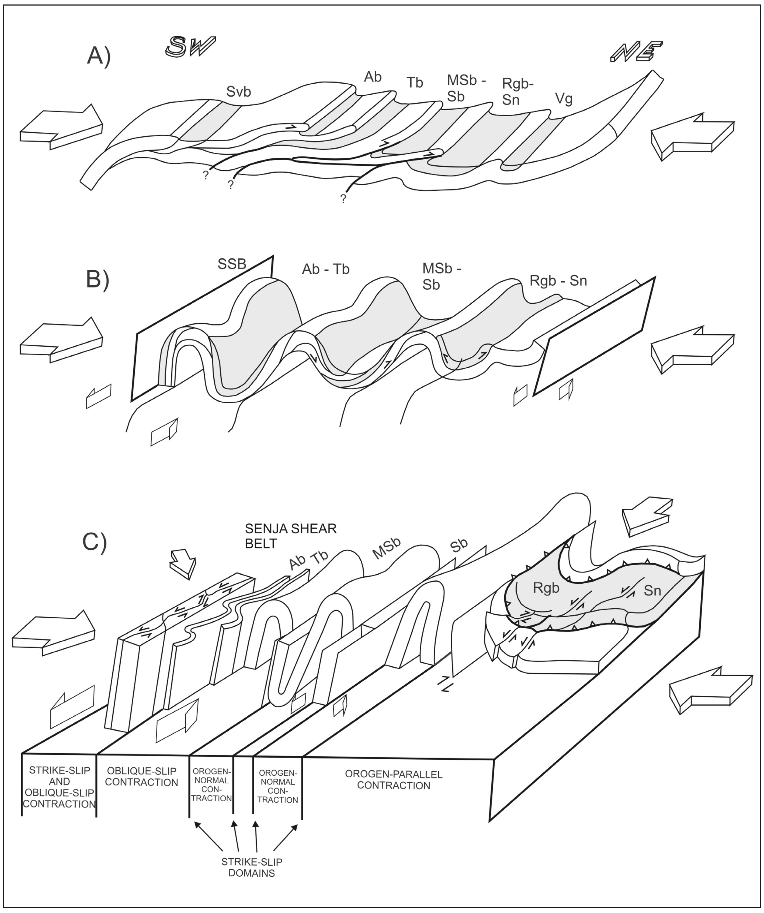

Figure 1.4: Schematic model displaying the development of presumed Svecofennian structures in the West Troms Basement Complex. (A) Formation of NE-directed thrusts and the main low angle mylonitic foliation (S1) in supracrustal belts from orogen-oblique NE-SW directed orthogonal shortening. (B) Continued orthogonal shortening produced upright macro-folds (F2) by folding of the earlier fabrics. (C) Late Svecofennian orogen-parallel to orogen-oblique directed contraction resulting in mostly sinistral strike-slip reactivation of steep macro-folds (D3). Figure from Bergh et al., (2010)
.

Whereas the Fennoscandian Shield in Finland, Sweden and Russia is well endowed in both base and precious metal deposits, few economic deposits have been found in the West Troms Basement Complex. Limited historic mining and exploration have mainly focused of base metals; Ni, Co, Cu ± PGE occurrences in layered mafic intrusions in the Hamm Gabbro was briefly mined in the 1860‘s (Bugge, 1935). During the same period, prospecting on Ringvassøya resulted in several known metal occurrences ranging from stratiform massive Fe-Cu sulphide deposits (assumed volcanic massive sulphide and/or sedimentary exhalatory deposits) and several different precious metal type occurrences found within the 2.8(?) Ga Ringvassøya Greenstone Belt (Bratrein, 1989; Zwaan, 1989). Several smaller orogenic gold deposits were also recognized in the 1980's (Sandstad and Nilsson, 1998). Despite recent advances in the geological knowledge of the region, both the syngenetic mineralization processes and the hydrothermal alteration and potential metal remobilisation caused by the later Svecofennian deformation is still poorly understood.

1.1.5 Study area - the geology of Vanna island

Vanna island (Fig. 1.5) is the study area of this thesis. It is located in the north-eastern part of the West Troms Basement Complex (Fig. 1.3), and is mainly composed of Archaean tonalite gneisses cut by 2.4 Ga mafic dike swarms (Binns et al., 1980; Opheim and Andresen, 1989; Bergh et al., 2007). Several metasedimentary cover sequences unconformably overlie the basement; the largest of these is the well-studied Vanna Group along the southern coast. In addition, several smaller and less studied cover sequences are found along the western coast of the island at Kvalvågklubben and Hamre, and farther north as lenses in, and structurally below, the Skipsfjord Nappe. The age of these cover sequences is constrained at Vikan by the erosional contact with the 2.4 Ga mafic dikes in the basement, and a diorite sill (2.2 Ga; Bergh et al., 2007) that has intruded the metasedimentary sequence. In the north, highly strained parautochtonous sequences, the Skipsfjord Nappe, is composed of variously mylonitized tonalitic gneisses and intercalated lenses of metasedimentary and mafic intrusive rocks (Opheim and Andresen, 1989).

Vanna Group metasedimentary sequence

The first geological mapping on the island was carried out by Pettersen (1887), who suggested that the island consisted mainly of Precambrian gneisses overlain by Caledonian metasedimentary rocks along the south-eastern coast. Mapping carried out by Binns et al., (1980) focussed on the stratigraphy of this metasedimentary sequence, now termed the Vanna Group, and informally divided the low-grade metasedimentary rocks into the lower psammitic Tinnvatn formation and the overlying mixed lithological Bukkheia Formation. The Tinnvatn Formation is $<$ 80 m thick and unconformably overlie the basement tonalites. It consists of quartzitic, arkosic to subarkosic, and calcareous metasedimentary rocks deposited in a deltaic environment (Binns et al., 1980). Detailed sedimentary facies analysis carried out by Johannessen (2012) further suggested that the upper parts (8-10 m) of the Tinnvatn formation was deposited in a transgressive shallow marine environment and represents a foreshore facies, while the rest was deposited by tidal streams as an upper shoreface facies. The much less studied overlying Bukkheia formation is thicker (< 150 m) and consists of partly calcareous mudstones with intermittent coarser sandstone layers. The Bukkheia formation is intruded by a diorite sill, locally up to 2 km thick. The diorite itself is composed of several intrusions ranging from intermediate to mafic, and whole-rock geochemical analyses show that the diorite has a continental tholeiitic signature (Johansen, 1987).

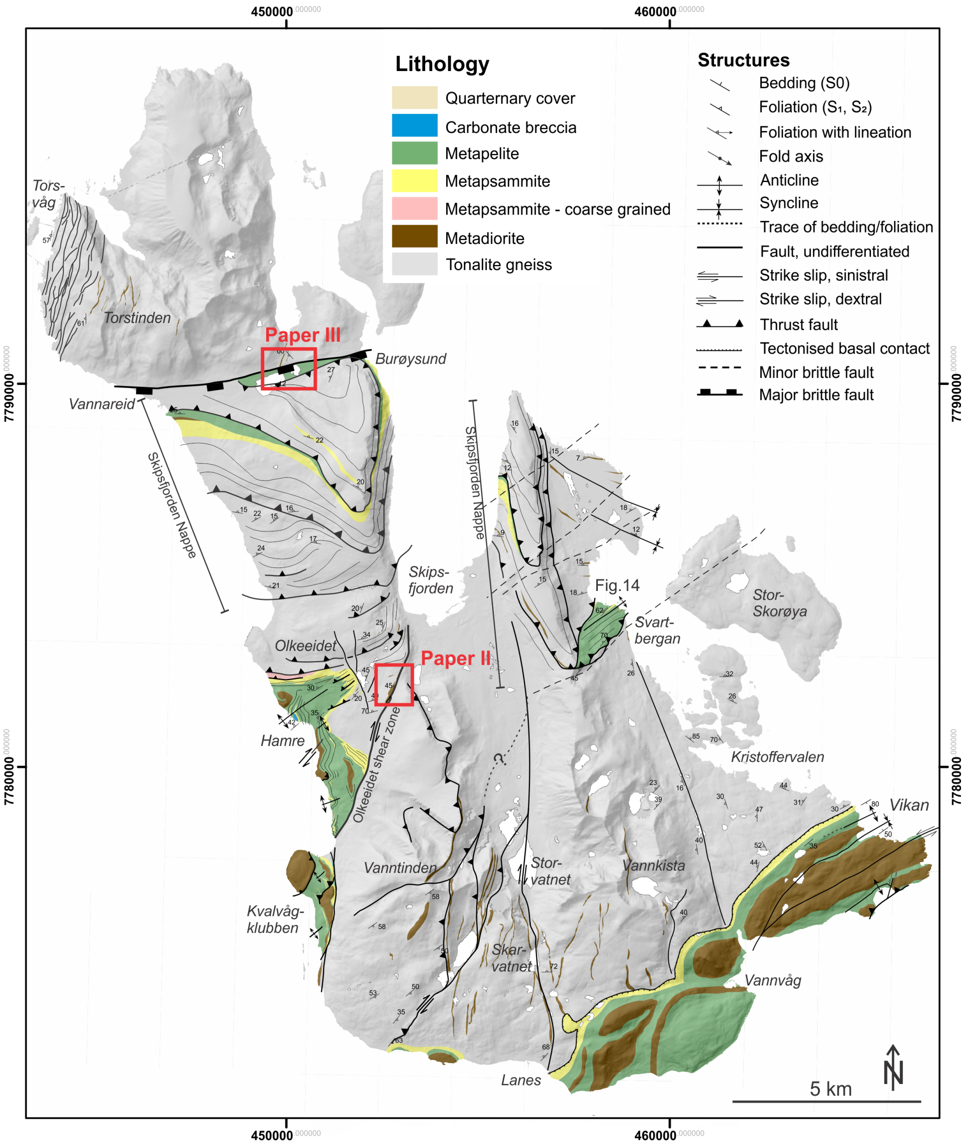

Figure 1.5: Geological and tectonic map of Vanna island (Modified after Bergh et al., 2007; Grogan and Zwaan, 1997; Opheim and Andresen, 1989; Roberts, 1974.) Red frames refer to the locations of Olkeeidet emerald occurrence in paper II and Vannareid Burøysund Cu-Zn mineralization in paper III.

Smaller metasedimentary sequences are also located at Hamre-Kvalvågklubben along the western coast of Vanna. These metasedimentary sequences have a similar stratigraphy as the Vanna Group, with metapsammites and quartzites overlain by intercalated metapelites, but the metamorphic grade is somewhat higher (upper-greenschist facies; this work; Bergh et al., 2007).

Skipsfjord Nappe

The parautochthonous Skipsfjord Nappe is a peculiar unit located in the northern part of Vanna (Fig. 2). It constitutes variously highly strained to mylonitized tonalitic gneisses and intercalated lenses of metasedimentary and mafic intrusive rocks of the Kvalkjeften Group (Opheim and Andresen, 1989). The metamorphic grade is generally higher than in the para-autochthonous units of the Vanna Group (lower amphibolite facies), and the rocks have a more pronounced foliation which coincides with ductile shear zones dipping gently NW. Individual units are separated by mylonitic high-strain ductile shear zones that dip gently NW and reveal mostly, top-to-the-SE thrust displacement. Oppheim and Andresen (1989) divided the Kvalkjeften Group into the lower mainly metapsammitic Geitdalen formation, and the upper mainly metapelitic Brattfjell formation. A depositional contact is suggested with the underlying mylonitic tonalite gneiss, however, strong deformation has obscured this relationship. A set of mafic dikes has intruded the upper parts of the Brattfjell formation.

Below the Skipsfjord Nappe, at Svartbergan (Fig. 1.5), recent mapping has unraveled a ca. 1km thick sequence of quartz-feldspathic metasandstones and siltstones, resembling rocks of the Vanna Group, although previously mapped as mylonitized basement gneisses. The strata are tilted to subvertical position, multiply folded, and truncated by the overlying Skipsfjord Nappe stack (Karlsen, 2019; Rønningen, 2019). The contact with basement gneisses below is marked by a moderate/steep oblique-slip shear zone at a high angle to the fold-thrust zones. In the north, the Skipsfjord Nappe is down-thrown > 3 km along the post-Caledonian brittle Vannareid-Burøysund normal fault (Opheim & Andresen 1989; Olesen et al. 1997), which hosts extensive Cu-Zn bearing quartz-carbonate veins (cf. paper III).

The Skipsfjord Nappe was originally suggested to be an allochtonous Caledonian thrust nappe correlated with the Kalak Nappe in Finnmark (Opheim and Andresen, 1989). Rice (1990) contradicted this interpretation and suggested that the rocks were a para-autochtonous basement-cover sequence. However, the Caledonian age of the Vanna Group deposition suggested by the similarities with the Cambro-Silurian Dividalen Group (Pettersen, 1887) and with Lyngsfjell Group (Landmark, 1973) was not disputed until Bergh et al., 2007 dated the diorite sill in the metapelitic Bukkheia formation to be 2221 +- 3 Ma, thereby constraining a Palaeoproterozoic minimum age to the deposition of the Vanna Group. Further, Bergh (2007) showed that the provenance of the sediments were locally derived from Archaean tonalite gneisses of Ringvassøya, Kvaløya and Senja.

In this thesis, we suggest that complex fold-thrust belt structures of presumed late-Svecofennian age characterize the deformation of the basement tonalites and the Palaeoproterozoic metasedimentary and intrusive rocks. This further implies that the structures formed in the foreland/frontal part of a transpressional deformation system adjacent to a continental accretionary orogen (Paulsen et al., 2019). In this setting, Palaeoproterozoic sedimentary basins controlled the location, extent and character of late-Svecofennian basement-seated folds, thrusts and orogen-parallel/oblique shear zones. However, the age of this deformation is still unresolved. This will be discussed further in Paper I in this thesis.

1.2 Aims of the project

The aim of this thesis is to investigate the controls on mineralization in the Archaean/Palaeoproterozoic basement rocks on Vanna island, northern Norway using a combination of structural and lithological field mapping and a suite of geochemical techniques. Although ore-mineralization on Vanna has been known since the 1860's (Bratrein, 1989), few analytical studies have been carried out prior to the work in this PhD thesis. A further aim is to understand the formation of local structures, and their role as fluid pathways for ore-bearing fluids. In addition, an attempt is made to place the local structures in a larger tectonic setting. This work also sets out to understand the ore-bearing fluids, and the key mechanisms that ultimately lead to the deposition of mineralization.

2

Approach

The aims of this thesis are approached using a combination of field work together with an extensive suite of analytical techniques. The methods compliment each other well as they each resolve a part of the complex interplay of structures that control the hydrothermal fluid flow used as pathways, and to understand the physiochemical properties of the fluids that further control the mineralization and alteration assemblage.

2.1 Field mapping and structural analysis

Approximately ten weeks over four field seasons were spent mapping selected areas of Vanna island. Field studies forms the basis for all three papers presented in this thesis. Paper I comprises a structural field study that focussed on mapping of the metasedimentary cover sequences (Vanna Group) and their relation to the basement seated structures in Vanna. The key outcrops were the metasedimentary cover sequences, as they have recorded these structural fabrics very well. Mapping carried out in paper I also forms the structural framework for the more detailed field investigation of the structural controls on mineralization discussed in papers II and III. Field work for papers II and III also included selected sampling of mineralization, altered host rocks and their unaltered equivalents. For paper III, field work was combined with investigations of c. 800 m of existing diamond drill-core bored by Store Norske Gull in 2008 (Ojala et al., 2013). The drill-core provided unique 3D understanding of the Vannareid-Burøysund fault, and its relationship to mineralization and hydrothermal alteration.

2.2 Analythical methods

A suite of different analytical methods were selected based on their usefulness to understand various properties involved in the deposition of ore-minerals in paper II and III, in particular to understand the metal-transport capabilities and deposition mechanisms of the ore-bearing fluid.

Scanning electron microscopy (SEM) including energy-dispersive X-ray spectroscopy (EDS), electron backscattered diffraction (EBSD), and cathodoluminescence (CL), was used to determine mineral chemistry, mineral parageneses, mineralogical changes, e.g. zonation in hydrothermal quartz, and textural relationships. The thin sections were coated with a thin carbon layer to avoid charging effects. All the analyses were carried out using a Zeiss Merlin VP Compact field emission SEM equipped with an X-max80 EDS detector and a Nordlys EBSD detector, both provided by Oxford Instruments, as well as a Zeiss valuable pressure secondary electron (VPSE) detector for CL imaging. The VPSE detector produces an image close to panchromatic CL under high vacuum conditions (Giffin et al., 2010). EDS chemical analysis of chlorite in fault rocks was used to estimate formation temperatures based on tetrahedral site occupancy (Cathelineau, 1988), which is accurate to within 30°C.

Fluid inclusions are microscopic bubbles of hydrothermal fluid trapped within a crystal, and are widely used to provide insight into the chemical and physical (pressure and temperature) properties of ore-forming fluids (Roedder, 1984; Wilkinson, 2001). Fluid inclusion studies were selected because it is one of the few methods that allows for semi-direct analysis of the fluids that deposited the various minerals, including ore-minerals. Fluid inclusion data were obtained from double polished wafers (100-250 µm thick) of hydrothermal gangue and ore minerals. Petrographic observations classified the fluid inclusions as primary, pseudosecondary or secondary based on their internal relationships with each other and their spatial distribution. Microthermometric measurements during the heating and freezing cycle allowed us to determine salinity, minimum fluid temperatures, and indicate the chemical composition of the fluid. All measurements were recorded using an Olympus BX 2 microscope coupled with a Linkam THMS 600 heating and cooling stage operating between -180 and +600°C at UiT-The Arctic University of Norway. For the equations used to calculate salinity and isochores see paper II and III. Despite the wide acceptance of usefulness of this method, there are several potential complications that can occur and lead to misinterpretations of the measurements. Fluid inclusions commonly deform and/or recrystallise post deposition (Roedder, 1984). If not recognised, this can lead to over/underestimation particularly of pressures in calculated isochores (Tarantola et al., 2010). In addition, failure to recognise solid phases because of their small size making them invisible under the microscope, or metastability can further complicate measurements and the subsequent interpretation. Most of these issues can, however, be minimised by careful and detailed observations by the person performing the analyses.

In addition, qualitative measurements of key elements present in the hydrothermal fluid were obtained by **decrepitating fluid inclusions** (c. 500°C for 3-4 minutes) and analysing the resulting evaporate mounds formed on the sample surface using an SEM/EDS technique modified after Kontak (2004). We performed both spot analyses of specific mineral phases and a map scan over the whole evaporate mound. This technique was useful for determining the major components present in the fluid inclusions. Its usefulness is, however, limited by the unpredictability in which of the individual fluid inclusion will decrepitate, and further if microthermometric measurements have been obtained from that particular fluid inclusion.

Raman Spectroscopy is used to characterize the structure of geologically interesting materials such as minerals. It is particularly useful as a non-destructive method to identify Raman active species in fluid inclusions, including CO_2. Raman spectroscopy was conducted at the Department of Earth Science, the Faculty of Mathematics and Natural Sciences, University of Bergen (UiB). A JobinYvon LabRAM HR800 confocal Raman spectrometer equipped with a frequency doubled Nd-YAG laser (100 mW, 532 nm) and LMPlan FI 50× objective (Olympus) was used to identify minerals based on Raman spectra published in the literature (Lafuente et al., 2015). CO_2 densities were calculated according to Fall et al., (2011).

Stable isotopic measurements of $\delta^{13}C$ and $\delta^{18}O$ can indicate the source of the CO_2 that formed carbonates. These analyses were obtained using a Thermo-Fisher MAT253 IRMS with a Gasbench II at UiT (site.uit.no/sil). Samples were placed in 4.5ml Labco vials, then flushed with He, and 5 drops of water-free H_3PO_4 were added manually with a syringe. The results were normalised to the Vienna Pee Dee Belemnite (VPDB) standard by three in-house standards with a wide range of $\delta^{13}C$ and $\delta^{18}O$ values, and reported with an uncertainty of standard deviation $\leqslant$ 0.1 ‰.

X-ray diffraction (XRD) analyses were used to study the structure, composition and physical properties of minerals. It was particularly useful to identify the mineralogy of fine-grained ultracataclasite material. The analyses were conducted at the University of Zagreb on a Philips PW 3040/60 X'Pert PRO powder diffractometer (45 kV, 40 µA), with CuKα-monochromatized radiation

(Δ= 1.54056 Å) and θ-θ geometry. The area between 4 and 63°2θ, with 0.02° steps was measured with a 0.5° primary beam divergence. Compound identifications were based on a computer program X'Pert high score 1.0B and literature data.

For further detail on the analytical methods used, see paper II and III.

3

Synthesis of papers

Paper I

Paulsen, H.K., Bergh, S.G., Strmić Palinkaš, S., Karlsen, S.E., Kolsum, S. & Rønningen, I.U., Nasuti, A. **Fold-thrust structures and oblique faults on Vanna island, West Troms Basement Complex, and their relation to inverted metasedimentary sequences**, *Manuscript*

The aim of this paper is to portray and discuss the structural architecture and tectonostratigraphic evolution of Vanna island by using field structural and lithological mapping in combination with reprocessed magnetic susceptibility data. Resolving the structural evolution of Vanna significantly improves the understanding of the northernmost low-grade portion of the West Troms Basement Complex, and shows that Vanna could represent a fold-thrust belt system related to accretionary tectonism documented in this basement complex. Further, we compare these observations with the larger-scale tectonic evolution of northern Fennoscandian Shield. Further, understanding the formation of the structural fabrics found on Vanna is valuable from an economic perspective, and the results from this paper form a framework to understand the structural controls on mineralization presented in paper II and III.

This manuscript focusses on a series of metasedimentary sequences that unconformably overlie the Archaean to Palaeoproterozoic basement rocks on Vanna (Fig. 1.5). The para-autochthonous metasedimentary sequences in Vanna, including those in the autochthonous Skipsfjord and Svartbergan Nappes were deposited in separate, pre-orogenic (2.4-2.2 Ga) rift basins bounded by NNW-SSE, NNE-SSW, and subordinate NE-SW trending, steep normal faults. The basins in Vanna comprise a lower series of metapsammites and overlying metapelites with subordinate horizons of peculiar calcareous metapelitic breccias, quartzites and conglomerates. Internal stratigraphy and preserved primary sedimentary structures indicate deposition in shallow marine, high-energy deltaic or tidal and shore face depositional environment.

Steep, pre-existing c. 2.4 Ga mafic dykes trending N-S in the tonalitic basement rocks of Vanna, provided favourable zones of weakness that helped localise the Palaeoproterozoic rift basins and their bounding normal faults. During the subsequent orogenic deformation, the rift-basins and enclosed metasedimentary sequences were subjected to two main shortening events (D1-D2). The D1-event involved ENE-WSW shortening, basement-involved folding and steep reverse faulting/thrusting. Pre-existing N-S trending normal faults were reactivated as steep west-dipping reverse and low-angle thrust faults with up-to-the-east displacement. A dextral strike-slip component of the steep reactivated faults, including the Olkeeidet shear zone, is also observed. The D2-event caused major SE-directed imbricate thrusting of the Skipsfjord and Svartbergan Nappes, basement-involved fold-thrust belt formation in the para-autochthonous Vanna Group in southeastern Vanna, and sinistral strike-slip reactivation of the steep N-S trending basement faults. These complex, two-stage fold- and thrust belt systems are considered to be Late-Svecofennian in age, from dating elsewhere in the West Troms Basement Complex. However, it is also possible that the D2 phase is Caledonian in age, or reactivated during the Caledonian Orogeny. Regardless of the age of these contractile deformations, metasedimentary units and associated D1-D2 thrusts, steep strike-slip shear zones, and intrusive contacts in both the metasedimentary units and basement gneisses suffered mineralization and quartz-carbonate veining, emerald-quality beryllium, and fuchsite-bearing fabrics, suggesting strong ductile structural control on the mineralization described in paper II.

Paper II

Paulsen, H-K, Bergh, S. G, Palinkaš, S. S. **Hydrothermal emeralds: a shear zone hosted mineralization on Vanna Island, northern Norway** *Manuscript*

This paper investigates the hydrothermal origin of recently discovered emeralds hosted by the Olkeeidet shear zone (OSZ) on Vanna island (Fig. 1.5). The formation of emerald (the green coloured variety of beryl) is a geological contradiction - it requires interaction of two geochemically contrasting components; one that brings highly incompatible Be, and another rich in compatible

Cr. Although emeralds are rare, they can form in a variety of geological settings, most commonly from beryllium-bearing pegmatites that intrudes Cr-rich ultramafic rocks. This occurrence on Vanna is unique, and is evidence that emerald can be deposited from fluids and not just granitic melts.

Detailed mapping of structural relations shows that the OSZ is a c. 50 m wide ductile shear zone that cuts Archaean/Palaeoproterozoic tonalite and tonalite gneisses with amphibolite layers. Within the OSZ, an array of internal splay faults, including minor thrust faults and strike slip faults, form a set of duplexes that indicate dextral movement along the OSZ. Hydrothermal fluid flow through this shear zone is evident from extensive metasomatic alteration of the host rocks that resulted in the formation of albitites and fuchsite schists, and the deposition of hydrothermal dolomite, quartz, tourmaline and emerald. The protolith of the strongly metasomatised rock is speculated to include a small lens of metasedimentary rocks; similar metasedimentary rocks are also found along the OSZ further south at Kvalvågklubben. The mineralogy of emerald and the surrounding alteration assemblage is confirmed using SEM, and X-ray diffraction analyses as well as Raman Spectroscopy.

The OSZ acted as a conduit for hydrothermal fluid flow. In addition, metasomatic alteration of the host rocks likely furthered the porosity, thereby creating a positive-feedback loop that allowed for increasing metasomatic alteration. Fluid composition is investigated by fluid inclusion microthermometry and decrepitation, which reveal that the hydrothermal fluids were highly saline (30-43 wt. % NaCl equiv.) and composed of $H_2O+NaCl\pm CO_2\pm KCl$. Estimates of formation conditions reveal minimum temperatures of 320-350°C and 0.7 kbar pressure. In addition, the stable isotopic C-O compositions suggest that the fluids were, at least in part, magmatic in origin. As fluid can migrate considerable distances within a shear zone environment, a deeper crustal level magmatic degassing is speculated as a possible source of highly saline fluids and CO_2. A genetic link with granitoid-associated veins is thus suggested for the fluids. Such a magmatic fluid can also contain significant beryllium, the highly incompatible element, needed to form emerald. Chromium is likely sourced from the local, possibly metasedimentary host rocks. From this, we suggest that emerald mineralization is epigenetic and has formed as a result of hydrothermal growth associated with tectonic activity. This locality evidences that emerald can be deposited from hydrothermal fluids of a magmatic origin, in contrast to the classic emerald formation models where emerald is deposited from a granitic melt intruding an ultramafic host rock.

Paper III

Paulsen, H-K., Bergh, S. B., Palinkaš, S. S., **Late Palaeozoic fault controlled hydrothermal Cu-Zn mineralization on Vanna Island, West Troms Basement Complex, northern Norway,** *Manuscript submitted to Norwegian Journal of Geology*

This paper focusses on hydrothermal Cu-Zn mineralization hosted by the Vannareid-Burøysund fault (VBF). In this paper we aim to identify the structural and physiochemical controls on mineralization. We analyse the structural architecture and textural relationships of host rocks, cataclasites and hydrothermal veins hosted by the VBF and attempt to resolve its role as a fluid pathway for the ore-bearing fluids. A second part of this work aims to determine the characteristics of the ore-bearing fluid to indicate a potential fluid source, identify controls on metal solubility and transport capabilities, and investigate the depositional mechanisms. For this second part, we use a multi-technique analytical approach including fluid inclusion studies, mineral and whole-rock geochemical-, and stable isotope analyses.

The VBF is exposed on the northern part of Vanna, where it separates Archaean tonalite gneiss from highly strained Skipsfjord Nappe with enclosed metasedimentary lenses (Fig. 1.5). This fault is a part of the Vestfjord-Vanna Fault Complex that bounds the West Troms Basement Complex horst against Caledonian Nappes to the east. Existing K–Ar illite dating of this fault yielded a late Carboniferous through early Permian age (Davids et al., 2013); concurrent with incipient continental rifting that resulted in the opening of the North Atlantic Ocean. The Cu-Zn mineralization was discovered in 2008. Following a brief exploratory diamond drilling carried out by the company Store Norske Gull in 2012 this occurrence was informally interpreted as the stringer zone of a Palaeoproterozoic volcanic massive sulphide deposit, related to the deposition of the metasedimentary sequences in the Skipsfjord Nappe (Ojala et al., 2013). However the results from this paper contradicts that interpretation; we suggest that mineralization is epigenetic and strongly structurally controlled by late Palaeozoic normal fault movement.

A model is proposed to explain the complex Cu-Zn mineralization in the VBF. This model shows successive and/or repeated supply of over-pressurized hydrothermal fluids to the VBF in a tectonic environment characterised by crustal extension and normal faulting. Two main stages of faulting/fracturing is observed, where the initial stages of syn-ore brittle faulting along VBF generated massive proto/ortho-cataclasites in a relatively narrow core zone, and the porosity created by the fracturing allowed for the deposition of massive quartz-sphalerite veins. The second stage in the fault evolution was progressive widening of the fault, the development of spatially more extensive damage zones, continued cataclasis, and injection of quartz-chalcopyrite veins. Additionally, during successive injection of quartz-sphalerite vein material, the initial fault core might have become partly or fully sealed, thus reducing the permeability and forcing the later fluids to flow into the damage zones. Although the fault cores acted as the main fluid conduits, the fluids also weakened the strength of the fault damage zones and contributed to the complex fault architecture.

Fluid inclusion microthermometry of inclusions hosted by quartz, sphalerite and calcite revealed that Cu and Zn were carried as chloride complexes in a highly saline (27-38 wt. % NaCl+$CaCl_2$ equiv.) fluid composed of NaCl+$CaCl_2$+H_2O at temperatures conditions of c. 250-330°C. The propylitic alteration mineralogy assemblage suggests that the ore-bearing fluid was near neutral and possibly reducing. In such a highly saline fluid, the physiochemical properties that control metal solubility is mainly temperature and concentration of ligands. The successive deposition of quartz sphalerite veins followed by quartz-chalcopyrite veins is also reflected in the interpreted depositional mechanisms. Sphalerite ore minerals were deposited by isothermal fluid mixing - by diluting the highly saline fluid and thereby lowering the solubility. The later chalcopyrite minerals were deposited by a combination of fluid mixing with a cooler fluid and wall-rock interactions. Further, this implies an influx of cooler ground/meteroric water into the fault system as the fault widens. A magmatic source, or a significant magmatic contribution, of CO_2 in hydrothermal calcite is indicated by stable $\delta^{13}C_{VPDB}$ and $\delta^{18}O_{SMOW}$ analysis. In addition, the different stable isotopic composition of calcite found in the metasedimentary sequence in the Skipsfjord Nappe is not directly the source of metals and salinity of the ore bearing fluid, as suggested by previous workers. No late Palaeozoic magmatism is observed in the region, however, we suggest that the fluids might be derived from a deeper magmatic source that is not found on surface. This study demonstrates that hydrothermal Cu-Zn mineralization in northern Norway may occur not only in old Precambrian and Caledonian basement rocks, but also in much younger, Palaeozoic to Cretaceous, rift-related, brittle fault zones. This provides an additional regional mineral exploration model for structurally controlled ore deposits in northern Norway.

3.1 Synthesis

This thesis focusses on the structural and tectonostratigraphic evolution of Vanna, and its associated controls on mineralization. The three papers presented in this thesis relate well as each paper aims to explain a separate part. The first paper discusses the early tectonic and structural evolution of Vanna, with a focus on the contractile ductile deformations forming fold and thrust belt structures. These contractionary fabrics are well-preserved in the metasedimentary strata that were deposited in Palaeoproterozoic continental rift basins that formed due to a E-W directed regional extension event. The subsequent multi-phase contractile deformation inverted these basins and their boundary faults and resulted in low-grade fold and thrust belt structures. The first phase (D1) of deformation is caused by WSW-ENE compression, and the second more spatially extensive phase (D2) was caused by later NNW-SSE compression. In paper II we investigate the Olkeeidet shear zone that hosts hydrothermal emerald mineralization deposited in relation to the dextral deformation. The Olkeeidet shear zone likely originated as a Palaeoproterozoic basin bounding normal fault, and the dextral movement along the fault suggests that the early D1 deformation was active at the time of emerald formation. In paper III we investigate Cu-Zn mineralization hosted by the brittle Vannareid-Burøysund fault. This brittle fault is associated with incipient rifting related to the late Palaeozoic opening of the Atlantic Ocean.

Considered together, the three papers in this thesis can be used to discuss the mineralization potential and the controls more broadly. The three papers cover a prolonged geological history, and shows that various types of mineralization occur in different geotectonic settings. Although the occurrences found on Vannareid and Olkeeidet are small and at this stage in time uneconomic, neither type of mineralization is previously described from the West Troms Basement Complex. This study provides valuable insight into the mineralization potential, key mechanisms that control mineralization, and highlights the potential for further undiscovered and significant structurally controlled mineralization to be found.

3.1.1 A transect though a continental accretionary orogen

The data presented in paper I suggest that the structures on Vanna formed in the foreland/frontal part of a transpressional deformation system adjacent to a continental accretionary orogen, likely the Svecofennian Orogeny. Considering the presumed metamorphic gradient in the West Troms Basement Complex where the hinterland (deep crust) is represented by the high-grade rocks found in Lofoten/Vesterålen in the south-west, to a foreland (upper crust) at Vanna in the north-east, a near-complete coastal transect through an orogenic event can be found in the West Troms Basement Complex. The excellent exposures makes the this coastal transect a key area for studying regional-scale tectonics of a presumed Late-Svecofennian age.

3.1.2 Age of D2 deformation on Vanna

The discussion regarding the depositional age of the Vanna Group metasedimentary sequence; whether it is Caledonian (Pettersen, 1887; Landmark, 1973) or Svecofennian, was put to an end by Bergh et al., (2007) whom proved a Palaeoproterozoic depositional age. The age of deformation, however, still remains an open question. Although in paper I we suggest that the deformation is likely Svecofennian, preliminary and unpublished Ar^{40}/Ar^{39} data of metamorphically formed muscovite from mylonitised metasedimentary rocks within the Skipsfjord Nappe yield a Caledonian age (c. 420 Ma; NGU pers. comm., 2019). Further studies are needed to determine whether this preliminary data suggests that the entire D2 deformation event on Vanna is Caledonian or whether it simply suggests a weak Caledonian metamorphic overprint. It has previously been suggested that the West Troms Basement Complex has not been substantially subjected to Caledonian deformation (Dallmeyer, 1992; Corfu et al., 2003).

When considering a potential Caledonian age of this D2 deformation, it is natural to compare with the lowermost Caledonian Nappe exposed in the region, the Kalak Nappe (Fig. 1.2), thus supporting the suggestions by Opheim and Andresen (1989). The Kalak Nappe is exposed on the islands on Arnøya and Uløya located just east of Vanna, and is composed of low-grade Precambrian gneisses and metapsammites with local intrusive mafic rocks (Faber et al., 2019). However, the metapsammites are Neoproterozoic and much younger than those found at Vanna (Kirkland et al., 2007). On Arnøya and Uløya, the pervasive Caledonian mylonitic foliation, associated mineral lineations and stretching lineations also plunge shallowly to the NW or SE (Faber et al., 2019). The orientation of these structural fabrics are similar to foliations and stretching lineations found in the D2 deformational fabrics of the Skipsfjord Nappe on Vanna (Fig. 1.5). Despite similar orientations with Caledonian structural fabrics further studies are needed to confirm or disprove the hypothesis of the Caledonian age.

Further, if the D2-Vanna deformation of the Skipsfjord Nappe indeed is Caledonian, it also warrants further investigations into the formation age of the assumed Svecofennian-aged, semi-ductile D3 event in the southern parts of the West Troms Basement Complex (Fig. 1.4) in Bergh et al., (2007; 2010). Currently, this is interpreted to be Late Svecofennian orogen-parallel contraction that resulted in sinistral strike-slip reactivation of steep macro-folds. However, if the D2-Vanna deformation is Caledonian it is not unlikely that Caledonian aged structures also exist further south in the West Troms Basement Complex.

3.1.3 Hidden magmatism or deep-seated structures as a source of magmatic CO_2

Stable isotopic $\delta^{13}C$ and $\delta^{18}O$ analyses of emerald-hosting dolomite (paper II) in the assumed Palaeoproterozoic ductile OSZ and of hydrothermal calcite in the Palaeozoic VBF both show a significant component of magmatic CO_2 (Fig. 3.1). These analyses are in contrast to those analysed from the calcite cement of the Vanna Group (Johannessen, 2012), from calcite veins hosted by metasedimentary sequences within the Skipsfjord Nappe, and from calcite veins in the magmatic diorite sill within the Vanna Group - all of which plot much closer to the field of marine sandstone. The source of this magmatic CO_2 is, however, enigmatic as no magmatism is recorded on Vanna since the intrusion of the diorite sill at 2.2 Ga.

Regionally, several Svecofennian aged magmatic events, possible Palaeoproterozoic sources for the magmatic signature of the emerald-hosting dolomite are recorded in the West Troms Basement Complex. These include a suite of 1.8 to 1.7 plutonic rocks in Lofoten-Vesterålen, and the Ersfjord Granite (1.3) on Kvaløya. The latter intrusion is thought have formed from partial melting of the TTG gneisses and was emplaced during the waning stages of the Svecofennian Orogeny (Haaland, 2018).

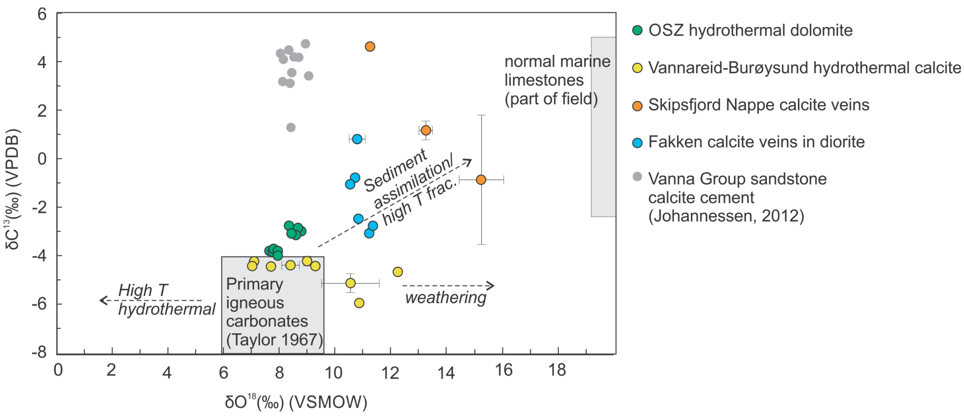

Figure 3.1: Isotopic compositions from Vanna

Regarding a possible magmatic source for some of the hydrothermal fluids in the much later brittle Palaeozoic Vannareid Burøysund fault, no direct evidence of a corresponding hot Permian magmatic and/or volcanic source/dike for the fluids have been observed in the Vanna island of western Troms. The closest in distance is the narrow (0.5 m wide) Carboniferous aged lamproite dike on Kvaløya farther south (Fig. 1.3) (Kullerud et al., 2011). Also, extensive rift-related mafic dike and sill intrusions of Carboniferous-Permian age do exist at northern Atlantic Ocean margins (Kirstein et al., 2006), including the continental margin of northern Finnmark (Lippard and Prestvik, 1997; Roberts et al., 2003; Roberts, 2011; Rice, 2014; Nasuti et al., 2015). However, CO_2 degassing is common in continental rift systems, and volatiles can travel far from its source along faults and fractures (Brune et al., 2017).

Rather, this suggests that although no direct local source of the magmatic CO_2 is found in either of the mineralized faults, both of the faults are likely deep-seated structures that can source CO_2 bearing fluids from deeper in the crust, and therefore can source CO_2 from more distal/deeper reservoirs.

3.1.4 Fennoscandian source of salinity

Hydrothermal fluids may derive their salinity and metal contents from a variety of sources that include magmatic, various non-magmatic, or more commonly a mixed source. In paper II we suggest that the salinity and the fluids are sourced from a deeper magmatic source, likely associated with granitoid felsic melt.

However, widespread Na-metasomatism is documented in the Palaeoproterozoic volcano-metasedimentary rocks throughout the northern Fennoscandian Shield, resulting in the formation of albite and scapolite, commonly accompanied by formation of carbonate and tourmaline (Frietsch et al., 1997). Albitisation in shear zones is also described predating orogenic gold, where albitisation makes the rock more competent and favourable for gold deposition (Eilu 2007; Hulkki and Keinanen, 2007). The source of these Fennoscandian extensive Na and Cl rich fluids is elusive, but it is suggested that hypothetical evaporite sequences deposited in rift basins with mafic volcanism around 2500-2000 Ma is the source of these highly saline fluids (Meleznic et al., 2015).

3.1.5 Implications for mineral exploration

The results from paper III show that the brittle Vannareid-Burøysund fault can host hydrothermal mineralization. The VBF fault is a part of the Vestfjord-Vanna Fault Complex that developed due to post-Caledonian orogenic collapse and subsequent incipient rifting prior to the opening of the Atlantic Ocean. Age dating of illite obtained by Davids et. al., (2013) gave an age of the last movement along the fault of 306-284 Ma. With continued rifting, this wide part of the margin on the coast of Vanna became passive as faulting moved further south to the Lofoten area (Mosar, 2003; Davids et al., 2013; Indrevær et al., 2013), by leaving the VBF is a part of the innermost boundary fault system. This is visible in (Fig. 1.1) where the continental margin along the Norwegian coast narrows northward towards Lofoten, and then abruptly widens again to the north of the Senja fracture zone that acted as a transfer zone.

Indrevær et al., (2013) suggested that these faults offshore could influence hydrocarbon migration and either act as fluid pathways for migration of fluids, or as hydrocarbon traps if the faults were sealed. The results from paper III also suggests that these faults could host hydrothermal mineralization and warrants further investigations into this extensive fault network that is found along most of the coastal margins of Norway.

3.2 Future research

The following suggestions on future research are given to further verify and/or evolve the results and models presented within this thesis:

- The age of the contractile deformation events on Vanna is uncertain. Absolute age dating of the ductile deformation that formed the fold and thrust belt system on Vanna would greatly improve the temporal relationship between the two ductile contractional phases (D1 & D2), and establish whether the deformation is late Svecofennian or Caledonian. Zircon age dating of the mafic layers in the Skipsfjord Nappe would also help constrain this age.

- The jump in metamorphic grade and age of supracrustal units from Ringvassøya to Vanna is not well understood, and further structural and lithological investigations of the islands of Nord-Kvaløya, Helgøy, Spenna and Nord-Fugløya could aid in understanding this gap.

- Further stable isotopic $\delta^{13}C$ and $\delta^{18}O$ studies of the various carbonate horizons and breccias found on the island, within the metasedimentary sequences and localised within various ductile and brittle faults, would further the understanding of the magmatic components in the hydrothermal fluids in paper II and III.

- The source of metals in the Vannareid-Burøysund fault could be further constrained by sulphur isotopic analyses of the sulphides sphalerite and chalcopyrite. Further, the source of the salinity in the fluid could be better constrained by analysing the halogen content of the fluid inclusions using a LA-ICP-MS method. In particular, measuring the Cr/Br ratio could indicate whether some of the salinity was derived from potential evaporites in metasedimentary sequences in the Skipsfjord Nappe. Further, this would aid exploration for similar metal occurrences to know whether such a source of salinity is needed to mobilise the metals.

- The verification of the brittle nature a Palaeozoic age of mineralization along the Vannareid-Burøysund fault warrants further investigations into other post-Caledonian extensional faults along the West Troms Basement Complex, including those described by Indrevær et al., (2013) and Koehl (2013).

Bibliography

Angvik, T. L. (2014). “Structural development and metallogenesis of Palaeoproterozoic volcano-sedimentary rocks of the Rombak Tectonic Window.” PhD Thesis. UiT - the Arctic University of Tromsø (cit. on p. 4).

Armitage, P. E. B. and Bergh, S. G. (2005). “Structural development of the Mjelde-Skorelvvatn Zone on Kvaløya, Troms: a metasupractustal shear belt in the Precambrian West Troms Basement Complex, North Norway.” In: *Norwegian Journal of Geology* **85**, p. 16 (cit. on p. 7).

Augland, L. E., Andresen, A., Gasser, D., and Steltenpohl, M. G. (2014). “Early Ordovician to Silurian evolution of exotic terranes in the Scandinavian Caledonides of the Ofoten - Troms area - terrane characterization and correlation based on new U-Pb zircon ages and Lu-Hf isotopes.” In: *New perspectives on the Caledonides of Scandinavia and related areas.* Ed. by Corfu, F., Gasser, D., and Chew, D. M. Vol. 390. Special publication. London: The Geological Society of London, pp. 655–678 (cit. on pp. 5, 6).

Bark, G. and Weihed, P. (2007). “Orogenic gold in the new Lycksele-Storuman ore province, northern Sweden; the new Palaeoproterozoic Fäboliden deposit.” In: *Ore Geology Reviews* **32**, pp. 431–451 (cit. on p. 4).

Bergh, S. G., Corfu, F., Myhre, P. I., Kullerud, K., Armitage, P. E. B., Zwaan, K. B., Ravna, E. J. K., Holdsworth, R. E., and Chattopadhya, A. (2012). “Was the Precambrian basement of Western Troms and Lofoten-Vesterålen in Northern Norway linked to the Lewisian of Scotland? A comparison of crustal components, tectonic evolution and amalgamation history.” In: *Tectonics - recent advances*. Chap. 11 (cit. on p. 7).

Bergh, S. G., Corfu, F., Priyatkina, N., Kullerud, K., and Myhre, P. I. (2015). “Multiple post-Svecofennian 1750-1560 Ma pematite dykes in Archean-Palaeoproterozoic rocks of the West Troms Basement Complex, North Norway: geological significance and regional implications.” In: *Precambrian Research* **266**, p. 15 (cit. on p. 8).

Bergh, S. G., Kullerud, K., Armitage, P. E. B., Zwaan, K. B., Corfu, F., Ravna, E. J. K., and Myhre, P. I. (2010). “Neoarchean to Svecofennian tectono-magmatic evolution of the West Troms Basement Complex, North Norway.” In: *Norwegian Journal of Geology* **90**, p. 28 (cit. on pp. 7, 8, 9, 25).

Bergh, S. G., Kullerud, K., Corfu, F., Armitage, P. E. B., Davidsen, B., Johansen, H. W., Pettersen, T., and Knudsen, S. (2007). “Low-grade sedimentary rocks on Vanna, North Norway: a new occurrence of a Palaeoproterozoic (2.4-2.2 Ga) cover succession in northern Fennoscandia.” In: *Norwegian Journal of Geology* **87**, p. 18 (cit. on pp. 7, 8, 10, 11, 12, 13, 25).

Bingen, B., Solli, A., Viola, G., Torgersen, E., Sandstad, J. S., Whitehouse, M. J., Røhr, T. S., Ganerød, M., and Nasuti, A. (2015). “Geochronology of the Palaeoproterozoic Kautokeino Greenstone Belt, Finnmark, Norway: Tectonic implications in a Fennoscandia context.” In: *Norwegian Journal of Geology* **95**, pp. 365–396 (cit. on p. 4).

Binns, R. E., Chroston, P. N., and Matthews, D. W. (1980). “Low-grade sediments on Precambrian Gneiss on Vanna, Troms, Northern Norway.” In: *Offprint NGU* **359**, p. 12 (cit. on p. 10).

Bleeker, W. (2003). “The late Archean record: a puzzle in ca. 35 pieces.” In: *Lithos* **71**, p. 28 (cit. on p. 4).

Bratrein, H. D. (1989). *Karlsøy og Helgøy bygdebok: folkeliv, næringsliv, samfunnsliv 3: Fra år 1860 til 1925*. Vol. X. Springer, p. 656 (cit. on pp. 10, 13).

Brune, S., Williams, S. E., and Müller, R. D. (2017). “Potential links between continental rifting, CO_2 degassing and climate change through time.” In: *Nature letters* **10**, pp. 941–946 (cit. on p. 27).

Bugge, C. (1935). *Rapport over Senjens nikkelverk*. Report. NGU (cit. on p. 9).

Cathelineau, M. (1988). “Cation site occupancy in chlorites and illites as a function of temperature.” In: *Clay Minerals* **23**, p. 15 (cit. on p. 16).

Corfu, F. (2004). “U-Pb age, setting and tectonic significance of the anorthosite-mangerite-charnockite-granite suite, Lofoten-Vesterålen, Norway.” In: *Journal of Petrology* **45**.9, p. 21 (cit. on p. 7).

Corfu, F., Armitage, P. E. B., Kullerud, K., and Bergh, S. G. (2003). “Preliminary U-Pb geochronology in the West Troms Basement Complex, north Norway:

Archean and Palaeoproterozoic events and younger overprints." In: *NGU Bulletin* **441**, p. 12 (cit. on pp. 7, 25).

Dallmeyer, R. D. (1992). "$^{40}Ar/^{39}Ar$ mineral ages within the Western Gneiss Terrane, Troms: evidence of polyphase Proterozoic tectonothermal activity (Svecokarelian and Sveconorwegian)." In: *Precambrian Research* **57**, p. 12 (cit. on p. 25).

Daly, J. S., Balagansky, V. V., Timmerman, M. J., and Whitehouse, M. J. (2006). "The Lapland-Kola orogen: Palaeoproterozoic collision and accretion of the northern Fennoscandian lithosphere." In: *Geological Society, London, Memoirs* **32**, pp. 579–598 (cit. on p. 4).

Davids, C., Benowith, J. A., Layer, P., Wemmer, K., Zwingmann, H., and Bergh, S. (2012). "$^{40}Ar/^{39}Ar$ dating of hydrothemally altered K-feldspar - Permian brittle faulting in northern Norway." In: *The 13th International Conference on Thermochronology*, p. 1 (cit. on p. 6).

Davids, C., Wemmer, K., Zwingmann, H., Kohlmann, F., Jacobs, J., and Bergh, S. (2013). "K-Ar illite and apatite fission track constraints on brittle faulting and the evolution of the northern Norwegian passive margin." In: *Tectonophysics* **608**, p. 16 (cit. on pp. 3, 6, 8, 22, 27).

Eilu, P. (2012). *Mineral deposits and metallogeny of Fennoscandia*. Special Publication 53. Geological survey of Finland (cit. on pp. 2, 3, 4).

Eilu, P., Sorjonen-Ward, P., Nurmi, P., and Niiranen, T. (2003). "A review of gold mineralisation styles in Finland." In: *Economic geology* **98**, p. 26 (cit. on pp. 3, 4).

Faber, C., Stünitz, H., Gasser, D., Jeřábek, P., Kraus, K., Corfu, F., Ravna, E. K., and Konopásek, J. (2019). "Anticlockwise metamorphic pressure–temperature paths and nappe stacking in the Reisa Nappe Complex in the Scandinavian Caledonides, northern Norway: evidence for weakening of lower continental crust before and during continental collision." In: *Solid Earth* **10**, pp. 117–148 (cit. on pp. 5, 25).

Fall, A., Tattitch, B., and Bodnar, R. J. (2011). "Combined microthermometric and Raman spectroscopic technique to determine the salinity of H_2O-CO_2-NaCl fluid inclusions based on clathrate melting." In: *Geochimica et Cosmochimica acta* **75**, pp. 951–964 (cit. on p. 17).

Gaál, G. and Gorbatschev, R. (1987). "An Outline of the Precambrian Evolution of the Baltic Shield." In: *Precambrian Research* **35**, p. 38 (cit. on p. 4).

Gabrielsen, R. H. and Braathen, A. (2014). "Models of fracture lineaments - joint swarms, fracture corridors and faults in crystalline rocks, and their genetic relations." In: *Tectonophysics* **628**, p. 19 (cit. on p. 1).

Giffin, B. J., Joy, D. C., and Michael, J. R. (2010). "A comparison of a luminescence-based VPSE and an electron-based GSED for SE and CL imaging in variable pressure SEM with conventional SE imaging." In: *Microscopy and Microanalysis* **160**, pp. 825–843 (cit. on p. 16).

Griffin, W. L., Taylor, P. N., Hakkinen, J. W., Heier, K. S., Iden, I. K., Krogh, E. J., Malm, O., Olsen, K. I., Ormaasen, D. E., and Tveten, E. (1978). "Archean and Proterozoic crustal evolution in Lofoten-Vesterålen, N Norway." In: *Journal of the Geological Society of London* **135**, p. 19 (cit. on p. 7).

Grogan, P. and Zwaan, B. (1997). *Geologisk kart over Norge, berggrunnskart Helgøy, M 1:250 000*. Report. Geological survey of Norway (cit. on p. 11).

Haaland, L. C. (2018). "Geometry and kinematic evolution of ductile shear zones in the Ersfjord Granite (1.79 Ga), West Troms Basement Complex: a Svecofennian accretionary thrust system." MSc Thesis. UiT - the Arctic University of Tromsø (cit. on pp. 7, 8, 26).

Hansen, J.-A., Bergh, S. G., and Henningsen, T. (2012). "Mesozoic rifting and basin evolution on the Lofoten and Vesterålen margin, North Norway; time constraints and regional implications." In: *Norwegian Journal of Geology* **91**, pp. 203–228 (cit. on p. 6).

Hanski, E., Huhma, H., and Vaasjoki, M. (2001). "Geochronology of northern Finland: a summary and discussion." In: *Special Paper 33*. Ed. by Vaasjoki, M. Geological Survey of Finland, pp. 255–279 (cit. on p. 4).

Henderson, I., Viola, G., and Nasuti, A. (2015). "A new tectonic model for the Palaeoproterozoic Kautokeino Greenstone Belt, northern Norway, based on high-resolution airborne magnetic data and field structural analysis and implications for mineral potential." In: *Norwegian Journal of Geology* **95**.3-4, p. 26 (cit. on pp. 4, 7).

Högdahl, K., Andersson, U. B., and Eklund, O. (2004). *The Transscandinavian Igneous Belt (TIB) in Sweden: a review of its character and evolution*. Geological Survey of Finland, p. 125 (cit. on p. 4).

Hölttä, P., Balagansky, V., Garde, A. A., Mertanen, S., Peltonen, P., Slabunov, A., Sorjonen-Ward, P., and Whitehouse, M. (2008). "Archean of Greenland and Fennoscandia." In: *Episodes* **13**.1, p. 7 (cit. on p. 3).

Indrevær, K., Bergh, S. G., Koehl, J.-B., Hansen, J.-A., Schermer, E. R., and Ingebrigtsen, A. (2013). "Post-Caledonian brittle fault zones on the hyper-extended SW Barents Sea margin: New insights into onshore and offshore margin architecture." In: *Norwegian Journal of Geology* **93**, p. 23 (cit. on pp. 3, 6, 27, 28, 29).

Johannessen, H. (2012). "Tinnvatnformasjonen i Vannas proterozoiske lagrekke: Sedimentære facies og avsetningsmiljø." MSc Thesis. UiT - the Arctic University of Tromsø (cit. on pp. 10, 26).

Johansen, H. (1987). "Forholdet mellom det prekambriske underlaget og overliggende sedimentære bergarter sør-øst på Vanna, Troms." MSc Thesis. UiT - the Arctic University of Tromsø (cit. on p. 11).

Karlsen, S. E. (2019). "Strukturell og kinematisk analyse av Skipsfjorddekket og underliggende bergarter i nordøstlige del av Vanna, Vest-Troms gneisregion." MSc Thesis. UiT - the Arctic University of Tromsø (cit. on p. 12).

Kirkland, C. L., Daly, J. S., and Whitehouse, M. J. (2007). "Provenance and Terrane Evolution of the Kalak Nappe Complex, Norwegian Caledonides: Implications for Neoproterozoic Paleogeography and Tectonics." In: *The Journal of Geology* **115**, pp. 21–41 (cit. on p. 25).

Kirstein, L. A., Davies, G. R., and Heeremans, M. (2006). "The petrogenesis of Carboniferous–Permian dyke and sill intrusions across northern Europe." In: *Contributions to Mineralogy and Petrology* **152**, pp. 721–742 (cit. on p. 26).

Koehl, J.-B. (2013). "Late Paleozoic-Cenozoic fault correlation and characterization of fault rocks in western Troms, North Norway." MSc Thesis. UiT - the Arctic University of Tromsø (cit. on pp. 3, 29).

Koehl, J.-B., Bergh, S., Henningsen, T., and Faleide, J.-I. (2018). "Middle to Late Devonian-Carboniferous collapse basins on the Finnmark Platform and in the southwesternmost Nordkapp basin, SW Barents Sea." In: *Solid Earth* **9**, p. 32 (cit. on p. 6).

Koistinen, T., Stephens, M. B., Bogatchev, V., Nordgulen, Ø., Wennerström, M., and Korhonen, J. (2001). *Geological map of the Fennoscandian Shield, scale 1:2 000 000*. Report. Geological surveys of Finland, Norway, Sweden, and the north-west department of ministry of Natural Resources of Russia (cit. on pp. 3, 4).

Kontak, D. J. (2004). "Analysis of evaporate mounds as a complement to fluid-inclusion thermometric data: case studies from granitic environments in Nova Scotia and Peru." In: *The Canadian Mineralogist* **42**, p. 16 (cit. on p. 17).

Kullerud, K., Skjerlie, K. p., Corfu, F., and de la Rosa, J. D. (2006). "The 2.40 Ga Ringvassøy mafic dykes, West Troms Basement Complex, Norway: The concuding act of early Palaeoproterozoic continental breakup." In: *Precambrian Research* **150**, p. 18 (cit. on p. 7).

Kullerud, K., Zozulya, D., Bergh, S., Hansen, H., and Ravna, E. J. K. (2011). "Geochemistry and tectonic setting of a lamproite dyke in Kvaløya, North Norway." In: *Lithos* **126**, p. 12 (cit. on p. 26).

Lafuente, B., Downs, R. T., Yang, H., and Stone, N. (2015). *Highlights in Mineralogical Crystallography*. *The power of databases: the RRUFF project*. Ed. by Armbruster, T. and Danisi, R. M. Berlin, Germany: W. De Gruyter, pp. 1–30 (cit. on p. 17).

Lahtinen, R., Hallberg, A., Korsakova, M., Sandstad, J. S., and Eilu, P. (2012). "Main metallogenic events in Fennoscandia: Summary." In: *Special Paper 53*. Ed. by Eilu, P. Geological Survey of Finland, pp. 397–401 (cit. on p. 4).

Lahtinen, R., Hölttä, P., Kontinen, A., Niiranen, T., Nironen, M., Saalmann, K., and Sorjonen-Ward, P. (2011). "Tectonic and metallogenic evolution of the Fennoscandian Shield: key questions with emphasis on Finland." In: *Special Paper 49*. Ed. by Neonen, K. and Nurmi, P. A. Geological Survey of Finland, pp. 23–33 (cit. on pp. 3, 4, 7).

Landmark, K. (1973). "Beskrivelse til de geologiske kartene Tromsø og Målselv II. Kaledonske bergarter." In: *Tromsø Museums Skrifter* **15**, pp. 1–263 (cit. on pp. 12, 25).

Larsen, R. B., Grant, T., Sørensen, B. E., Tegner, C., McEnroe, S., Pastore, Z., Fichler, C., Nikolaisen, E., Grannes, K. R., Church, N., ter Maat, G. W., and Michels, A. (2018). "Portrait of a giant deep-seated magmatic conduit system: the Seiland Magmatic Province." In: *Lithos* **299**.22, pp. 600–622 (cit. on p. 5).

Laurent, O., Vander, J., Bingen, B., Bolle, O., and Gerdes, A. (2019). "Building up the first continents: Mesoarchean to Paleoproterozoic crustal evolution in West Troms, Norway, inferred from granitoid petrology, geochemistry and zircon U-Pb/Lu-Hf isotopes." In: *Precambrian Research* **321**, pp. 303–327 (cit. on pp. 7, 8).

Lippard, S. J. and Prestvik, T. (1997). “Carboniferous dolerite dykes on Magerøy; new age determinations and tectonic significance.” In: *Norsk Geologisk Tidsskrift* 77, pp. 159–163 (cit. on pp. 5, 27).

Mosar, J. (2003). “Scandinavias North Atlantic passive margin.” In: *Journal of Geophysical Research* **108**.B8, p. 18 (cit. on pp. 6, 27).

Motuza, G. (2000). *Description to the geological map of the central part of the Ringvassøya Greenstone Belt, Troms county, northern Norway*. Report. Geological survey of Norway (cit. on p. 7).

Myhre, P. I., Corfu, F., Bergh, S. G., and Kullerud, K. (2013). “U-Pb geochronology along an Archean geotransect in the West Troms Basement Complex, North Norway.” In: *Norwegian Journal of Geology* **93**, p. 24 (cit. on p. 7).

Nasuti, A., Roberts, D., and Gernigon, L. (2015). “Multiphase mafic dykes in the Caledonides of northern Finnmark revealed by a new high-resolution aeromagnetic dataset.” In: *Norwegian Journal of Geology* **95**.3-4, pp. 285–298 (cit. on p. 27).

Nironen, M. (1997). “The Svecofennian Orogen: a tectonic model.” In: *Precambrian Research* **86**, p. 24 (cit. on p. 4).

Ojala, J. V., Hansen, H., and Ahola, H. (2013). “Cu-Zn mineralisation at Vannareid, West Troms Basement Complex: a new Palaeoproterozioc VMS occurrence in the northern Fennoscandian Shield.” In: *12th Biennial SGA Meeting* (cit. on pp. 15, 22).

Olesen, O., Lundin, E., Nordgulen, Ø., Osmundsen, P. T., Skilbrei, J. R., Smethurst, M. A., Solli, A., Bugge, T., and Fichler, C. (2002). “Bridging the gap between the onshore and offshore geology in Nordland, northern Norway.” In: *Norwegian Journal of Geology* **82**, p. 20 (cit. on p. 3).

Olesen, O., Torsvik, T. H., Tveten, E., Zwaan, K. B., Løseth, H., and Henningsen, T. (1997). “Basement structure of the continental margin in the Lofoten-Lopphavet area, northern Norway: constraints from potential field data, on-land structural mapping and palaeomagnetic data.” In: *Norwegian Journal of Geology* 77, pp. 15–30 (cit. on p. 5).

Opheim, J. A. and Andresen, A. (1989). “Basement-cover relationships on northern Vanna, Troms, Norway.” In: *Norsk Geologisk Tidsskrift* **69**, p. 5 (cit. on pp. 10, 11, 12, 25).

Paulsen, H., Bergh, S., Strmic Palinkas, S., Armitage, P., Karlsen, S., Kolsum, S., Rønningen, I., and Nazuti, A. (2019). "Late-Svecofennian fold-thrust belt and oblique-slip structures on Vanna island, West Troms Basement Complex, and their relation to meta-sedimentary sequences." In: *Geological Society of Norway Wintermeeting*. Program with Abstracts. Bergen (cit. on p. 13).

Pettersen, K. (1887). *Den nord-norske fjeldbygning I*. Vol. 10. Tromsø Museums Årshefte. Tromsø Museum, p. 174 (cit. on pp. 10, 12, 25).

Rice, A. H. J. (1990). "A discussion: Basement-cover relationships on northern Vanna, Troms, Norway." In: *Norsk Geologisk Tidsskrift* **70**, p. 8 (cit. on p. 12).

Rice, A. H. N. (2014). "Restoration of the external Caledonides, Finnmark, North Norway." In: *Geological Society of London Special Publication* **390**, pp. 271–299 (cit. on p. 27).

Roberts, D. (1974). *Kartblad Hammerfest. Beskrivelse til det 1:250 000 berggrunns-geologiske kart*. Report. Geological survey of Norway (cit. on p. 11).

Roberts, D. (2011). "Age of the Hamningberg dolerite dyke, Varanger Peninsula, Finnmark: Devonian rather than Vendian - a revised interpretation." In: *Norges Geologiske Undersøkelse Bulletin* **451**, pp. 32–36 (cit. on p. 27).

Roberts, D. and Lippard, S. J. (2005). "Inferred Mesozoic faulting in Finnmark: current status and offshore links." In: *NGU Bulletin* **443**, p. 6 (cit. on p. 5).

Roberts, D., Torsvik, T., Andersen, T. B., and Rehnström, E. F. (2003). "The Early Carboniferous Magerøy dykes, northern Norway; palaeomagnetism and palaeogeography." In: *Geological Magazine* **140**, pp. 443–451 (cit. on p. 27).

Roedder, E. (1984). *Fluid inclusions*. Vol. 12. Reviews in Mineralogy. Blacksburg, Virginia: U S geological Survey, p. 644 (cit. on pp. 16, 17).

Rønningen, I. U. (2019). "Geometrisk og kinematisk analyse av paleoprotero-zoiske duktile skjærsoner i Skipsfjorddekkets undre del, Vanna, Vest-Troms gneisregionen, og relasjon til metasedimentære bergarter i Vannagruppen." MSc Thesis. UiT - the Arctic University of Tromsø (cit. on p. 12).

Sandstad, J. S. and Nilsson, L. P. (1998). *Gullundersøkelser på Ringvassøy, sammenstilling av tidligere prospektering og feltbefaring i 1997*. Report. NGU (cit. on p. 10).

Sibson, R., Moore, J., and Rankin, A. H. (1975). "Seismic pumping - a hydrothermal fluid transport mechanism." In: *Journal of the Geological Society of London* **131**, p. 7 (cit. on p. 1).

Tarantola, A., Diamond, L. W., and Stünitz, H. (2010). "Modification of fluid inclusions in quartz by deviatoric stress I: experimentally induced changes in inclusion shapes and microstructures." In: *Contributions to Mineralogy and Petrology* **16**, p. 624 (cit. on p. 17).

Thorstensen, L. (2011). "Land-sokkel korrelasjon av tektoniske elementer i ytre del av Senja og Kvaløya i Troms." MSc Thesis. UiT - the Arctic University of Tromsø (cit. on p. 8).

Weihed, P., Arndt, N., Billström, K., Duchesne, J.-C., Eilu, P., Martinsson, O., Papunen, H., and Lathinen, R. (2005). "Precambrian geodynamics and ore formation: The Fennoscandian Shield." In: *Ore Geology Reviews* **27**, p. 49 (cit. on p. 4).

Wilkinson, J. (2001). "Fluid inclusions in hydrothermal ore deposits." In: *Lithos* **55**, p. 44 (cit. on p. 16).

Zwaan, K. B. (1989). *Berggrunnsgeologisk kartlegging av det prekambriske grønnsteisbelte på Ringvassøya, Troms*. Report. NGU (cit. on pp. 7, 10).

Zwaan, K. B. (1995). "Geology of the West Troms Basement Complex, northern Norway, with emphasis on the Senja Shear Belt: a preliminary account." In: *NGU Bulletin* **427**, pp. 33–36 (cit. on p. 7).

Late Palaeozoic fault controlled hydrothermal Cu-Zn mineralization on Vanna Island, West Troms Basement Complex, northern Norway.

Hanne-Kristin Paulsen[1], Steffen G. Bergh[1], Sabina Strmić Palinkaš[1]

[1] University of Tromsø (UiT) – The Arctic University of Norway, N-9037 Tromsø, Norway

hanne-kristin.paulsen@uit.no

Abstract

The Vannareid-Burøysund fault is a major, brittle normal fault in northern Norway, with cohesive fault rocks (cataclasites) that host Cu-Zn bearing quartz-carbonate veins. The fault is exposed on the island of Vanna in the Neoarchaean to Palaeoproterozoic West Troms Basement Complex, separating variably deformed tonalitic gneisses in the footwall from mylonitized meta-sedimentary rocks and tonalites in the hanging wall. Radiometric dating (K–Ar illite) of normal fault movement along the Vannareid-Burøysund fault yielded a late Permian age, concurrent with incipient post-Caledonian continental rifting. The fault evolution and internal architecture of the Vannareid-Burøysund fault largely controlled the spatial distribution of mineralization, and two main phases of the Cu-Zn mineralization have been discerned. Early quartz-sphalerite veins are deposited in the cataclastic fault core zone, where initial movement along the fault created a fluid conduit that allowed for fluid flow and sphalerite deposition. With subsequent movement and widening of the fault zone, a later and spatially more extensive generation of quartz-chalcopyrite veins were deposited in both the fault core and damage zones. Fluid inclusion microthermometry revealed that the ore-forming fluids were highly saline aqueous solutions (20-37 wt. % $NaCl+CaCl_2$) that carried base metals and sulphur. Further, the isotopic composition of hydrothermal carbonates indicates a magmatic source of CO_2. The structural data and obtained geochemical results indicate that the Cu-Zn mineralization in the Vannareid-Burøysund fault was epigenetic and strongly controlled by extensional brittle faulting and cataclasis during early stages of post-Caledonian (Permian) continental rifting, thus providing a new model for exploration of post-Caledonian hydrothermal ore deposits in basement rocks of northern Norway.

Introduction

Cu-Zn mineralization is found in a variety of geological settings, such as volcanogenic massive sulphide (VMS) deposits (Franklin et al. 1981; Galley et al. 2007), skarn deposits (Meinert et al. 2005), black shale hosted Cu-Zn deposits (Kupferschiefer; Kucha and Pawlikoswki, 1986; Oszczepalski 1999), sediment hosted Cu-Zn deposits (Perello et al. 2015), and hydrothermal vein deposits (Corbett and Leach 1998; Simmons et al. 2005). Key factors that may control the deposition of significant Cu-Zn mineralization include a source of metals (Rye and Ohmoto 1974; Boiron et al. 2010), an aqueous fluid capable of transporting metal complexes (Hemley and Cygan 1992; Zhong et al. 2015), rock permeability that allows fluid flow (Sibson et al. 1975; Ingebritsen and Manning 2010), and favourable physicochemical conditions for Cu and Zn deposition (Seward and Barnes 1997; Vaughan and Craig 1997; Corbett and Leach 1998). In crystalline rocks in the upper crust, brittle faults and fracture systems represent important conduits for ore-bearing fluids in otherwise non-permeable rocks (Braathen and

Davidsen 2000; Gabrielsen and Braathen 2014; Schmid and Handy 1991; Sibson 1977; Wise et al. 1984).

In this study, we analyse a major brittle normal fault in northern Norway, the Late Palaeozoic/Permian Vannareid-Burøysund fault (VBF), and its cohesive brittle fault rocks (cataclasites) hosting Cu-Zn bearing quartz-carbonate veins. The fault is situated along the contact between Neoarchaean tonalitic basement gneisses and an overlying, mixed basement and meta-sedimentary thrust unit, the Skipsfjord Nappe (Opheim and Andresen 1989; Monsen, 2014). The Cu-Zn mineralization was discovered in 2008 and briefly explored in 2012 when an exploration company (Store Norske Gull) bored eight drill holes totalling a length of 880 m, and informally interpreted the mineralized occurrence as a Palaeoproterozoic VMS type (Ojala et al. 2013). Follow-up studies showed Cu-Zn and sulfide enrichment in vein and brecciated/cataclastic fault rocks indicating extensive hydrothermal alteration (Monsen, 2014). This paper expands the goals to explore ore-forming processes based on fault rock architectures, ore-hosting vein and host rock mineral geochemistry, fluid inclusion microthermometry and decrepitation studies, and stable isotope data.

These goals are achieved by studying the brittle fault zone architecture (domains in section across the fault) and meso- and micro-scale textures of the resulting fault rocks in relation to ore-hosting hydrothermal quartz-carbonate veins. The mineralogical and geochemical changes of the host rock during infiltration of ore-bearing fluids and the mineralization process are studied in detail. In addition, P-T-X conditions estimated by use of microthermometric data obtained from fluid inclusions in quartz, sphalerite and calcite in hydrothermal veins are discussed. These data are also used to calculate the fluid composition in order to discuss metal mobility and depositional mechanisms of mineralization relative to the brittle faulting events. Fluid composition and stable isotope geochemistry of carbonates are used to infer potential sources of the Cu-Zn-bearing hydrothermal fluids.

Geological setting

Vanna is a coastal island located in the Neoarchaean-Palaeoproterozoic West Troms Basement Complex (WTBC) in northern Norway (**Fig.** 1; Bergh et al. 2010). This basement province is located west of, and structurally below, the much younger Palaeozoic Caledonian thrust nappes (Augland et al. 2014; Roberts and Lippard 2005), which to the east are down-faulted several km by the regional Vestfjord-Vanna Fault Complex (**Fig.** 1; Olesen et al. 1997; Indrevær et al. 2013). The WTBC (**Fig.** 2) is composed of segmented crustal blocks of tonalitic, trondhjemitic to granitic gneisses (2.9-2.6 Ga) overlain by supracrustal units (2.8-1.9 Ga; Armitage and Bergh 2005; Myhre 2011; Myhre et al. 2013), and intruded by felsic and mafic igneous rocks (c. 1.8 Ga; Bergh et al. 2010; Corfu et al. 2003). In the north of the WTBC, on the islands of Ringvassøy and Vanna, mafic dike swarms (2.4 Ga) intruded the basement gneisses (Kullerud et al. 2006).

In southern parts of Vanna (**Fig.** 3), a para-autochthonous meta-sedimentary sequence, the Vanna Group, unconformably overlies the basement gneisses (Binns et al. 1980; Johansen 1987). Its age is constrained by the older 2.4 Ga dikes present below the unconformity, and an intrusive diorite sill in the meta-sedimentary rocks dated at 2.2 Ga (Bergh et al. 2007). The Vanna Group meta-sedimentary rocks are composed of arkosic, shallow deltaic sandstones and calcareous mud- and siltstones (Binns et al. 1980; Johannessen 2012). These cover units and the tonalitic basement in Vanna were all affected by contractional deformation and low-grade metamorphism (greenschist facies) during the Svecofennian orogeny (c. 1.8-1.77 Ga) and/or during younger Caledonian tectono-thermal events (Bergh et al. 2010; Bergh et al. 2007; Dallmeyer 1992; Myhre et al. 2013). The Svecofennian event produced a foreland fold and thrust belt in Vanna (Bergh et al. 2007), which in the northern part of the island included the Skipsfjord Nappe (Binns et al. 1980; Opheim and Andresen 1989; Rice 1990). The Skipsfjord Nappe consists of repeated thrust sequences of locally highly strained and mylonitized basement tonalites, alternating with lenses/sheets of relict Vanna Group meta-sedimentary rocks, and sheared mafic and felsic intrusive rocks. Its thrust contact to autochthonous gneisses is exposed in the south at Skipsfjorden and Slettnes (**Fig.** 3).

In the northern part of Vanna island (**Fig.** 3), the Skipsfjord Nappe is down-faulted in the hanging wall by the VBF (Bergh et al. 2007; Opheim and Andresen 1989). This fault is a splay fault to the regional, ENE-WSW trending, zigzag-shaped Vestfjord-Vanna Fault Complex (**Fig.** 2) that bounds the WTBC horst against Caledonian nappes to the east (Forslund 1988; Olesen et al. 1997; Indrevær et al. 2013, 2014). Offshore to the northwest the WTBC horst abuts against the Troms-Finnmark Fault Complex (Indrevær et al. 2013) (**Figs.** 1 & 2). The WTBC horst and its bounding normal faults all formed during incipient rifting of the North Atlantic Ocean in the Early Permian-Triassic (**Fig.** 1; Blystad et al. 1995; Mosar et al. 2002; Faleide et al. 2008; Davids et al. 2013, 2018; Gabrielsen and Braathen 2014; Koehl et al. 2018a, b), and this rifting event affected the entire North-Norwegian passive continental margin (Mosar 2003).

The present study focuses on a mineralized segment (**Fig.** 4) of the VBF (Opheim and Andresen 1989) that hosts Cu-Zn mineralization. The VBF is a brittle oblique-normal fault striking ENE-WSW and dipping c. 50-60° to the SSE. It separates variably deformed Neoarchaean tonalitic gneisses intruded by mafic dikes (2.2-2.4 Ga), diorite and gabbro, in the footwall from mylonitized tonalites and meta-sedimentary rocks of the Skipsfjord Nappe in the hanging wall, with a minimum vertical throw in the order of 2-3 km (Opheim and Andresen 1989). A section through the VBF shows a < 100 m wide fault complex including fault gouge core and damage zones. K-Ar illite dating and $^{40}Ar/^{39}Ar$ dating of K-feldspar in the fault gouge core yielded Late-Carboniferous (348.5 Ma) through Early Permian (283.9 Ma) ages (Davids et al. 2013, 2018), concurrent with known periods of incipient rift-margin extensional faulting and associated fluid infiltration and reactivation (Indrevær et al. 2014; Davids et al. 2018).

We analyse the VBF and its mineralized sections, and attempt to resolve its role as a pathway for hydrothermal fluids and the conditions that caused ore mineral deposition along the VBF. The results may have important implications for understanding ore genesis and for exploration purposes of Cu-Zn deposits in northern Norway.

Methodology

Field work and drill core data

Fieldwork (c. five days) and structural analysis of the VBF focussed on characterization of the fault core and damage zones surrounding the mineralized fault segment and adjacent host rocks. These studies were combined with four days of detailed core logging of c. 880 m of non-oriented drill cores bored by Store Norske Gull (SNG) in 2012, to identify and describe fault rocks, fabric domains, and cross-cutting relationships of fabrics and hydrothermal veins. Sixty-one drill core samples and five outcrop rock samples were collected from the VBF core zones, damage zones, hydrothermal mineralized veins, and the surrounding host rocks. Microtextural analysis of polished thin-sections was undertaken using conventional transmitted and reflected light microscopy. We used an existing dataset obtained by SNG of 783 drill core assays (0.15-2 m sample length) of host rocks, fault rocks, and mineralized hydrothermal veins analysed by ALS-Geochemistry Analytical Lab. This dataset contains analyses of whole rock geochemistry (analysed fused pellets using XRF) and a 48-element suite (analysed using four-acid digest and ICP-MS finish). Samples with ore grade Zn and Cu (> 10 000 ppm) were re-analysed using sodium peroxide fusion with an ICP-AES finish.

Scanning electron microscope data

Scanning electron microscope (SEM) analysis including energy-dispersive X-ray spectroscopy (EDS), electron backscattered diffraction (EBSD), and cathodoluminescence (CL), was used to determine mineral chemistry, mineral parageneses, mineralogical changes, e.g. zonation in hydrothermal quartz, and textural relationships. The thin sections were coated with a thin carbon layer to avoid charging effects. All the analyses were carried out using a Zeiss Merlin VP Compact field emission SEM equipped with an X-max^{80} EDS detector and a Nordlys EBSD detector, both provided by Oxford Instruments, as well as a Zeiss variable pressure secondary electron (VPSE) detector for CL imaging. The VPSE detector uses the CL signal and produces an image close to panchromatic CL under high vacuum conditions (Griffin et al., 2010). EDS measurements were done at 20 kV acceleration voltage and a 60 µm aperture size. For EBSD, the sample was tilted to 70 degrees; 20 kV acceleration voltage and a 240 µm aperture was applied. A step-size of 5 µm was chosen for EBSD mapping and a minimum number of 6 detection bands was applied for indexing. The AZtec software by Oxford Instruments was used for data acquisition further post-processing of the EDS and EBSD data. Backscatter images (BSE) were acquired under the same conditions as EDS measurements. For VPSE imaging an acceleration voltage of 20 kV was applied as well as an aperture of 120 µm. The vacuum conditions were higher than

$1x10^{-5}$ mbar within the sample chamber. EDS chemical analysis of chlorite in fault rocks was used to estimate formation temperatures based on tetrahedral site occupancy (Cathelineau, 1988), which is accurate to within 30°C. EDS measurements were standardised using a cobalt standard.

X-ray diffraction data

X-ray diffraction (XRD) analyses were performed on consolidated fault rocks (cataclasites) to determine mineralogy of very fine-grained samples. The analyses were conducted at the University of Zagreb on a Philips PW 3040/60 X'Pert PRO powder diffractometer (45 kV, 40 µA), with CuKα-monochromatized radiation (λ = 1.54056 Å) and θ-θ geometry. The area between 4 and 63° 2θ, with 0.02° steps was measured with a 0.5° primary beam divergence. Compound identifications were based on a computer program X'Pert high score 1.0B and literature data.

Fluid inclusion data

Fluid inclusion data were obtained from double polished wafers (100-250 µm thick) of hydrothermal quartz, sphalerite, and calcite. Homogenisation temperatures (T_h), halite melting temperatures (T_s), final ice melting temperatures ($T_{m\ Ice}$), and eutectic temperatures (T_e) were recorded using an Olympus BX 2 microscope coupled with a Linkam THMS 600 heating and cooling stage operating between -180 and +600°C at UiT-The Arctic University of Norway. Fluid inclusions were classified according to Roedder (1984) and Sheperd (1985). Salinities of the H_2O-NaCl-$CaCl_2$ system were calculated in NaCl+$CaCl_2$ weight percent using known eutectic temperature as well as halite and ice melting temperatures (Bodnar and Vityk 1994; Steele-MacInnis et al. 2011). In addition, qualitative measurements of key elements and complexes present in the hydrothermal fluid were obtained by decrepitating fluid inclusions (c. 500°C for 3-4 minutes) and analysing the resulting evaporate mounds formed on the sample surface using SEM/EDS technique according to the procedure modified after Kontak (2004). We performed both spot analysis of specific mineral phases and a map scan over the whole evaporate mound.

Stable isotope data

We achieved twenty-two $\delta^{13}C$ and $\delta^{18}O$ stable isotope analyses of hydrothermal calcite veins, calcite from host rock mica-schists in the Skipsfjord Nappe hanging wall to the VBF, and calcites from veins and hydrothermal breccia adjacent to an intrusive diorite sill in the Vanna Group farther south (see **Fig.** 3 for location). These analyses were obtained using a Thermo-Fisher MAT253 IRMS with a Gasbench II at UiT (site.uit.no/sil). Samples were placed in 4.5ml Labco vials, then flushed with He, and 5 drops of water free H_3PO_4 were added manually with a syringe. The results were normalised to Vienna Pee Dee Belemnite (VPDB) standard by three in-house standards with a wide range of $\delta^{13}C$ and $\delta^{18}O$ values, and reported with an uncertainty of standard deviation ≤ 0.1 ‰.

Results

Fault geometry and textural subdivision

From a regional perspective, the VBF is discernible on ortho-photos and digital elevation maps as an ENE-WSW trending linear valley between Vannareid and Burøysund on the island of Vanna (**Fig.** 3). The fault itself is partly exposed in a road section in this valley (**Fig.** 4), but is otherwise mostly covered by glacial and valley debris. The surrounding basement gneisses in footwall and meta-psammites and schists of the Skipsfjord Nappe in hanging wall, are however, well exposed along the shores of Vanna both to the east and west. Where exposed, splays of the VBF strike ENE-WSW and dip 45-50° to the SSE (**Fig.** 4; Opheim and Andresen 1989; Monsen 2014). The foliation of the quartz-mica schists in the hanging wall of VBF strikes mostly ENE-WSW and dips gently to the NNW, but adjacent to the VBF the foliation on a large scale is tilted to a c. 50° dip to the SSE. This change in dip may be due to drag folding caused by normal, down-to the SSE movement of VBF.

This study focuses on the mineralized part of the VBF (**Figs.** 4 & 5). The surface expression of the fault is a scarp with c. 10 m thick core zone that can be followed for c. 25 m along strike. In outcrop, the fault zone is pronounced (**Fig.** 6A) and made up of pale green chlorite-rich proto- and ultracataclasite cut by networks of irregular quartz and calcite veins with sphalerite and chalcopyrite (**Fig.** 6B). Where exposed, the fault surface itself is planar and coated with green-coloured chlorite and epidote (**Fig.** 6A). Local presence of epidote slickenside fibres indicate normal-oblique, down-to the SSE movement along the fault.

Combined surface mapping, logged drill-core, and petrographic data show six textural domains across the c. 120 m thick VBF (**Fig.** 5). These include two fault core zones (**Fig.** 5; domains A1 & A2), characterized by various types of cataclastic fault rocks (**Figs.** 6 & 7), and two damage zones (**Fig.** 5; domains B1 & B2), with complex internal veins and fracture networks (**Figs.** 8 & 9). The remaining domains, domain C and domain D, occur in the surrounding host rocks of hanging wall (**Fig.** 10) and footwall, respectively. Notably, the fracture networks in both core and damage zones contain an extensive number of hydrothermal quartz-calcite veins with pronounced Cu-Zn mineralization (**Fig.** 11), described below.

Domain A1 (core zone) is c. 15 m thick and the principal fault core zone located in the footwall, at the contact between host rocks of tonalitic gneiss and a gabbroic dike. It is characterized by multiple generations of cohesive cataclasites with 20-50% sub-rounded, polymict clasts of tonalite gneiss, older cataclasite, sphalerite, and quartz in a pale green fine-grained quartz-chlorite matrix (**Figs.** 7 & 11A). Multiple generations of hydrothermal veins are identified within the cataclasites of domain A1 and make up c. 60 % of the material in this core zone (**Fig.** 11A).

In thin section, the cataclasites have a dismembered texture with sub-rounded to rounded, consolidated clasts of at least two generations of fine-grained cataclasite embedded as new clasts within a third generation (**Fig.** 7A-C). The matrix of all generations of cataclasite is microcrystalline with internal grain size of 0.1 to 5 mm, and composed of quartz (c. 98 %), chlorite, microcline and minor albite and cookeite (based on XRD and SEM analyses).

Along strike farther west, the texture and mineralogy of core zone A1 changes and is a c. 15 m wide complex cataclasite containing decimetre-sized clasts of mainly calcite and sphalerite cemented by calcite veins (**Fig.** 11B).

Domain A2 (core zone) defines a c. 4 m thick cataclasite zone, which is texturally similar to that of domain A1, but which affected weakly foliated tonalite gneiss host rocks of the footwall. This domain has the same types and amount of cohesive cataclasites and surrounding matrix components as domain A1 (**Fig.** 7), and also contain an extensive network of hydrothermal veins ranging in width from 1 mm to >1 m, which makes up c. 60% of the material in this zone. This vein material is are also present as matrix cement enclosing rounded to sub-angular, polymict clasts of embedded older cataclasite, tonalites, and fractured hydrothermal quartz and sphalerite grains (**Figs.** 11C & D). In addition, this core zone contains abundant networks of pale green ultra-cataclasites with internal banding (**Figs.** 8A-D & 11C-D). Thin section observations show that the apparent banding of the ultracataclasites is caused by minor variations in grain size (**Figs.** 8A-B), and that these ultra-cataclasites fill open space between quartz veins (**Fig.** 8C), and/or define consolidated sub-angular clasts within quartz breccias (**Figs.** 8 D-E & 11C). Acicular grains observed within the ultra-cataclasites (**Fig.** 8E) suggests grain-growth and that the original grain size was smaller.

Domain B1 (damage zone) is c. 40 m thick and located in tonalitic gneisses of the footwall to the VBF. It defines a link zone or fracture corridor between core zones A1 and A2 (**Fig.** 5), and is characterized by heavily fractured, weakly foliated tonalite gneiss with narrow (<60 cm thick) localized cataclastic zones parallel to the main and subsidiary fault surfaces of the VBF. Most of the fractures are infilled with multiple cross-cutting stock work veins (**Fig.** 11E), ranging in thickness from 1 mm to c. 80 cm.

In thin section, the relict gneiss foliation in the tonalitic gneiss host rock is observed as of 1-2 mm long composite bands of muscovite (**Fig.** 9C). This fabric is cut at a low angle by semi-brittle, chlorite-rich shear bands (**Figs.** 9A-C), indicating the fracturing produced a retrogressed shear band texture. Larger (<2 mm) plagioclase grains have commonly healed microfractures filled by microcrystalline quartz and chlorite; some are dilated by hydrothermal veinlets (**Fig.** 9C).

Domain B2 (damage zone) is c. 15 m thick and present in the footwall of core zone A1 (**Fig.** 5). This fractured zone is located mainly within a thick, foliated meta-gabbro dike, and it is truncated by networks of irregular brittle fractures, locally with narrow (<40 cm thick) cataclasite zones. Most of the fractures are filled by chalcopyrite-bearing quartz and calcite veins (**Figs.** 11F & G). In contrast to the damage zone of domain B1, the quartz veins define parallel sets of sheeted veins close to the core zone, changing texturally into stock work vein networks with a more random orientation when farther from the core zone.

The typical mode of the foliated meta-gabbro identified in thin section is 70 % dark green, strongly pleochroic amphibole, 20 % partly sericitised plagioclase, 10 % fine-grained quartz as well as trace magnetite, garnet and ilmenite. In the fractured meta-gabbro, amphibole and ilmenite/magnetite grains are partly to completely replaced by chlorite, quartz, anorthite feldspar, and minor pyrite, titanite, apatite and rutile. Hydrothermal alteration of the meta-gabbroic host rock is outlined texturally as haloes along contacts to quartz veins and stock networks (**Fig.** 11F).

Domain C (hanging wall) represents the down-dropped hanging wall strata of the Skipsfjord Nappe (**Fig.** 5) with strongly foliated quartz-mica schists and intercalated mafic schists and lenses (**Fig.** 10A). In contrast to the core and damage zones of the VBF, the hanging wall schists are less fractured and comprise no Cu or Zn bearing hydrothermal mineralization (**Fig.** 5). The contact with cataclasites of the VBF itself (**Fig.** 5, domain A2) is marked by a narrow c. 1-2 m thick zone of unconsolidated, green-coloured fault gouge with sub-rounded clasts of quartz ($\leq$ 1 cm) in a fine-grained, clay-rich matrix (**Fig.** 10B), made of illite and smectite–vermiculite (cf. Davids et al. 2013). This gouge zone is irregular in shape and may disappear along strike, but where present, it truncates (post-dates) the cataclasites of domain A2. No hydrothermal veining or mineralization is observed in the gouge material.

In thin section, alternating layers of recrystallized quartz (50%), white mica (40%), and plagioclase (10%) make up the ductile foliation of the Skipsfjord Nappe schists with accessory tourmaline (dravite), apatite, and uranothorite. The foliation itself shows clear evidence of internal shearing, by sigmoidal quartz porphyroblasts, mica fish and remnants of intrafolial tight folds (**Fig.** 10C). These ductile fabrics are all truncated by the brittle VBF.

Domain D (footwall) represents weakly foliated basement tonalite gneiss in the footwall to the VBF. This domain is weekly fractured and contain no significant mineralization.

Hydrothermal veins hosting Cu-Zn mineralization

Hydrothermal networks of Cu-Zn-mineralized quartz and calcite veins exist in variable amounts and geometric relationships both in the core (domains A1-A2) and damage zones (domains B1-B2) of the VBF (**Fig.** 11). In the core zones, matrix-bearing cataclasites are the main mineralized zones, whereas in the damage zones, secondary quartz and calcite are present as mineralized stock-work and/or parallel/sheeted veins. Notably, complex and multiphase microtextural and cross-cutting relationships of the Cu-Zn bearing veins are observed (**Figs.** 11H-L). These relations provide the basis for evaluating temporal and mineralogical changes of the hydrothermal veins/fluids. By use of such criteria, we propose a succession of veining from early to late-stage as: (i) quartz-sphalerite (QS) veins (10-30 mm wide; **Fig.** 11A), (ii) quartz-chalcopyrite (QCp) veins ± calcite (1 mm to 1 m wide; **Figs.** 11C, D, F & G), (iii) calcite (Ca) veins (5 mm-1 m wide; **Fig.** 11B), and (iv) minor narrow (<10 mm wide) quartz-calcite-fluorite-sulfosalt veins (QCF) (**Figs.** 11H, I). Further details of these vein types are as follows:

QS veins (stage i) are mainly restricted to core zone A1 (**Fig.** 5) and are characterised by euhedral, zoned and massive quartz associated with sphalerite mineralization (**Figs.** 11A, H & I). Sphalerite is brown to deep orange in colour (**Figs.** 11A, B & H), commonly colour zoned, and is observed both as small (<1 mm) inclusions within larger (<10 mm) quartz grains and as interstitial material between quartz grains (**Fig.** 11I). In addition to vein style mineralization (**Fig.** 11H), individual grains of quartz and sphalerite are partly dismantled and now present as clasts within even younger generations of cataclasites (**Figs.** 11A-B & J-L), and truncated by a younger generation of quartz-chalcopyrite veins (QCp veins; **Figs.** 11J-L). These textural relationships indicates that the QS veins are the earliest observed hydrothermal veins.

QCp veins (stage ii) are composed of quartz and chalcopyrite with minor calcite. They are the most voluminous and spatially most extensive generation of quartz veins, and are in contrast to QS veins present in both the core and damage zones. Within the core zones (Domains A1, A2) quartz of the QCp veins exist as fine-grained matrix and as massive to euhedral grains in a hydrothermal breccia, enclosing rounded to sub-angular, displaced polymict clasts of basement tonalite gneiss, injected cataclasite (**Fig.** 11C), and earlier generations pf hydrothermal quartz and sphalerite (QS veins; **Fig.** 11A). Within the damage zones (Domains B1, B2), these quartz-chalcopyrite veins define cross-cutting stockwork-veins or parallel sets of sheeted-veins (**Figs.** 11E-G). In both cases, chalcopyrite is commonly deposited as a rim around clasts or at the inner edges of the veins (**Fig.** 11C), in direct contact with Fe-bearing minerals like chlorite or pyrite, or in contact with chlorite-rich cataclasite (**Figs.** 8C & 11D)

Notably, within the core zone of domain A2, multiple repeated quartz veins and injected ulatracataclasites are observed (**Figs.** 8A, B), outlined by euhedral quartz grains growing from the vein wall and having zoned cores and feathery/plumose textures on the rims (**Figs.** 8C-E). In addition, injected cataclasite is also present as fracture infill (**Fig.** 8D) and as matrix within broken hydrothermal quartz clasts (**Fig.** 8E). Multiple criss-cross networks of QCp veins exist, but an attempt to separate them into further generations and/or sub-stages has not been succesful.

Ca veins (stage iii) are characterised by various barren carbonate (calcite) veins cross-cutting previous generations of veins, or in conjunction with minor sphalerite and chalcopyrite. Calcite, however, is also present in all other vein types, where it represents the last infill stage in veins, and such calcite clearly post-dates the deposition of sphalerite (**Figs.** 11J-L), since sphalerite grains are fractured and show a jig-saw pattern. Calcite matrix observed in a coarse-grained breccia at the top of core zone A1 (**Fig.** 11B) with a high number of sphalerite clasts is also interpreted to be a late phase Ca vein. However, the lack of cross-cutting relationship with QCp veins makes this interpretation uncertain.

QCF veins (stage iv) are the youngest veins observed in the VBF, and they are only identified locally in core zone A1. These are narrow veins (<4 mm) of equant grains of massive quartz, calcite, fluorite and notably with Pb-As-Ag-Bi sulphides (**Figs.** 11J-L). This vein type will not be analysed further because of its limited spatial extent.

Alteration mineralogy and chlorite geochemistry

The secondary minerals associated with each of the above described vein types is commonly expressed as alteration haloes along rims of quartz-veins, but the mineral assemblages changes as these veins extended into different host rock types. Chlorite is the dominant alteration mineral and gives the altered rocks a pale green colour. In cataclasites, chlorite is found in close association with the main gangue minerals such as quartz and calcite, but also with minor albite, clinozoizite, titanite, rutile, apatite and cookeite. In tonalite host rock gneisses of the footwall to VBF, chlorite (±titanite) replaces host rock biotite and amphibole. Some epidote alteration of feldspar is also observed. In the gabbroic dike host rock tabular amphibole is replaced by chlorite and titanite/rutile; most feldspar is partly or fully replaced by epidote/clinozoizite; and ilmenite/magnetite is partly replaced by pyrite/chalcopyrite and titanite (**Fig.** 12). XRD analyses of very fine-grained ultracataclasite rocks show that quartz, chlorite, chalcopyrite and minor aggregates of microcline have completely replaced the original mineralogy.

We analysed the mineral chemistry of fine-grained chlorite present as matrix in cataclasites in core zones A1 and A2 of the VBF (**Fig.** 13), with an aim to estimate temperature of the hydrothermal alteration (Table 1). Chlorites were selected for analysis based on textural proximity to Cu-Zn bearing veins, to ensure that they were formed synchronously.

The chemical composition classifies the chlorite as clinochlore to chamosite (Table 1), with formation temperatures ranging from 280-305°C ± 30°C (Cathelineau, 1988). For example, chlorite analysed from surface outcrops of cataclasite in core zone A2 indicated a temperature of 280°C (**Fig.** 13A), whereas analysed chlorite from core zone A1 in drill cores at 70 m depth yielded a temperature of c. 295°C. In addition, at 93 m depth in domain B2, two generations of chlorite in the gabbroic host rocks (**Fig.** 13B) displayed a drop in the Mg/Fe ratio from core to rim, where the Mg-rich chlorite in the core indicates a formation temperature of 285°C, while the Fe-rich rim indicates growth at 305°C (cf. Table 1).

Fluid inclusions

The fluid inclusion study was conducted on quartz, calcite, and sphalerite from three generations of hydrothermal veins (i.e, QS veins, **Fig.** 14A; QCp veins, **Fig.** 14B; and Ca-veins, **Fig.** 14C). The microthermometric measurements were used to determine the salinity and density of the hydrothermal fluids that circulated along VBF as well as to indicate P-T-X conditions during faulting events. Further, the resulting fluid properties are used to infer the metal solubility potential of the ore-forming fluids and investigate the depositional mechanisms.

Fluid inclusion petrography

Primary fluid inclusions occur along growth zones and within isolated clusters. Primary fluid inclusion assemblages are usually cross-cut by trails of less common pseudosecondary and secondary inclusions (**Fig.** 14K). The microthermometry was conducted only for primary and pseudosecondary fluid inclusions, whereas a small size of secondary inclusions (<2 μm) precluded reliable measurements. Based on their petrographic characteristics, primary and pseudosecondary inclusions from all three generations of veins can be divided into three types:

Type 1 represents primary multiphase (liquid-vapour-solid) inclusions (**Fig.** 14D) containing an aqueous liquid (70 vol. %), a vapour bubble (15 vol. %), and a cubic solid phase (halite) (15 vol. %). Occasionally, assumed incidentally entrapped phases of elongated/tabular or fibroradial minerals are also observed (**Fig.** 14E). Type 1 inclusions are generally sub-rounded or with negative crystal shapes. These inclusions are found in all vein-types, but mostly in QS veins, in both quartz (**Fig.** 14D) and sphalerite (**Fig.** 14F). In QCp veins they are much less frequent and are hosted within the cores of euhedral and zoned quartz. Type 1 inclusions are also found in Ca veins.

Type 2 inclusions are also primary in their origin but, in contrast to Type 1, they do not contain a cubic solid phase. According to their petrographic properties, inclusions of this type can be divided into two subtypes, Type 2a and 2b. Type 2a inclusions are two-phase inclusions (liquid-vapour) that have sub-rounded to negative crystal shapes and contain a liquid phase (80 vol. %) and a vapour phase (20 vol. %; **Figs.** 11G & H). Type 2a inclusions are found in sphalerite and in calcite. Type 2b inclusions are irregularly shaped and can in addition to liquid (75-80 vol. %) and vapour (15-20 vol. %) also contain between <1 to 10 vol. % of solid phase (s) that are irregular, tabular, or radiating tabular in shape (**Figs.** 14I & J). Type 2b inclusions are found in quartz from both QS and QCp vein.

Type 3 inclusion are pseudosecondary inclusions grouped in narrow trails of coexisting, small (<20 μm), L+V and monophase L-only inclusions (**Fig.** 14K). The L+V inclusions have c. 90-98 vol. % liquid and 2-10 vol. % vapour, while L-only inclusions (at room temperature) commonly developed a vapour bubble during the freezing cycle. Type 3 veins are found in QS vein quartz.

Fluid inclusion microthermometry

Microthermometric measurements were performed on fluid inclusions in quartz, calcite and sphalerite, but the most numerous data, however, were obtained from fluid inclusions in quartz, because they are generally larger and easier to measure accurately. By contrast, fluid inclusions in sphalerite were usually too dark for phase changes to be observed, whereas calcite-hosted inclusions are too small (<20 μm).

During the freezing cycle, all fluid inclusions were undercooled to -100 to -130°C. Upon heating, frozen inclusions would turn dark brown around -80°C followed by first melt occurring around T_e of around -52°C indicating a fluid composed of H_2O-NaCl-$CaCl_2$ (cf. Roedder 1984; Steele-MacInnis et al. 2011).

Fluid inclusions in the of H_2O-NaCl-$CaCl_2$ system are notorious for metastable behaviour, which includes absence of phases that are expected to be present and occurrence of phases that are not expected to be present (Chu et al., 2016). In the following, we will describe the behaviour of each type of fluid inclusion and also note assumptions, possible metastable behaviour, and present alternative calculations for salinities. Despite uncertainties in the salinity calculations, the accuracies of the salinities presented is acceptable within the scope of this paper.

Type 1 (L+V+H) inclusions froze to a dark fine-grained mass during the freezing cycle. When heated the inclusions would turn dark brown around -80°C followed by first melt occurring around T_e of around -52°C. Ice, observed as a globular transparent phase, melted over a large range of temperatures from -52.3 to -37.5°C. It is assumed that antarcticite that melts at the eutectic temperature. Upon further heating, the isotropic solid in Type 1 inclusions melted around +70 to +151°C, and total homogenisation was characterized by a vapour to liquid transition in the temperature range from +70 to +239°C. The elongated solid in was insoluble up to 400°C. Based on the eutectic temperature of -52°C, total salinities are expressed as NaCl + $CaCl_2$ wt. % according to Steele-MacInnis et al. (2011). The total salinity for Type 1 inclusions was calculated from the peritectic $T_{m\ Ice}$ and final melting temperature of halite (T_s) based on the methods of Vanko et al., (1988). This resulted in salinities (33-36 wt. % NaCl+$CaCl_2$; Table 1). However, it should be noted that in some Type 1 inclusions, poor optical properties hindered accurate measurement of $T_{m\ Ice}$ and for these inclusions salinities are calculated based on ice (and antarcticite) melting at the eutectic; this assumption yields higher salinities (up to 5 wt. % NaCl+$CaCl_2$) and higher NaCl/$CaCl_2$ ratios (up to 0.5). Further, salinities for Type 1 inclusions can also be calculated as NaCl wt. % equivalents using halite melting temperatures according to Bodnar and Vityk (1994); such a calulation would yield salinities in the range of 27 to 30 wt. % NaCl equivalents. $T_{m\ Ice}$ temperatures observed below the eutectic possible for the $CaCl_2$ system (< -52°C; Steele-MacInnis et al. 2011) were interpreted as metastable (Wilkinson 2001). Salinities for these inclusions were calculated based on $T_{m\ Ice}$ of -52°C.

Type 2 inclusions showed two styles of freezing when cooled; 1) the inclusion froze to a dark fine-grained mass; or 2) the inclusion did not freeze and no phase transitions was observed. No correlation between the content of the fibroradiate solids and freezing style was observed. Upon warming the frozen inclusions would turn dark brown around -80°C followed by first melt occurring around T_e of around -52°C. Ice, observed as a globular transparent phase, melted over a large range of temperatures from -54.4 to -18.3°C. Total homogenisation occurred by a vapour to liquid transition in the temperature range from +35 to +220°C. The various fibroradiate solids observed in Type 2b inclusions were insoluble up to 400°C. Salinities were calculated as wt. % NaCl + $CaCl_2$ according to Steele-MacInnis et al. (2011; Table 1). It was not possible to identify which phase melted at the eutectic, antarcticite or hydrohalite, however, the differences in salinity (< 0.2 wt. % NaCl+$CaCl_2$) and NaCl/$CaCl_2$ ratios (<0.03) calculated for either option is negligable. In addition, metastable behaviour is suspected for inclusions where no freezing behaviour was be observed (Chu et al., 2016). Alternatively, it is possible that freezing in these inclusions were hindered by small amounts of lithium in the fluid (Dubois et al., 2010).

Type 3 inclusions showed similar microthermometric behaviour to Type 2 inclusions; first melting was observed at T_e, and $T_{m\ Ice}$ occurred at -48.2 to -40.3°C, resulting in salinities of 28.6-30.6 wt. % NaCl + $CaCl_2$. The majority of Type 3 inclusions were liquid only at room temperature, but several developed vapour bubbles during freezing and T_h occurred by vapour to liquid transition at 19 to 36°C.

The microthermometric results of fluid inclusions in quartz, sphalerite and calcite from QS, QCp and Ca veins is summarised in Table 2 and **Fig.** 15A. **Fig.** 15A displays the last phase melting temperature on the X-axis; for Type 1 inclusions this is the cubic solid (halite), and for Type 2 and 3 inclusions ice melting ($T_{m\ Ice}$) is the last phase observed. Homogenisation temperatures (T_h) are plotted on the Y-axis. All together, the multiphase, two-phase and monophase fluid inclusions show that the fluids were low-to moderate temperature (<240°C) and moderate to highly saline (13-37 wt. % $CaCl_2$ + NaCl). **Fig.** 15B plots total salinity versus T_h and two clusters of fluid inclusions; Type 1 inclusions with higher salinities (33-36 wt.% NaCl+$CaCl_2$) and Type 2 and Type 3 inclusions with lower salinities (20-31 wt.% NaCl+$CaCl_2$). A salinity gap from c. 31-33 wt. % total salinity separates Type 1 from Type 2 and Type 3 inclusions in the **Fig.** 15B. This gap could be caused by metastability by failing to nucleate NaCl near the saturation point (Roedder, 1984), or it could be a result of the assumptions used to calculate the salinities of Type 1 inclusions as outlined above.

The temporal relationships between the vein-types as established by the cross-cutting relationships above are also included in the legend of **Fig.** 15B, and the data displayed are described accordingly. Overall the dataset shows a general positive correlation between total salinity and T_h. This positive correlation is also observed in sphalerite-hosted inclusions in QS veins (Type 1 and Type 2a) that show a weak positive correlation between total salinities (27-35 wt. % NaCl+$CaCl_2$) ranging over a rather narrow temperature range (155-218°C). Quartz-hosted inclusions (Types 1 and 2b) from QS veins are also highly saline inclusions (25-36 wt. % NaCl+$CaCl_2$) that homogenise over a larger T_h span (70-205°C). Inclusions in individual QS quartz veins (displayed as light and dark green colours) show overlap, however the light green vein has more inclusions with higher salinities than the vein plotted with darker green. Quartz hosted inclusions from QCp veins show two trends, the pale grey vein (inclusion type 1 and 2b) show similar T_h and salinities to those from QS veins. The pale blue and dark blue coloured dots representing Type 2b inclusions show relatively narrow range of salinities (25-31 wt.% NaCl+$CaCl_2$) over a large range of T_h (35-210°C). Type 3 pseudosecondary inclusions from QS veins show a weak overlap with these low-temperature Type 2b inclusions from QCp veins. Type 1 and 2a inclusions from Ca veins show the largest range in salinities (20-36 wt. % NaCl+$CaCl_2$), also with a positive correlation with T_h (94-175°C).

Fluid inclusion decrepitation

Qualitative chemical analyses of major elements in fluid inclusions in quartz were carried out by decrepitating individual inclusions and analysing the evaporate mounds formed on the sample surface (**Fig.** 16). SEM spot analyses of individual crystals enabled us to identify three major phases in the mounds: NaCl, $CaCl_2$, and $CaSO_4$ (anhydrite/gypsum; **Figs.** 16A, B). SEM map-scan analyses are presented in **Figs.** 16C-F and highlight the chemical composition of the mounds. Relative concentrations of Na, Ca, K, Cl and S are plotted in **Fig.** 17, and show two general trends based on the sulphur content: (1) mounds with varying amounts of Na, Ca, S, Cl and very minor K (e. g.); (2) mounds without S but with Na, Ca, Cl and very minor amounts of K. These trends likely reflect two different fluids.

Hydrothermal alteration of host and fault rocks

In order to resolve geochemical changes in fault and host rocks during deposition of the VBF hydrothermal mineralization, we performed lithogeochemical analyses of unaltered host tonalite gneiss and gabbro from footwall domain D. The obtained data were compared with the data gathered from altered host rock equivalents, including mineralized veins and cataclasites from core zones A1 and A2 (**Fig.** 5). The lithogeochemical data were used for construction of isocon diagrams (**Fig.** 18), following the method proposed by Grant (1986). In the diagrams, Al_2O_3 and TiO_2 are considered immobile and are for each sample used to delineate a second reference line, which takes into account apparent depletion of elements in the host rock when injected by hydrothermal quartz and calcite veins.

Separate isocon diagrams are constructed for the alteration of host rock tonalite gneiss (**Fig.** 18A) and gabbro (**Fig.** 18B), respectively. For both rock types, similar mobility trends are observed for ore-bearing elements: Zn and Cu are the major metals hydrothermally added to the system, together with minor amounts of S, Pb, As, Bi, Cd, Li, Ag and trace Sb. On the other hand, the major elements (expressed as oxides) show much larger variations; e.g. Na_2O is depleted in both of the altered host rocks of core zones A1 and A2, relative to unaltered host rocks (domain B2), whereas MgO and Fe_2O_3 is enriched. Other oxides like K_2O are slightly depleted in altered tonalite gneiss and enriched in altered gabbro, while MnO show opposite trends in altered tonalite gneiss versus gabbro, respectively.

$\delta^{13}C$ and $\delta^{18}O$ stable isotope data

Stable isotope data of calcite from various geological settings on Vanna were analysed, in order to infer potential sources of CO_2. Analysed samples show a wide range of $\delta^{13}C$ and $\delta^{18}O$ isotope values (**Fig.** 19). The hydrothermal vein calcites from VBF yielded $\delta^{13}C$ values in the range of -5.7 to -4.0 ‰, and $\delta^{18}O$ values from +7.1 to +12.3 ‰, overlapping with igneous carbonates (Taylor et al. 1967). In contrast, calcite from hanging wall Skipsfjord Nappe (for location see **Fig.** 5) shows distinctly higher $\delta^{13}C$ (-1 to +5 ‰) and $\delta^{18}O$ values (+11 to +16 ‰) than hydrothermal calcite in the VBF. Calcite samples from veins and breccia in diorite of the Vanna Group meta-sedimentary rocks (see **Fig.** 3 for location; Bergh et al. 2007) all yielded $\delta^{13}C$ (-4 to +1 ‰) and $\delta^{18}O$ isotope values (+8 to +12 ‰), i.e. consistently higher than for the VBF calcites, but lower than for calcites in the Skipsfjord Nappe. By comparison, $\delta^{13}C$ (+1 to +5 ‰) and $\delta^{18}O$ (+8 to +10‰) values for calcite cement in meta-sandstones of the Vanna Group (Johannessen, 2012) differ from all the other analysed samples.

Discussion

The data presented above show that the Cu-Zn mineralized zones in the VBF resulted from a multiphase history of fracturing, cataclasis, and hydrothermal vein injections into Neoarchaean gneisses as host rocks and the VBF acting as a conduit for the hydrothermal fluids. Mineral chemistry, fluid inclusion microthermometry, and stable isotope results were used to gain insight into the ore-forming processes and P-T-X conditions during mineralization. Based on these data, a tentative, paragenetic model is proposed for the Cu-Zn mineralization in the VBF (**Fig.** 20), and this model is discussed and argued for below.

Fault zone architecture, evolution and relation to Cu-Zn mineralization

The brittle VBF developed as a normal fault zone affecting Neoarchaean tonalite/gneisses in the footwall and down-faulted Palaeoproterozoic, meta-sedimentary rocks of the Skipsfjord Nappe/Vanna Group in the hanging wall (Bergh et al. 2007). These basement host rocks comprise a main ductile fabric/foliation which formed in a fold-thrust belt system during the Svecofennian orogeny at greenschist facies conditions (Bergh et al. 2007). A younger retrogressive, semi-ductile/brittle tectono-thermal event produced chlorite shear bands that may record the onset of Palaeozoic (Carboniferous-Permian) brittle faulting along the VBF (cf. Davids et al. 2013).

The brittle VBF is composed of two core zones surrounded by damage zones and undeformed host rocks, with fracture networks cemented by quartz-carbonate veins (**Figs.** 5 & 6). The structural evolution of the VBF included up to four stages of brittle normal faulting, hydrothermal veining (**Figs.** 7 & 11), and alteration of the crystalline bed rocks (**Fig.** 12). These events seem to have controlled the Cu-Zn mineralization (as summarized in **Figs.** 20B1-B3). To further, argue for the evolution and relative timing of textures and veins, the structures are discussed chronologically, in terms of pre-, syn-, or post-tectonic relative to the ore-forming processes.

The ductile, pre-ore fabrics of the host rock tonalitic gneisses and quartz-feldspatic schists in footwall and hanging wall of the VBF, respectively, are presumed to be Neoarchaean (ca. 2.7 Ga) to Palaeoproterozoic (c. 1.8 Ga) in age (Corfu et al. 2003; Myhre et al. 2013). These host rocks, however, were affected by networks of truncating chlorite-rich shear bands (**Fig.** 9) that may record the onset of brittle faulting along the VBF.

The initial stages of syn-ore brittle faulting along VBF generated massive proto/ortho-cataclasites in core zone A1 along the contact between the host tonalites and gabbroic dikes (**Figs.** 20A, B1). These cataclasites were enclosed by a matrix of injected quartz-sphalerite (QS) hydrothermal veins, as evidenced by crosscut relationships (**Figs.** 7 & 11H-L). This early process of brittle fracturing and cataclasis may have increased the porosity of the fault rocks and created space for further hydrothermal fluid flow, and thus suggest that the fault core A1 at least initially acted as a fluid conduit. It is, however, reasonable to conclude that during successive injection of QS vein material, this fault core became partly or fully sealed, thus reducing the permeability and forcing the later fluids to flow into the damage zones (cf. Indrevær et al. 2014).

The next stage in the fault evolution was continued cataclasis and injection of quartz and chalcopyrite bearing (QCp) veins. This significantly more extensive syn-ore faulting and hydrothermal event produced ultra-cataclasites and QCp vein breccia infill that post-dated the QS veins in core zone A1. QCp veins are the first and dominant generation of vein material to be deposited in core zone A2, and also formed as stockwork and sheeted veins in fractures within damage zones B1 and B2 (**Fig.** 20B2), in close association with secondary chlorite, cookeite and microcline in the matrix of the ultra-cataclasites.

The presence of multiple generations of cataclasites and Cu-Zn bearing vein injections, as observed in core zone A2, suggests that the porosity of the fault rocks increased by continued fault movement, and allowed episodic flow of over-pressurised fluids capable of transporting fine-grained, crushed material from elsewhere along the fault. Episodic fluid flow is supported by several phases of injected flow-banded ultracataclasites (**Figs.** 11C, D & J-L) in close spatial relationships to zoned euhedral quartz with plumose textured rims (**Fig.** 8). The matrix between such zoned quartz grains were filled by new injected cataclasite and QCp veins. This abrupt change in texture from zoned quartz cores, where the rate of deposition is considered slow, to plumose quartz textures at the rims, indicating faster rate of silica deposition, may be caused by a change in pressure from lithostatic to hydrostatic due to fracturing along the fault (Fournier and Potter, 1982; Dong et al. 1995; Rimstidt 1997). This process with cyclic opening of a fault due to overpressured fluids is known as seismic pumping (Sibson et al. 1975).

The last main syn-tectonic hydrothermal events (stages iii) affecting the VBF included infill of calcite in QS and QCp veins, growth of calcite as the main gangue mineral in the late cross-cutting barren veins in all fault domains (Ca veins), and possibly also formation of sphalerite-calcite breccias near the rim of core zone A1, although timing of the latter is uncertain. However, textural observations suggest that sphalerite was deposited as part of the early QS vein phase, subsequently brecciated and cemented by latest-stage calcite (see **Fig.** 11B).

Post-ore brittle fault movements along VBF generated unconsolidated fault gauge (**Fig.** 10B) which is observed along the contact with Skipsfjord Nappe rocks, thus separating the Cu-Zn mineralized fault core-damage zones from the non-mineralized hanging wall (**Fig.** 20B3).

Our data show that the VBF acted as a fluid conduit infiltrating permeable fault rocks with reduced host rock strength, during several stages (i-iv) of brittle fracturing and cataclasis. The mapped VBF architecture, and close relation of microtextures and accumulated ore forming hydrothermal veins confirms that Cu-Zn mineralization was controlled by evolution of the fault rocks. The VBF also, clearly must have acted, at least intermittently and locally, as a barrier that helped localization and enrichment of Cu-Zn mineralization. Fluids migrating in the crust may effectively reduce the strength of the rock by increasing the pore pressure and decreasing the frictional resistance (Hubbert and Rubey 1959; Sibson et al. 1975). Changes in pore pressure and frictional characteristics may have occurred along the VBF. For example, the pore pressure may have approached lithostatic values during the syn-ore forming hydrothermal events (**Figs.** 20A, B), as inferred from: (i) growth of euhedral zoned quartz on fracture surfaces, and (ii) injections of multiple generations of flow-banded ultra-cataclasites, likely from reworked fault core rocks. One requirement for fluids to hold fractures open allowing euhedral quartz growth, is a pore pressure that at least, exceeds the confining pressure (Hubbert & Rubey 1959). Conversely, if over-pressurized fluids injected the fault zone, such fluids may have contributed to enhance faulting and further evolution of the fault architecture itself. Therefore, we favour a model of successive and/or repeated supply of over-pressurized hydrothermal fluids, from a variety of sources (**Fig.** 20C), in a tectonic environment characterised by crustal extension and normal faulting (cf. Indrevær et al. 2013, 2014) to explain the complex Cu-Zn mineralization in the VBF.

P-T-X conditions

Temperature constraints during brittle faulting and injection of Cu-Zn-bearing hydrothermal veins are indicated from chlorite geochemistry and by microthemometric measurements of primary fluid inclusions. Homogenisation temperatures measured from spahlerite-hosted inclusions range from 164 to 218°C, and represent the minimum fluid temperature for the ore-bearing fluids during the first mineralisation phases. Combining this data with chlorite geochemistry that indicate formation temperatures of 280-305°C ± 30°C, does provide some additional constraints. However, chlorite geochemistry is extremely sensitive to later overprints and temperature estimates should be treated with care (Vidal et al., 2006). This is exemplified by the prograde overprint shown in **Fig.** 13B (Table 2) where a c. 20°C increase in core to rim is suggests, likely as a result of seismic pumping allowing fluxes of hotter ore-bearing fluids through the fault.

Ideally, formation pressures could be constrained from isochores constructed based on mictrothermometric measurements of fluid inclusions combined with temperature estimates from chlorite geothermometry. However, the steepness of isochores from these highly saline (and dense) fluids, combined with the rather large temperature range (including uncertaincies) in the chlorite geothermometric estimates cannot provide adequate constrainst on the pressure/depth of ore formation. Previous work from Indrevær (2014) who studied several onshore Late Permian normal faults of the Vestfjord-Vanna fault complex in western Troms, containing hydrothermal quartz and K-feldspar, yielded minimum P-T conditions of 300-275°C and 2.4-2.2 kbar. The temperature range overlap with that estimated from VBF, and we cautiously suggest that similar PT conditions could be used for VBF.

Fluid inclusion data microthermometric measurements suggest that the ore-bearing fluid is composed of H_2O-NaCl-$CaCl_2$ with a general NaCl/$CaCl_2$ ratio of c. 0.3 (Table 2). Regardless of the uncertainties in the accuracy of the salinity calculations, the various calculations show that the fluids are highly saline fluids (20-37 wt. % NaCl + $CaCl_2$). Analyses of evaporate mounds also suggested two different fluid compositions: one fluid with a significant proportion of sulphur, and one without. In addition, isocon diagrams suggests that sulphur was added to the mineralizing system, and we therefore suggest that the ore-bearing fluid also contained sulphur. In addition to sulphur and the ore-forming metals Zn and Cu, the isocon diagrams suggest that the ore-bearing fluid likely also contained (or remobilised) minor amounts of metals including Pb, As, Bi, Cd, Li and Ag (**Fig.** 18).

Redox potential of ore bearing fluids

As suggested above, the ore-bearing fluids at VBF contains sulphur (**Figs.** 16 & 17), but the speciation of sulphur is not known, and depends on whether the fluids have reducing or oxidizing properties. According to Zhong et al., (2015), given a high salinity fluid (>22.6 wt. % NaCl) sulphur would be present as sulphate (SO_4^-) in an oxidising fluid, and as H_2S in a reducing fluid.

At VBF, the alteration of host rock ilmentite to pyrite (**Fig.** 12), and general abundance of sulphide ore minerals suggests that the these minerals were formed under near neutral pH and reducing conditions, further implying that the ore-bearing fluids were reducing. However, fluids circulating in the upper crust with low water/rock ratios are commonly, at least in part, rock-buffered with sulphate is a common component - produced from oxidation of accessory sulphide minerals present in the basement (Bucher and Stober, 2010). In addition, sulphate is identified from the evaporate mounds (**Figs.** 16 & 17); this sulphate could have formed two ways, either it was already present in an oxidising ore-forming fluid, or the sulphur was oxidized to sulphate during the decrepitation process when exposed to atmospheric oxygen.

Two equations below exemplifies the two potential fluids (reducing fluid in equation 1 and oxidizing fluid in equation 2). In Equation 1, zinc is carried as a chloride complex in a reducing fluid and sulphur is present in the form of H_2S. The presence of H_2S in the fluid will destabilise the chloride complex carrying the zinc and significantly reduce the solubility of Zn (by shifting the equation to the right). However, higher salinities will increase the amount of H_2S the fluid can carry without precipitating sphalerite. Reversely, by diluting the fluid the decreasing Cl^- content will shift the equilibrium to the right, and sphalerite will precipitate.

Equation 1: $$ZnCl_{2\,(aq.)} + H_2S_{(aq.)} \rightleftharpoons ZnS_{(s)} + 2Cl^- + 2H^+$$

Equation 2: $$ZnCl_{2\,(aq.)} + SO_4^{2-} + CH_4 \rightleftharpoons ZnS_{(s)} + CO_{2(aq.)} + 2Cl^- + 2H_2O$$

Equation 2 describes an oxidising fluid that contains Zn as a chloride complex and sulphur as sulphate (SO_4^{2-}). However, to deposit sphalerite (ZnS) a reducing agent is needed, in this equation exemplified by CH_4. A reducing agent in this type of geological environment could be organic matter, however no evidence for such matter is found.

Ore-forming processes

Physicochemical properties of fluids control transport and deposition of metals in hydrothermal systems. In the upper crust these fluids are commonly, at least in part, rock-buffered. As a result of these buffering processes, the range in pH and oxygen fugacity of the fluid is relatively narrow and the major controls on metal solubility are temperature and concentration of ligands like chloride and sulphur (Yardley 2005; Zhong et al., 2015). At VBF, the ore-bearing fluids have a near neutral pH, have a salinity of c. 27-36 wt. % NaCl+$CaCl_2$, and a temperature estimated in the range of c. 250-335°C. The progressive enrichment of Zn in QS veins (first) followed by Cu in QCp veins (second), and the possible depositional mechanisms for each of these metals will be discussed below.

Zinc and copper in a highly saline fluid at a temperature of c. 300°C is likely transported as a chloride complex, regardless of the oxidation state of the fluid (Zhong et al. 2015). The positive correlation between T_h and salinity from fluid inclusions in sphalerite and in associated QS vein quartz (**Fig.** 15B) indicate mixing with a colder and less saline fluid, possibly originating as groundwater (table 2). Mixing and dilution of the fluid would efficiently precipitate sphalerite.

The progressive widening of the fault and repeated injections of fluid through the fault (and deposition of injected cataclasites) is associated with QCp vein deposition. Seismic pumping could lead to an increase in fluid flow, and also further influx of a colder and slightly less saline fluid. Such a process is supported by the salinity decrease observed in fluid inclusions from QS to QCp veins. It is further supported by the significant temperature decrease recorded in primary fluid inclusion in QCP vein quartz, and pseudosecondary inclusions in QS veins (**Fig.** 15B). It is likely that some of the solid material in the Type 2b fluid inclusions is accidentally entrapped microscopic minerals, like chlorite and microcline, from the material that deposited injected cataclasites.

A second contribution to the deposition of chalcopyrite is suggested by textural relationships; chalcopyrite have grown as a rim around clasts, or at the inner edges of the QCp veins, in direct contact with Fe-rich chlorite or pyrite, or chlorite-bearing cataclasite. This suggests that Fe was sourced locally from the host rocks, while sulphur could be sourced from the hydrothermal fluid (**Fig.** 17), and that chalcopyrite deposition was furthered by wall-rock interactions. Wall-rock interactions as a source of Fe may also explain why chalcopyrite mineralization is chiefly deposited in fractures hosted by mafic (Fe-rich) dike host rock (domain B2) and in domains A1-A2 fault cores with chlorite (Fe-) rich injected ultracataclasites.

Stable isotopic composition of vein-forming fluids

The stable isotope data for hydrothermal calcite from the VBF (**Fig.** 19) yielded $\delta^{13}C$ values in the range of -5.7 to -4.0 ‰, and $\delta^{18}O$ values from +7.1 to +12.3 ‰, which plot close to that of igneous carbonates (Taylor et al. 1967). In general, alteration of igneous carbonate by oxygen-rich atmosphere (e.g. weathering) may cause an increase in the value of $\delta^{18}O$ at a fairly constant $^{13}C/^{12}C$ ratio (Taylor et al. 1967), and such a trend is apparent for hydrothermal calcite associated with the VBF (**Fig.** 19). Alternatively, the large spread in $\delta^{18}O$ values for the VBF calcite may reflect fluid mixing in the hydrothermal system (Savard and Kontak 1995; Kontak et al. 2006) and/or assimilation with sedimentary carbonates, as inferred from a pronounced increase of $\delta^{13}C$ in calcite veins of the diorite and matrix of the Vanna Group sedimentary rocks (**Fig.** 19). The narrow compositional range of $\delta^{13}C$ for VBF calcite, however, strongly supports a magmatic origin of CO_2, and also suggests that factors such as boiling, temperature, and oxidation state of the hydrothermal fluid did not influence the $\delta^{13}C$ signature (Rye and Ohmoto 1974). The fact that calcite from veins in the Skipsfjord nappe, and Vanna Group sedimentary rocks, display much higher values of $\delta^{13}C$ and $\delta^{18}O$, larger compositional variations, and more variable trends than calcite in the VBF (**Fig.** 19) suggests a different origin, and/or possibly more diverse enrichment history of these carbonates.

Potential origin of the ore-forming fluids

Fluids of the composition described above may have been sourced from several possible hydrological reservoirs, including sediment-derived or shallow marine brines and entrapped formation water, brine fluids from deeper in the crust, or magmatic and hydrothermal fluids (Yardley 2005). At Vanna, the relict sedimentary formations are represented by the Palaeoproterozoic Vanna Group rocks deposited in a shallow marine environment (Binns et al. 1980; Bergh et al. 2007; Johannessen 2012) and portions of the Skipsfjord Nappe (Opheim and Andresen 1989), in hanging wall of the VBF. Deeper brine sources may include the metamorphic tonalitic gneiss and mafic dike host rocks, or alternatively, magmatic fluids released from a hot magma and transported through faults, fractures, and/or along lithological contacts as pathways, and final emplacement in e.g. major faults/shear zones (**Fig.** 20C).

The role of basinal brines as ore forming fluids has been widely discussed (Yardley 2005) and two main models are suggested for their formation (Walter et al. 2016). In the first model, low salinity fluids circulating in the crust are modified by wall-rock interactions and enriched in solutes through hydrothermal alteration of e.g. feldspar and mica to clay. This model is questioned from experiments by Burisch et al. (2016), indicating that wall-rock interactions are not sufficient to produce brines over 28 wt. % salinities, and therefore, an additional source is required for highly saline fluids. The second model poses an external source of salinity, for example, dissolution of previously deposited evaporates in a sedimentary rock sequence (Mississippi Valley Type deposits; Kesler et al. 1995), or the development and downward migration of so-called bittern brines, a residual brine produced by the precipitation of halite in shallow marine basins. This process is suggested for the formation of the continental basement brines at Schwarzwald (Walter et al. 2016). Although no evaporates have been observed within the relict shallow-water sedimentary sequences at Vanna, it is not unlikely that at least some of the salinity in the ore-forming fluid could be derived from this sequence. However, the $\delta^{13}C$ vs. $\delta^{18}O$ values of VBF calcite veins are distinctly different from those of the Skipsfjord Nappe and Vanna Group (**Fig.** 19), suggesting that a different source of CO_2 formed these carbonates.

Low Na/Ca ratios, like those at VBF, have been accredited to fluid-rock interactions by several workers. Banks et al. (1991) suggested a strong host rock control causing the fluid evolving to a lower Na/Ca ratio for brines analysed in the Central Pyrenees; Boiron et al. (2010) also suggested brine $CaCl_2$-enrichment caused by albitisation and Na-metasomatism, while Bucher and Stober (2010) show that brines may vary from NaCl-rich when residing in granites to $CaCl_2$-rich in mafic rocks like amphibolites and gabbros.

From the discussion above, a possible model for the Cu-Zn bearing fluid source in the VBF is that the first phase of fluids, associated with QS veins, originated as continent-internal basinal brines with Zn sourced mainly from the surrounding host rocks, possibly with some salinity derived from the meta-sedimentary sequence within the Skipsfjord Nappe. During continental rifting, the increasing amount of Cu associated with the second vein phase (QCp veins) was derived from either a Permian aged hot mafic melt/dike (see discussion below), or in combination with wall-rock interactions of a mafic component within the Neoarchaean host rock gneisses. A magmatic source for the CO_2 in the temporal late hydrothermal calcite veins (Ca veins) is suggested by the low $\delta^{13}C$ and $\delta^{18}O$ values (**Fig.** 19), indicating that the later fluids included some magmatic CO_2, possibly relating to Permian age rift-related magmatism.

Regional implications

A Palaeozoic (348-284 Ma) age of fault rocks along the VBF is well constrained from recent K-Ar dating of illite in late stage fault gouge (Davids et al. 2013). Such an age contrasts with previous workers arguing for a Palaeoproterozoic VMS stringer zone origin of the Cu-Zn mineralization, linked with the 2.4 Ga mafic dike swarm (Ojala et al. 2013; Monsen 2014) and subsequent spread of metals into sediments now present in the Skipsfjord Nappe (Opheim and Andresen 1989). The new dating results are consistent with formation of the VBF and enclosed Cu-Zn mineralized fault rocks/veins as part of an early Permian rifting event in the North Norwegian continental margin producing NE-SW striking brittle normal faults and associated fracture sets (Gabrielsen et al. 1990; Faleide et al. 2008; Smelror et al. 2009; Hansen et al. 2012), which later on evolved to major fault zones like the Vestfjord-Vanna and Troms-Finnmark fault complexes (Olesen et al. 1997; Indrevær et al. 2013, 2014; Koehl et al. 2018). Most of these Permian faults, including the VBF, contain features that indicate complex fluid flow and fault-rock interactions, however, yet very few of them seem to be accompanied by ore mineralization (cf. Koehl, 2013; Indrevær et al. 2014).

The wide K-Ar illite age range obtained for the VBF (Davids et al. 2013) could reflect a multiphase kinematic and very complex reactivation history of the fault rocks, as outlined in this work. If a minimum Early Permian age is linked to our post-ore movement unconsolidated fault gauge, the main fault zone movement may have initiated as early as in the Carboniferous, even Late-Devonian (cf. Koehl et al. 2018b). Carboniferous rifting is known to have produced mafic dike swarms on the Finnmark portion of the North Norwegian margin (Roberts et al. 2003, 2011; Nasuti et al. 2015) and numerous brittle normal faults with extensive hydrothermal alteration and cataclasis (Indrevær et al. 2013, 2014; Koehl et al. 2018a, b). Specifically, the Langfjorden-Vargsundet fault zone, which can be traced from Troms all along the coast of western Finnmark northward to Magerøya (**Fig.** 1), experienced multiphase movement and hydrothermal activity (Indrevær et al. 2013, 2014; Koehl et al. 2018a, b). In this fault zone early stage quartz- calcite- and laumontite-rich cataclasites initiated at a temperature of about 350-200°C and depth of 2-8 km, and were followed by a main, second period of faulting in the Mid-Permian (315–265 Ma) that exhumed basement rocks to shallow depths of 1-3.5 km (Koehl et al. 2018b). Similar results were obtained from several onshore Late Permian normal faults of the Vestfjord-Vanna fault complex in western Troms yielding minimum P-T conditions of 300-275°C and 2.4-2.2 kbar (Indrevær, 2014). These temperature estimates, as discussed above for PT conditions at VBF (this work) are altogether similar to those of the VBF, i.e. temperatures of 250-335°C. Based on the nature of the brittle faulting and the similar P-T conditions it is therefore likely that the hydrothermal Cu-Zn mineralization in the VBF was concurrent with the Carboniferous-Permian brittle extensional events that involved multiple brittle faulting, cataclasis, and hydrothermal Cu-Zn mineralization, coupled with a complex reactivation and exhumation history for the faults (cf. Davids et al. 2013).

Regarding a possible magmatic source for some of the hydrothermal fluids in the VBF (see **Fig.** 20C), no direct evidence of a corresponding hot Permian magmatic and/or volcanic source/dike for the fluids in the VBF have yet been observed in the Vanna island of western Troms. An exception is a lamproite dike in Kvaløya farther south, which yielded an Nd- and Sr-isotope age of ca. 333 Ma (Kullerud et al. 2011). Extensive rift-related mafic dike and sill intrusions of Carboniferous-Permian age, however, do exist at northern Atlantic Ocean margins (Kirstein et al. 2006), and also are recorded along portions of the Norwegian continental margin, including northern Finnmark (Lippard and Prestvik, 1997; Roberts et al. 2003, 2011; Rice et al. 2014; Nasuti et al. 2015). Thus, and since an increased geothermal gradient exceeding more than 50°C km^{-1} often accompanies incipient continental rifting events, we cannot rule out that a hidden subsurface, Carboniferous-Permian mafic magma source for hydrothermal Cu-Zn bearing fluids in the VBF may exist.

Conclusions

1) The Cu-Zn mineralization in the brittle, late Palaeozoic Vannareid-Burøysund fault on the island of Vanna, West Troms Basement Complex, is hydrothermal, epigenetic and localized within major core and damage zones, suggesting a strong structural (fault) control on the mineralization.
2) The brittle fault movement and cataclasis of the VBF created porosity allowing fluid flow and deposition of hydrothermal veins and Cu-Zn mineralization in the core and damage zones, possibly during two main stages of faulting/fracturing. Although the fault cores acted as the main fluid conduits, the fluids also weakened the strength of the fault damage zones and contributed to the complex fault architecture and development history.
3) A paragenetic model is developed for the successive deposition of i) quartz-sphalerite veins, ii) quartz-chalcopyrite veins and iii) calcite veins. Quartz-sphalerite veins deposited first in the core zone in conjunction with early brittle fracturing and cataclasis, increasing the porosity of the fault rocks and creating space for further hydrothermal fluid flow, confirming that the fault core at least initially acted as fluid conduit. With further fault movement and widening of the fault, quartz-chalcopyrite veins were deposited in fault core and damage zones. During successive injection of quartz-sphalerite vein material, the initial fault core became partly or fully sealed, thus reducing the permeability and forcing the later fluids to flow into the damage zones (cf. Indrevær et al. 2014).
4) The hydrothermal ore-bearing fluids in the VBF indicate temperature conditions of c. 250-335°C. Microtextural observations, including injected ultracataclasites, strongly indicate repeated phases of dilation, infill, and sealing of the fault. Such seismic pumping processes therefore indicate that the pressure conditions changed repeatedly between lithostatic and hydrostatic endmember values. Similar fault rock textures are documented from other Permian faults in the West Troms Basement Complex (Indrevær et al. 2014).
5) Ore forming fluids were near neutral, highly saline (c. 27-36 wt. % $NaCl+CaCl_2$) and composed of H_2O-NaCl-$CaCl_2$±S. A fluid with this high salinity is capable of transporting both Cu and Zn as chloride complexes. The ore-bearing fluid was likely a basinal brine with Zn sourced from tonalite gneiss host rocks. Sphalerite was deposited by fluid mixing with a colder and less saline fluid. Chalcopyrite in QCp veins deposited after sphalerite, likely by a combination of fluid mixing and wall-rock interactions. The stable isotope composition of calcite indicate a magmatic source of CO_2, suggests a later magmatic fluid influx, a common feature during continental extension/rifting.
6) The VBF comprises illite-bearing fault gouge yielding a Palaeozoic (Carboniferous) K-Ar age, thus linking the VBF to a period of incipient extensional faulting and rift basin formation in

the Norwegian–Greenland–Barents Sea. Several other faults in the west Troms Basement Complex are related to these early rifting events.

7) This study demonstrates that hydrothermal Cu-Zn mineralization in northern Norway may occur not only in old Precambrian and Caledonian basement rocks (Sandstad et al., 2015) but as well in much younger, Palaeozoic to Cretaceous (?), rift-related, brittle fault zones, and thus provides an additional mineral exploration model for structurally controlled ore deposits.

Acknowledgements

Tobias Bauer and Kristian Drivenes are kindly thanked for reviewing this manuscript. This work was funded by UiT – the Arctic University of Norway. We thank Øystein Rushfeld for access to assay data. Andrea Cobic with the University of Zagreb is thanked for XRD analyses. Kai Neufeld at UiT is acknowledged for his aid and input with SEM analyses. We also acknowledge Mattheus Lindgren at the Centre for Arctic Gas Hydrate, Environment and Climate at UiT for preforming stable isotope analyses.

Figures

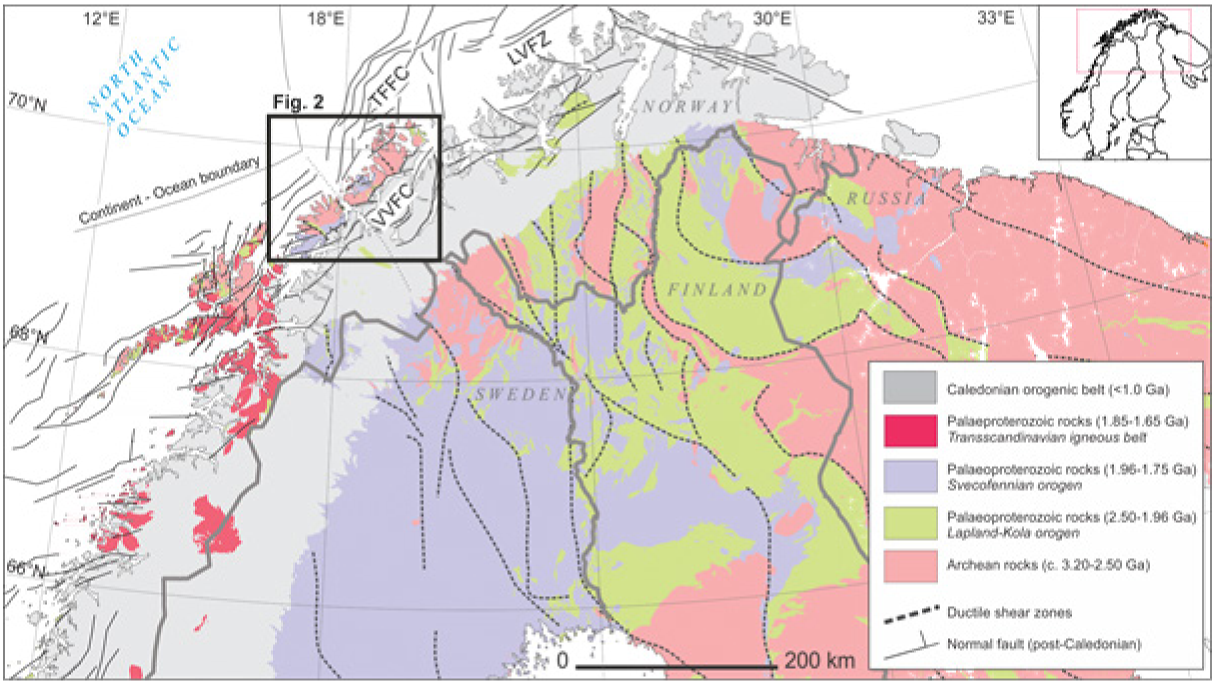

Figure 1. Regional geological map of the northern Fennoscandian Shield (based on Koistinen et al. 2001; Olesen et al. 2002; Eilu et al. 2008; Bergh et al. 2010; Davids et al. 2013; and Koehl et al. 2018). The black frame outline the West Troms Basement Complex (Fig. 2), a basement horst controlled by the onshore Vestfjorden-Vanna fault complex (VVFC) that down faults the Caledonian rocks to the east. This Permian-Early Triassic rift related activity can also be correlated with offshore fault systems including Troms-Finnmark fault complex (TFFC) and Langfjorden-Vargsundet fault zone (LVFZ).

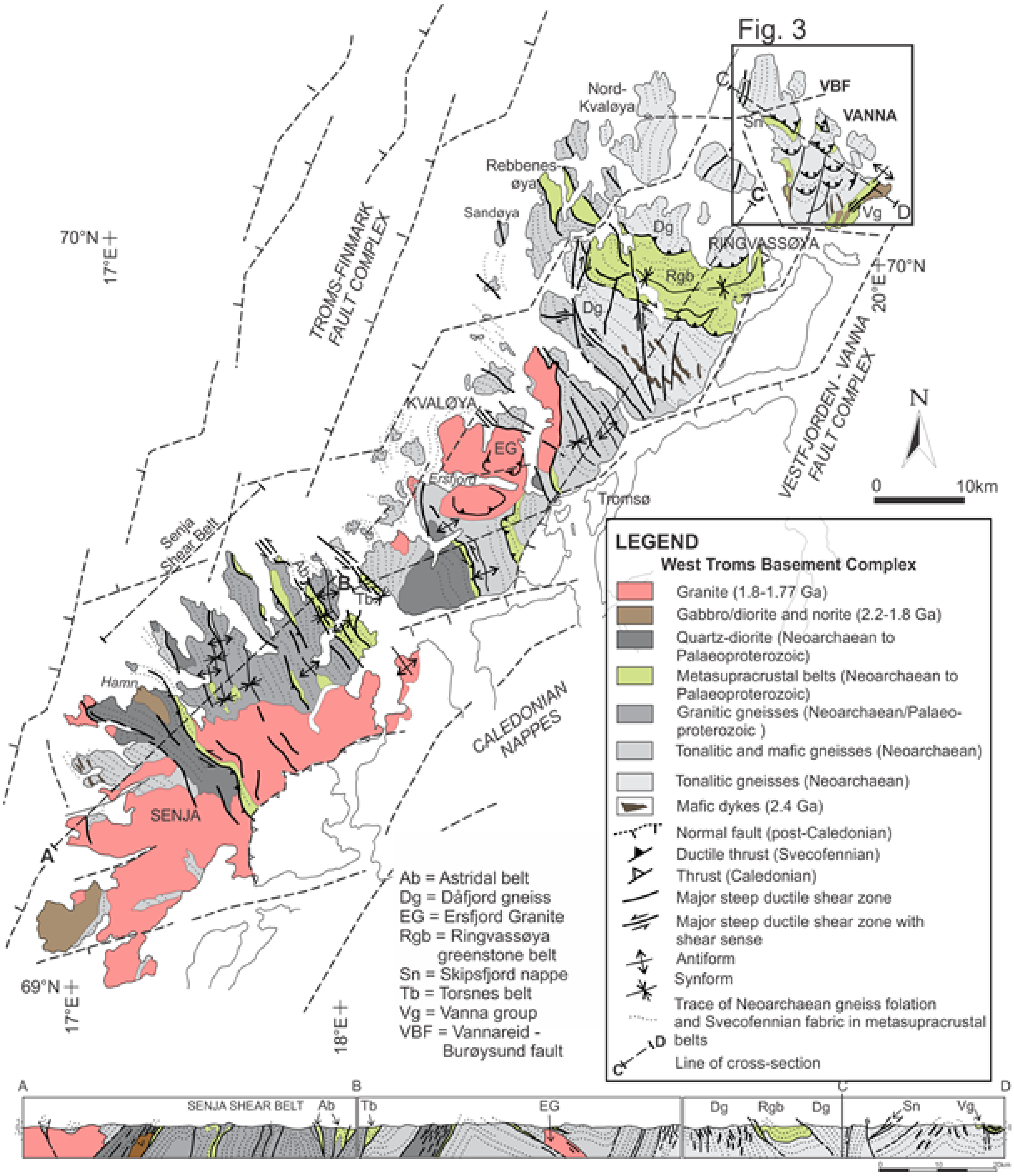

*Figure 2. Geology of the West Troms Basement Complex (Bergh et al. 2010; Thorstensen 2011; Davids et al. 2013; Haaland 2018). Vanna Island is located at the northern end of the complex. The location of the mineralized Vannareid-Burøysund fault (VBF) is marked on the map. The VBF is part of the Vestfjorden-Vanna and Troms-Finnmark Fault Complexes offshore and along fjords and sounds. Black frame outlines the island of Vanna (**Fig.** 3).*

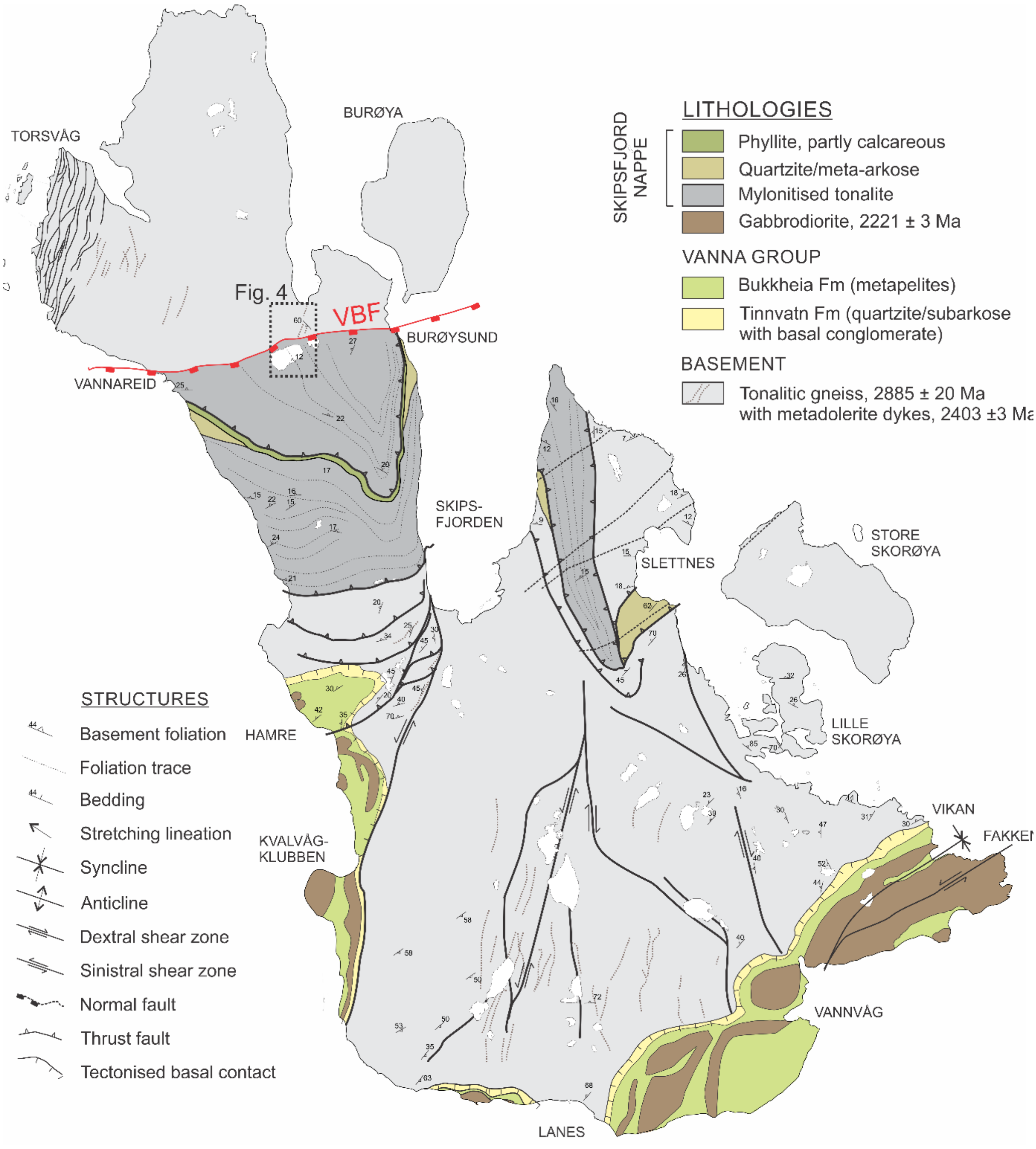

*Figure 3. Geological map of Vanna Island (Bergh et al. 2007). The mineralized Vannareid-Burøysund fault (VBF) separates variably deformed tonalite gneiss to the north from highly strained and mylonitized Skipsfjord Nappe rocks to the south. Black frame outlines the mineralized segment of the VBF (**Fig.** 4).*

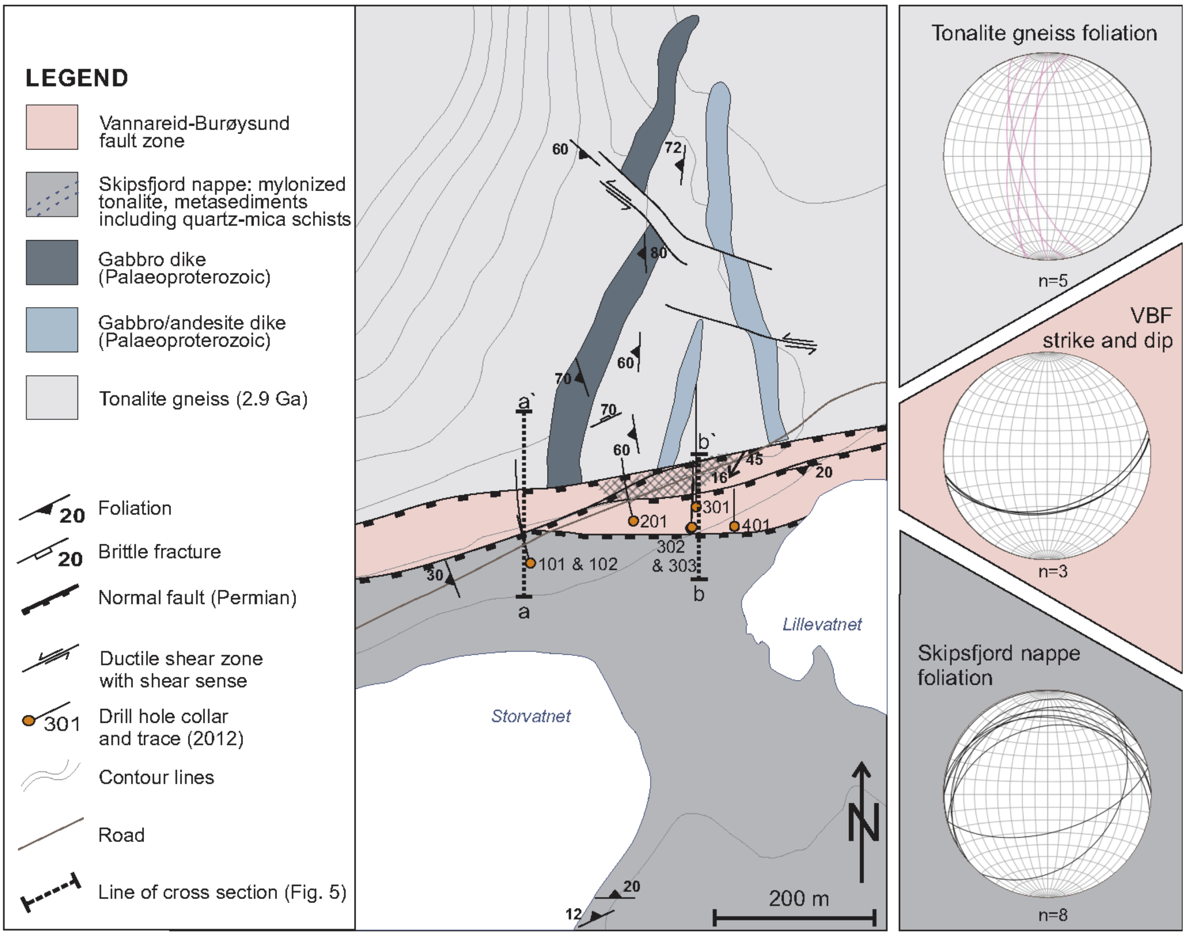

Figure 4. Geological map of the mineralized segment of the VBF in the valley between Vannareid and Burøysund (see **Fig.** *3 for location), with enclosed fault details to the right outlined as great circles in lower-hemisphere stereo plots. Note several splay faults of the VBF, a gentle NW-dip of the foliation in Skipsfjord Nappe changing to a SE-dip close to the VBF. Map is modified after Monsen (2014). Existing drill core locations are marked on the map (Ojala et al. 2013). Profile lines a-a' and b-b' mark the location of profiles shown in* **Fig.** *5.*

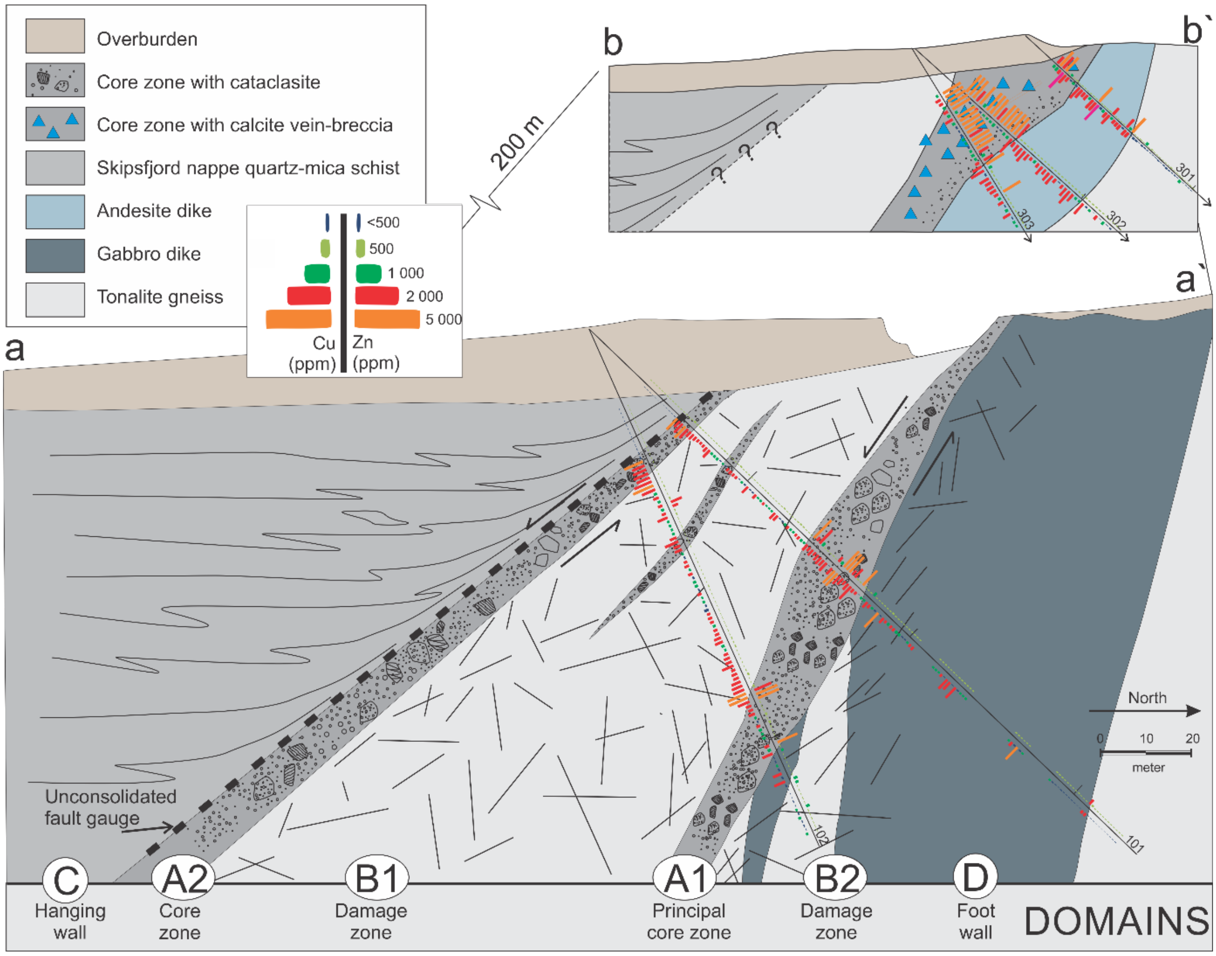

Figure 5. Cross-section a-a' through VBF showing the two drill cores and interpreted textural domains in mineralized fault rocks (core zone A1 and A2) and surrounding host rocks (damage zones B1 and B2; hanging wall domain C; and footwall domain D). The coloured assay data reflect amount of Zn (ppm), plotted on the right side of the drill core, and Cu (ppm) on the left side. Note enrichment of Cu-Zn in core zones A1 and A2, whereas lower values exist in damage zones B1 and B2. The down-dropped, non-deformed hanging wall rocks of the Skipsfjord Nappe are barren of ore mineralization. The inset figure on top right shows cross-section b-b' through VBF c. 200 m farther east, with thick calcite-breccias making up the fault core zone A1.

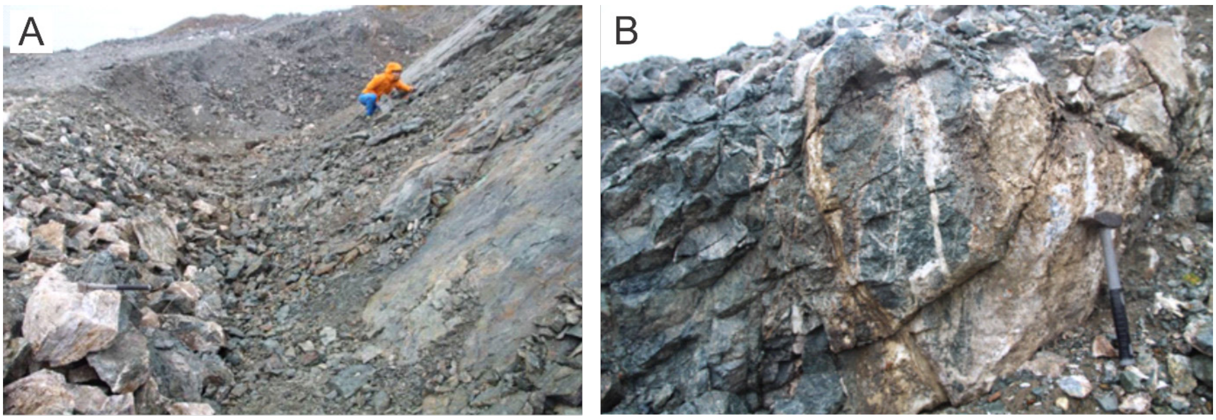

Figure 6. (A) Outcrop photo of the VBF, expressed as a planar, moderately dipping, locally striated surface, with malachite and epidote staining. Person for scale. (B) Outcrop photo of altered/chloritized (green colour) bed rocks and proto-cataclasites in damage zone B1 of the VBF. Note presence of abundant hydrothermal quartz and calcite veins as infill in brittle fractures.

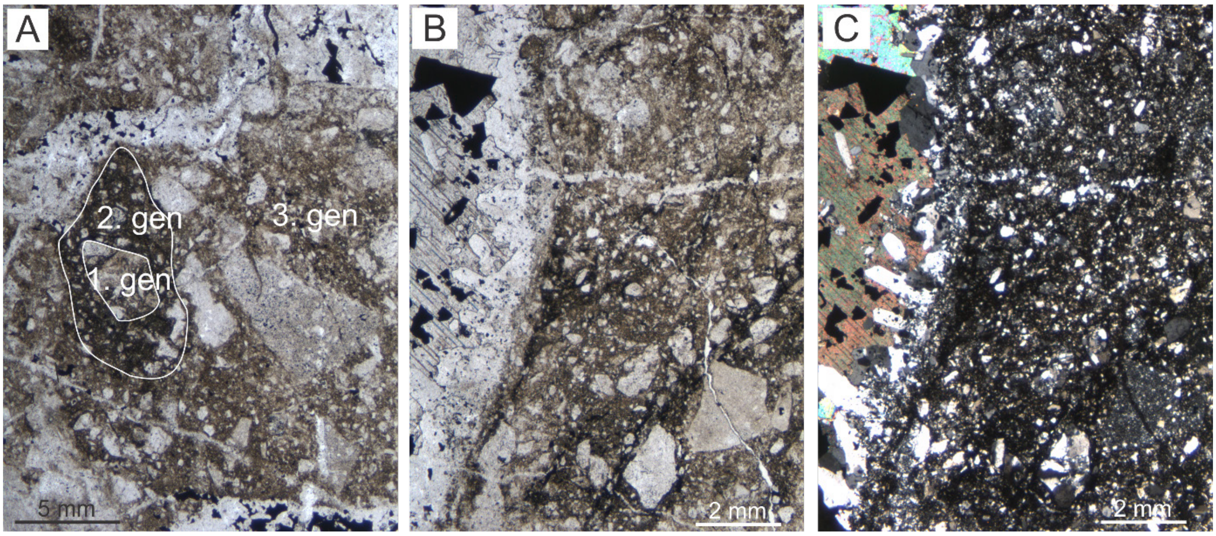

Figure 7. (A) Microphotograph (PPL) of three generations of cataclasite from core zone A1. These cataclasites are cross cut by a younger, hydrothermal chalcopyrite bearing quartz vein (top right to middle left). (B) Photomicrograph (PPL) from core zone A1 showing details several generations of cataclasite to the right and hydrothermal quartz-calcite vein to the left that is growing from the consolidated clast(s) of cataclasite. The rims of this vein is euhedral quartz with calcite infill. (C) Same as in B but as XPL.

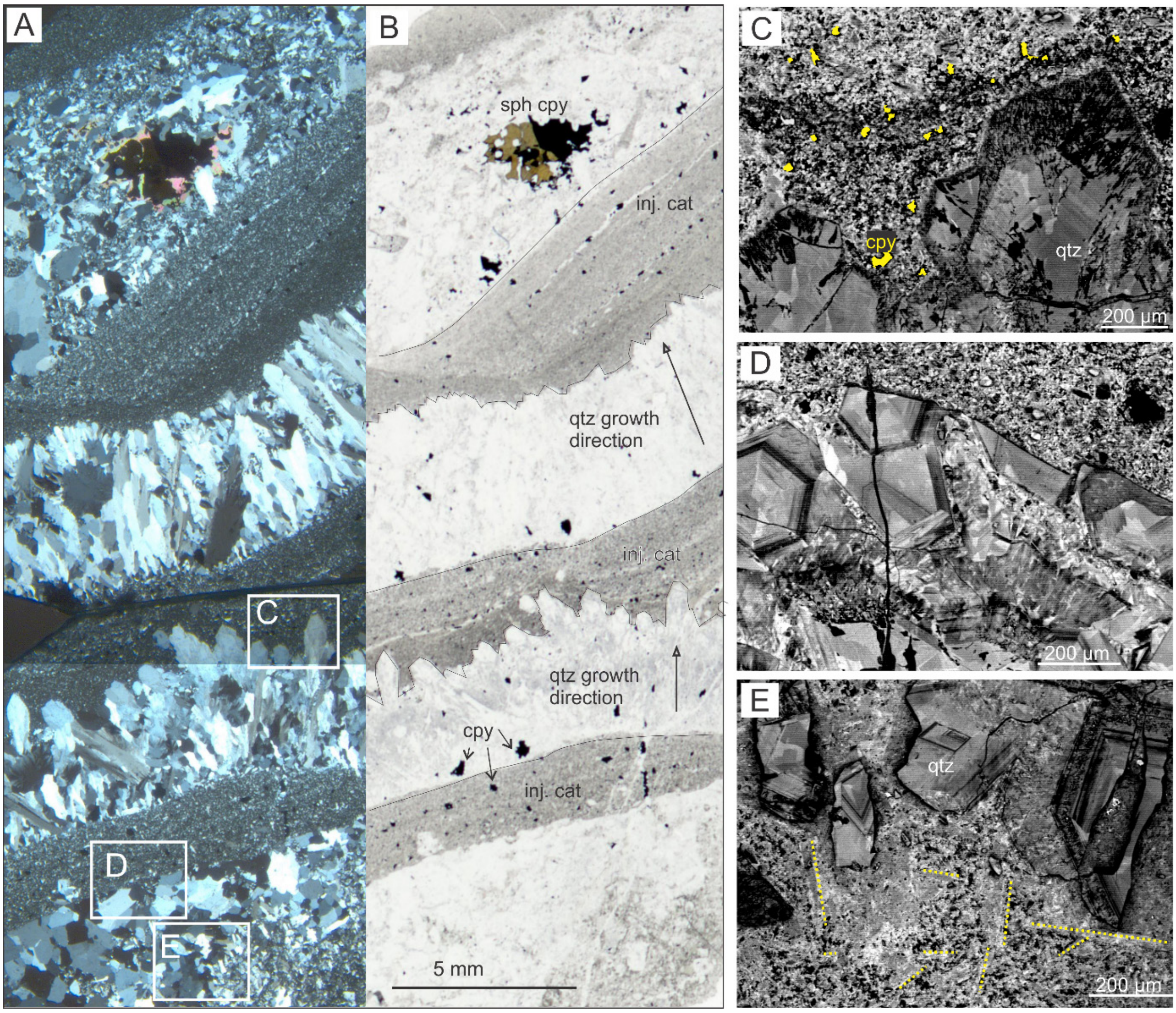

Figure 8. Microphotographs of hydrothermal veins and episodic injected ultracataclasites. XPL (A) and PPL (B) micrographs showing episodic quartz and injected cataclasites from core zone A2. Note location of C, D and E in frames. (C) Cathodoluminescence SEM image showing zoned euhedral quartz cores with plumose textured rims. Matrix between such quartz grains were then, later on filled by new injected cataclasite with chalcopyrite (yellow grains). (D) Cathodoluminescence SEM image showing fractured clasts of zoned quartz with fractures filled by injected ultracataclasite. (E) Fractured clasts of hydrothermal zoned quartz with plumose rims and surrounding infill of ultracataclasite with acicular new-grown minerals, in yellow (bottom half of photo. Abbreviations: inj. cat.-injected cataclasite, qtz -quartz, cpy -chalcopyrite, sph -sphalerite.

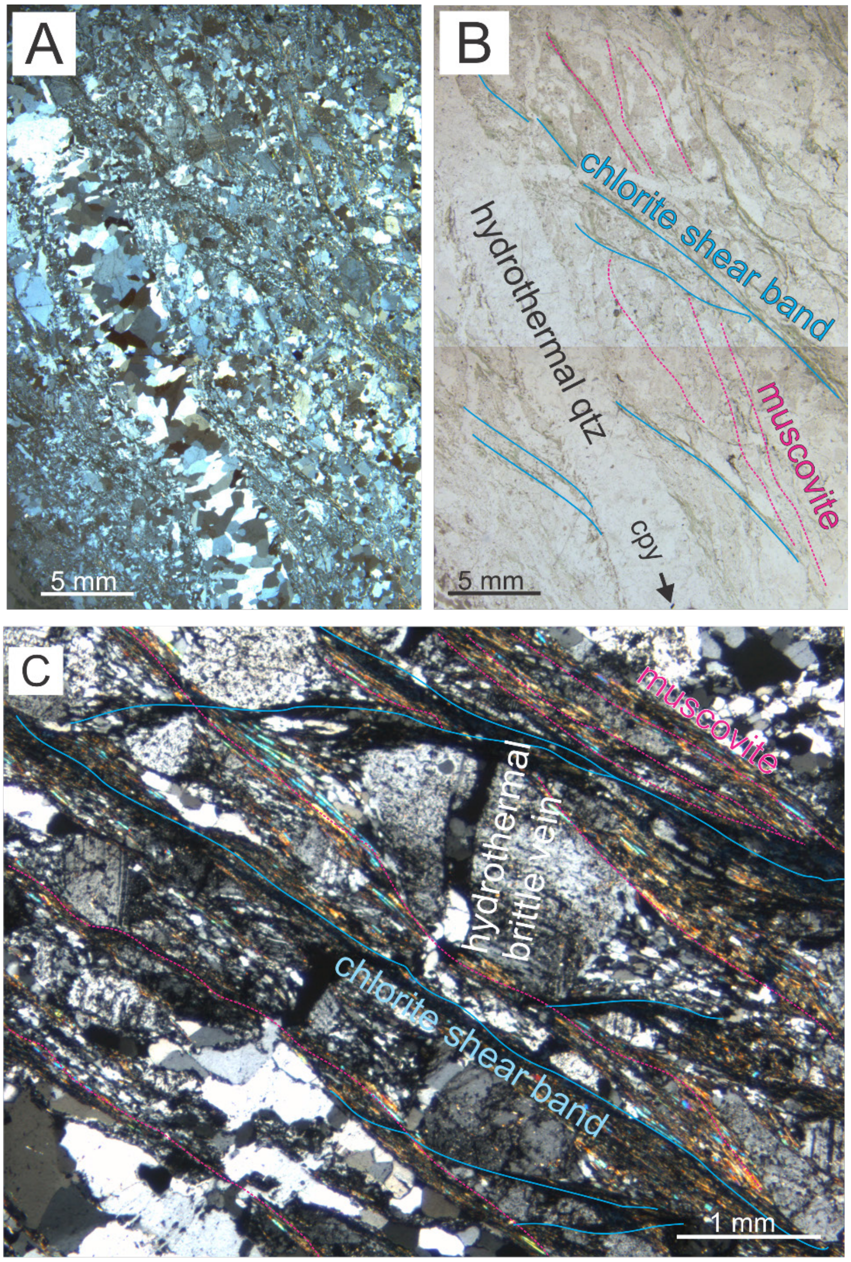

Figure 9. (A & B) XPL and PPL microphotographs from damage zone B1 showing weakly foliated tonalite gneiss with muscovite (pink) bands cut at a low angle by chlorite shear bands (blue). Younger hydrothermal quartz and chalcopyrite veins truncate, but are arranged parallel to the old, ductile fabric of the gneisses. (C) XPL micrograph of tonalitic gneiss with foliation composed mostly of aligned muscovite, which is superposed at low angle by chlorite shear bands in tonalite gneiss. Note the large, sigmoidal feldspar crystal in the middle of the micrograph which is fractured and dilated by quartz.

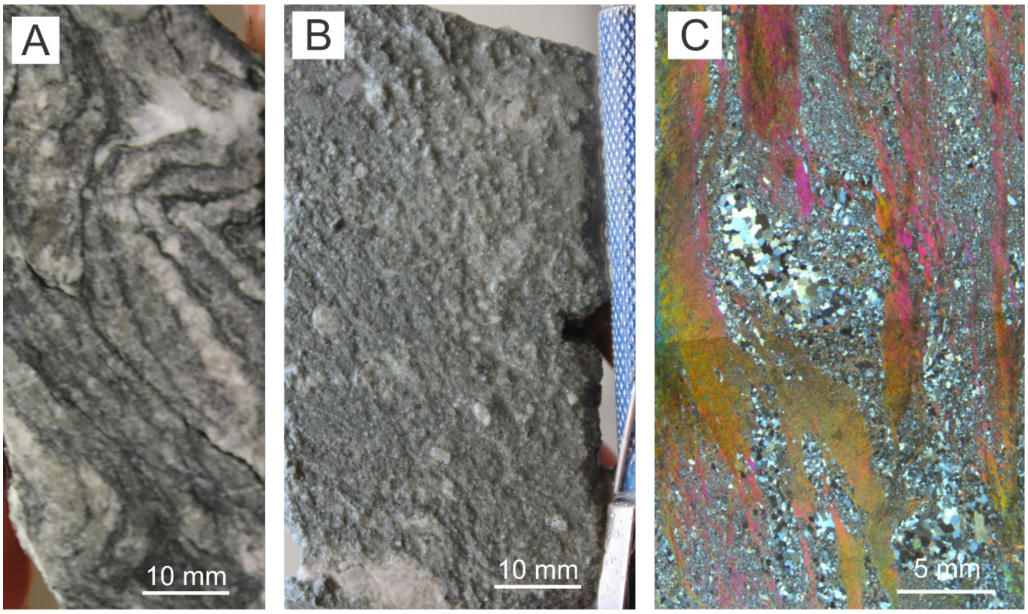

Figure 10. (A) Hand-specimen photo of folded, well-foliated, non-mineralized quartz-mica schist in Skipsfjord Nappe host rocks of the hanging wall to VBF. (B) Hand specimen photo of unconsolidated fault gouge (core zone A2) at the contact between quartz-schists in hanging wall and the mineralized footwall of VBF. (C) Photomicrograph (XPL) of quartz-mica schists from Skipsfjord Nappe rocks showing muscovite foliation and sigmoidal-shaped quartz crystal.

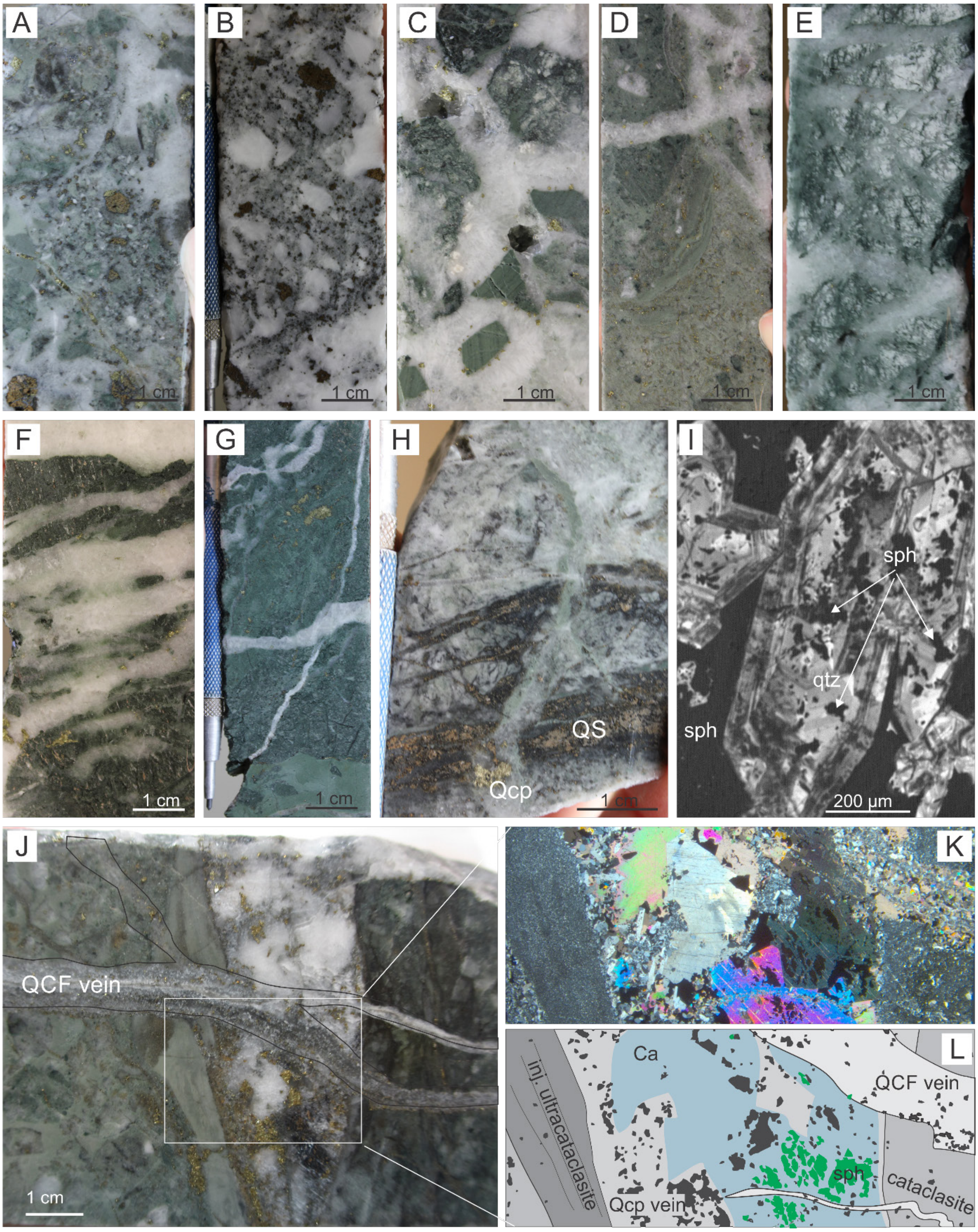

Figure 11. Drill core photographs (A-H and J) and microphotographs (I, K and L) of typical mineralization textures and quartz-carbonate veins. (A) Cataclasite with enclosed, early-stage sphalerite mineralization (QS) outlined as clasts cemented by a later phase of quartz-chalcopyrite veining material (QCp). From core zone A1. (B) Calcite-cemented sphalerite-rich breccia located at the top of core zone A1 (see Fig 5). (C) Clasts of banded ultracataclasites cemented by hydrothermal (QCp) veins in cataclasite of domain A2. Note that chalcopyrite is present as rims around chlorite-bearing clasts. (D) Cataclasite from core zone in domain A2, with clasts of quartz and several older generations of cataclasite, cemented by injected ultracataclasites, and cross cut by hydrothermal

quartz veins. (E) Damage zone B1 is characterised by fractured and weakly foliated tonalite gneiss cut by stock work QCp veins and chlorite alteration. (F) Chloritized gabbro in damage zone, domain B2, cut by parallel QCp veins. (G) Fine-grained cataclasite cut by QS veins in damage zone, domain B2. (H) Direct cross cutting relationship between early QS veins and later QCp veins, in core zone A1. (I) SEM cathodoluminescence image of a QS vein. Note zoned, euhedral quartz crystals with sphalerite occurring as small inclusions in quartz, and as interstitial sphalerite between quartz crystals. (J) Cross cutting relationships observed in core zone A1: Injected ultracataclasite is cut by QS and QCp veins, with a later infill of massive calcite. Early sphalerite grains are fractured in a jig-saw pattern by the later calcite infill. A narrow QCF vein with massive textures is the youngest vein observed. (K, L) Uninterpreted XPL (K) and interpreted (L) microphotograph of a portion (frame) of sample (J) outlining the relative timing (stages i-iv) of QS (green sphalerite), QCp (pale grey quartz and black chalcopyrite), Ca (pale blue calcite and black chalcopyrite), and QCF veins (palest white quartz-calcite-fluorite and black chalcopyrite and Pb-Ag-Bi sulphides), respectively. Injected cataclasites with apparent banding are outlined in darkest grey colour.

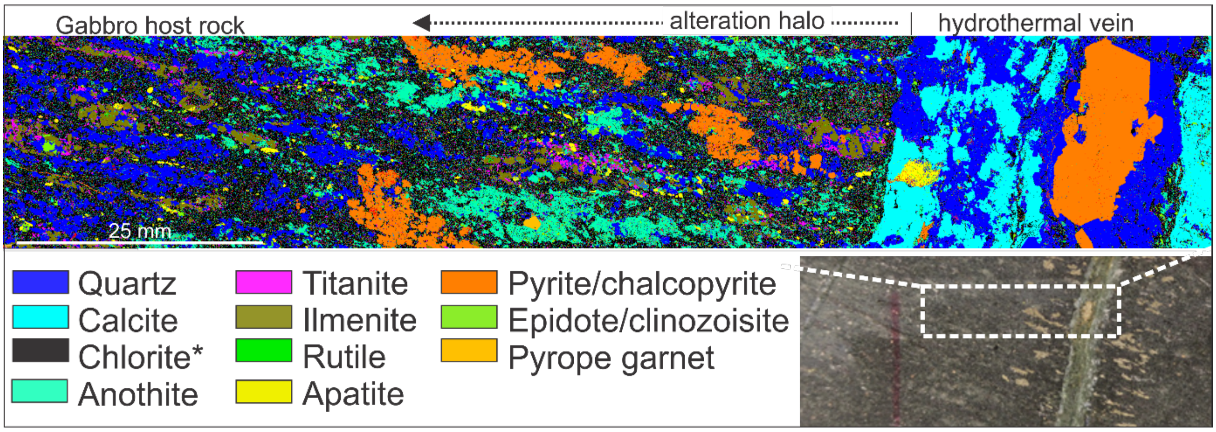

Figure 12. Secondary mineral growth expressed as alteration halo adjacent to a QCp vein, in gabbro from damage zone B2 (see inset photo of hand specimen and location of section, white stippled frame). SEM EBSD image (upper part) showing secondary alteration minerals replacing original minerals (in colour) along existing foliation in gabbro. The QCp vein is composed of quartz, calcite, and pyrite/chalcopyrite, with minor apatite and epidote. The mineral replacement is more pronounced close to the QCp vein where amphibole is replaced by chlorite; ilmenite/magnetite is replaced by pyrite/chalcopyrite and titanite; and feldspar is partly replaced by epidote.

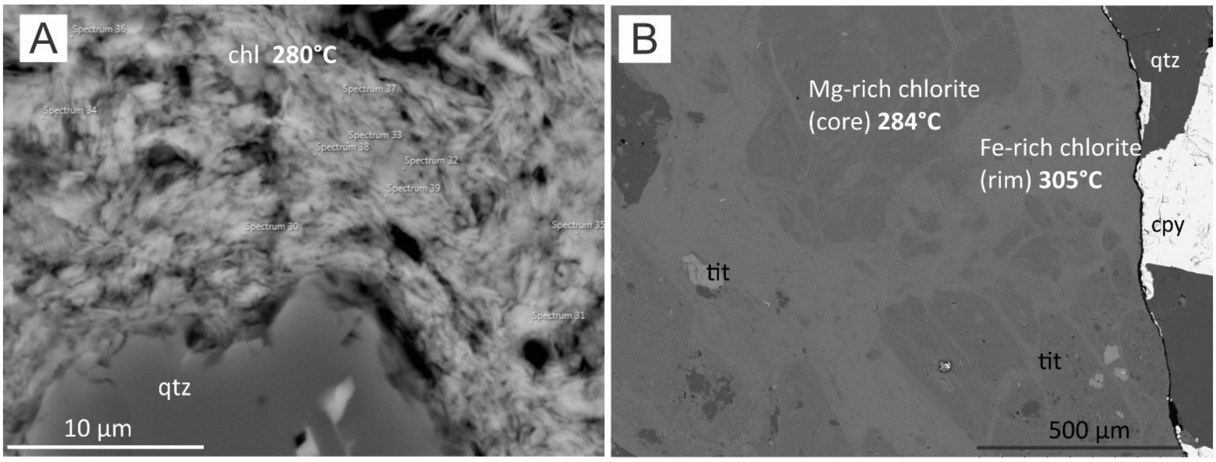

Figure 13. SEM images of different chlorite associations analysed for chlorite geothermometry. (A) Fine grained chlorite in cataclasite from top of core zone A1 (B) Two generations of cataclasite with chlorite alteration of amphibole in gabbro dike in damage zone B2.

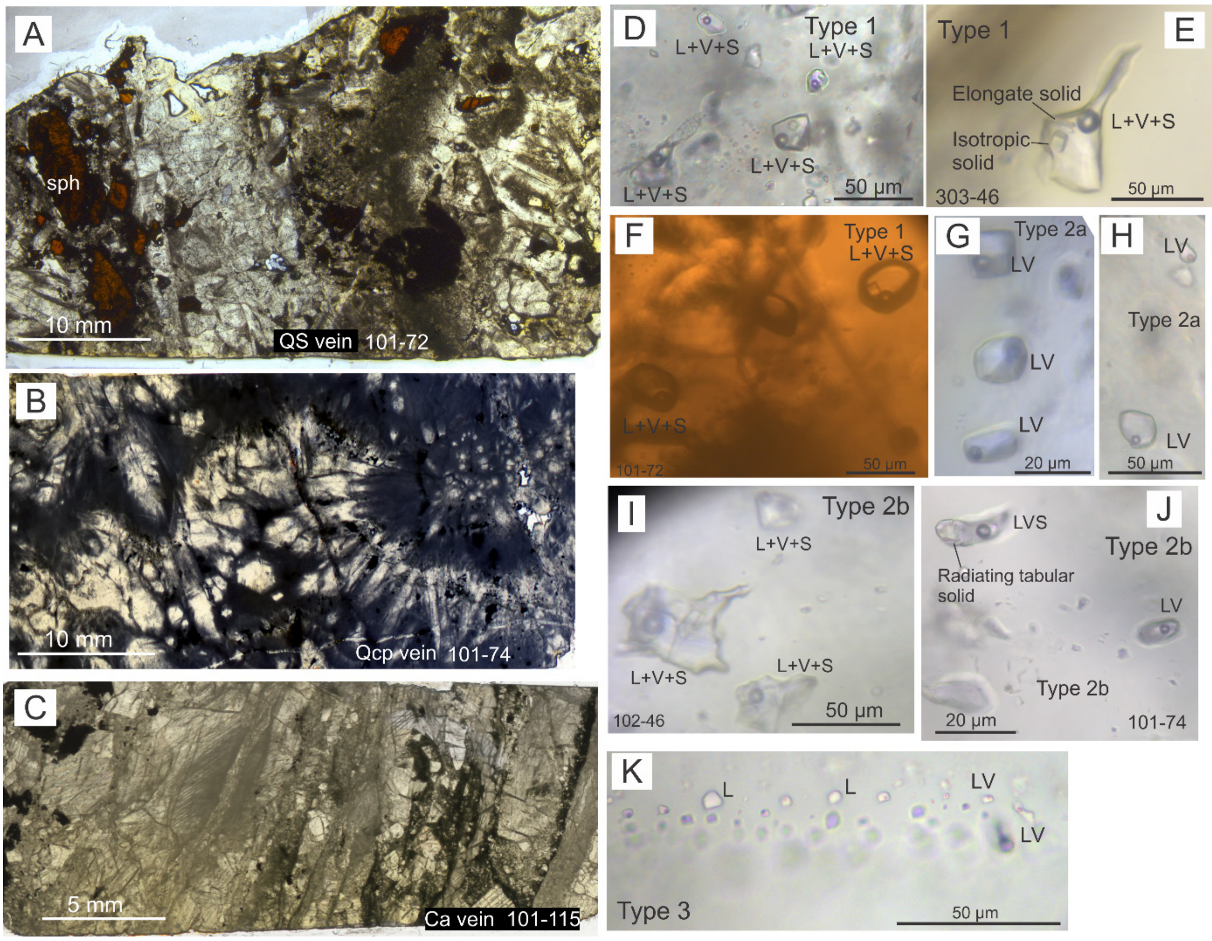

Figure 14. Compiled photographs double-polished wafers (A-C) and microphotographs of selected fluid inclusion types (D-K). A) Double polished wafer of QS vein from core zone A1. (B) Double polished wafer of typical textured QCp vein where quartz have zoned cores and feathery/plumose rims. C) Double-polished wafer of brecciated Ca vein. D) Composite photo of type 1 L+V+S fluid inclusion in quartz with cubic solid. E) Type 1 inclusion in quartz with two types of solids; an isotropic cubic solid which commonly melted around 70-200°C and a second, less common, elongate tabular crystal that did not melt when heated. The latter is possibly an incidentally entrapped solid. F) Type 1 L+V+S inclusions in sphalerite. G&H) Type 2a L+V inclusions in calcite. I) Type 2b L+V+S inclusions in quartz with <1-10% solids. J) Type 2b inclusion in quartz that contain a radiating tabular solid. K) Type 3 L+V and L-only pseudosecondary inclusions in quartz with negative crystal shapes. Note that L-inclusions lack vapour bubble at room temperature, but may develop vapour bubbles during freezing.

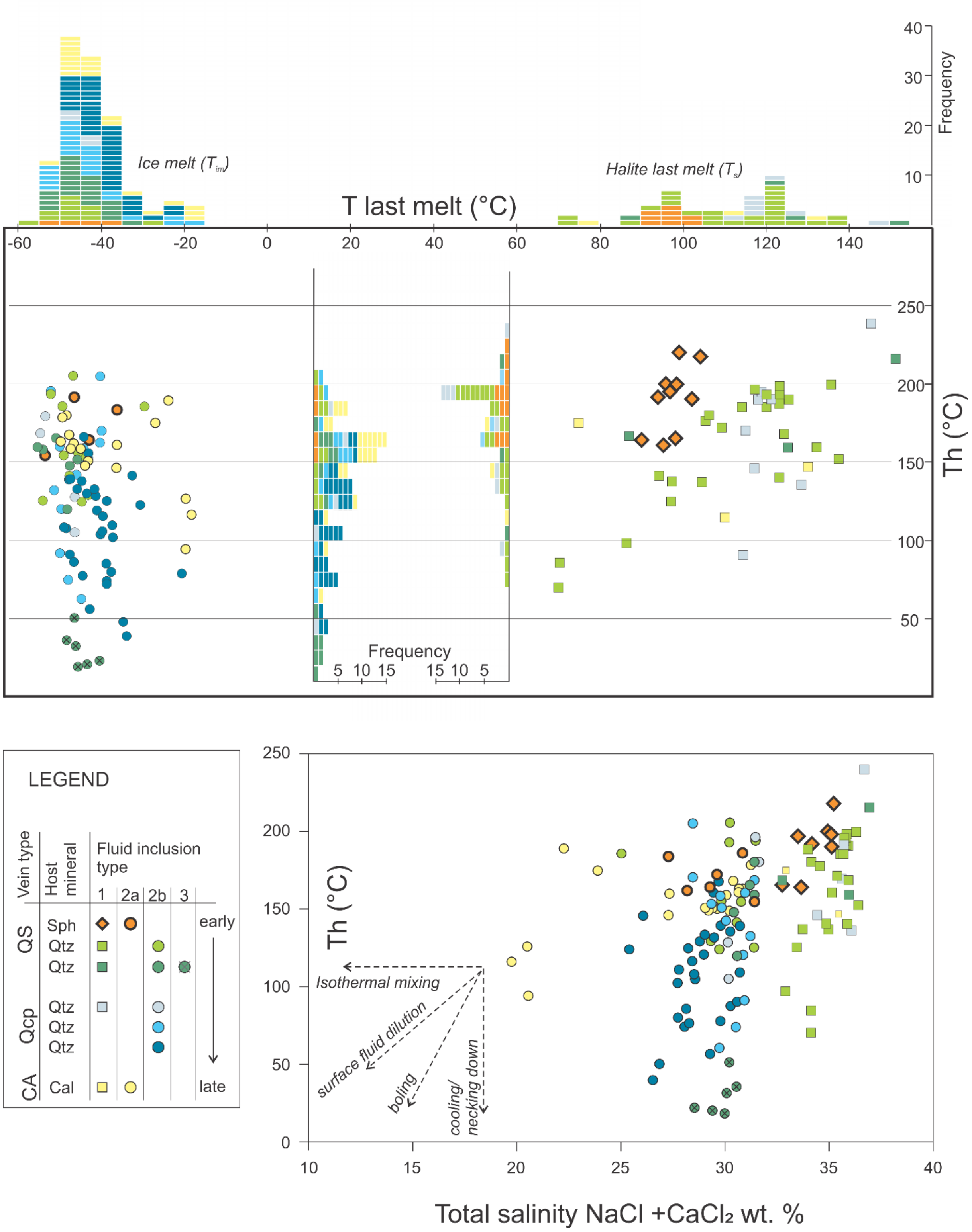

Figure 15. Summary of fluid inclusion microthermometric data. A) Measured ice melting temperatures ($T_{m\ Ice}$) for Type 2a, 2b and 3 inclusion are plotted on the X-axis. Halite melting temperatures for Type 1 inclusions are also plotted along the same axis. Homogenisation temperatures T_h (°C) is plotted on the Y axis. Note that frequency histograms are plotted separately for all measurements. B) Calculated total salinity ($NaCl+CaCl_2$) versus T_h (see also Table 2). The colours correspond to different vein samples from different vein types. Temporal relationships indicated in the legend is based on cross cutting relationships described in the text.

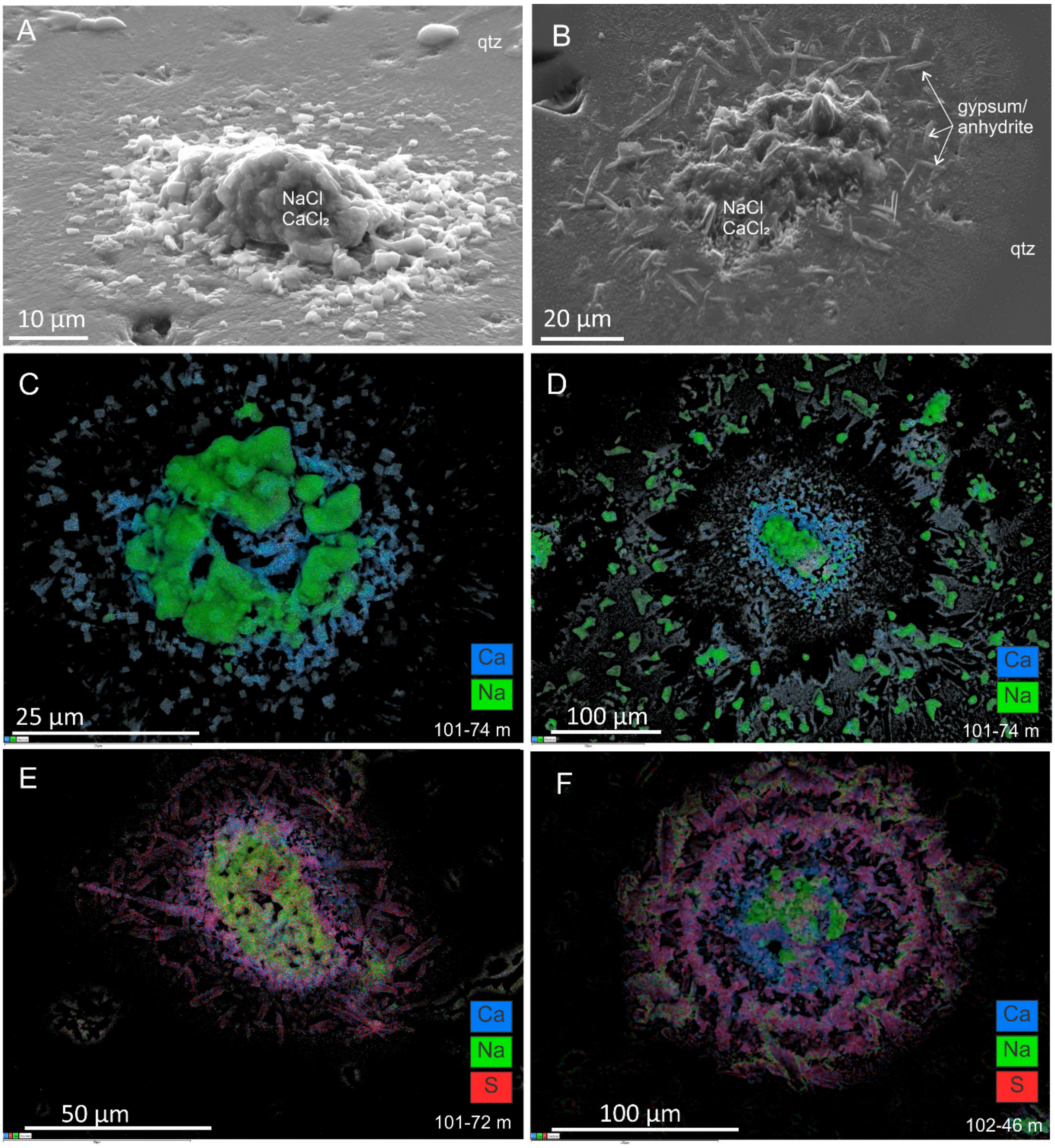

Figure 16. SEM images of evaporate mounds in quartz. (A) 3-D image of evaporate mound where cubic NaCl and $CaCl_2$ crystals from QCP vein (sample 101-74). (B) 3-D image of NaCl, $CaCl_2$ and $CaSO_4$ crystals (C & D) SEM-image with color code overlay, showing distribution of Na and Ca in QCp vein (sample 101-74). (E) NaCl, $CaCl_2$ and $CaSO_4$ in evaporate mounds from a QS vein (sample 101-72) F) NaCl, $CaCl_2$ and $CaSO_4$ in evaporate mounds from a QCp vein (sample 102-46)

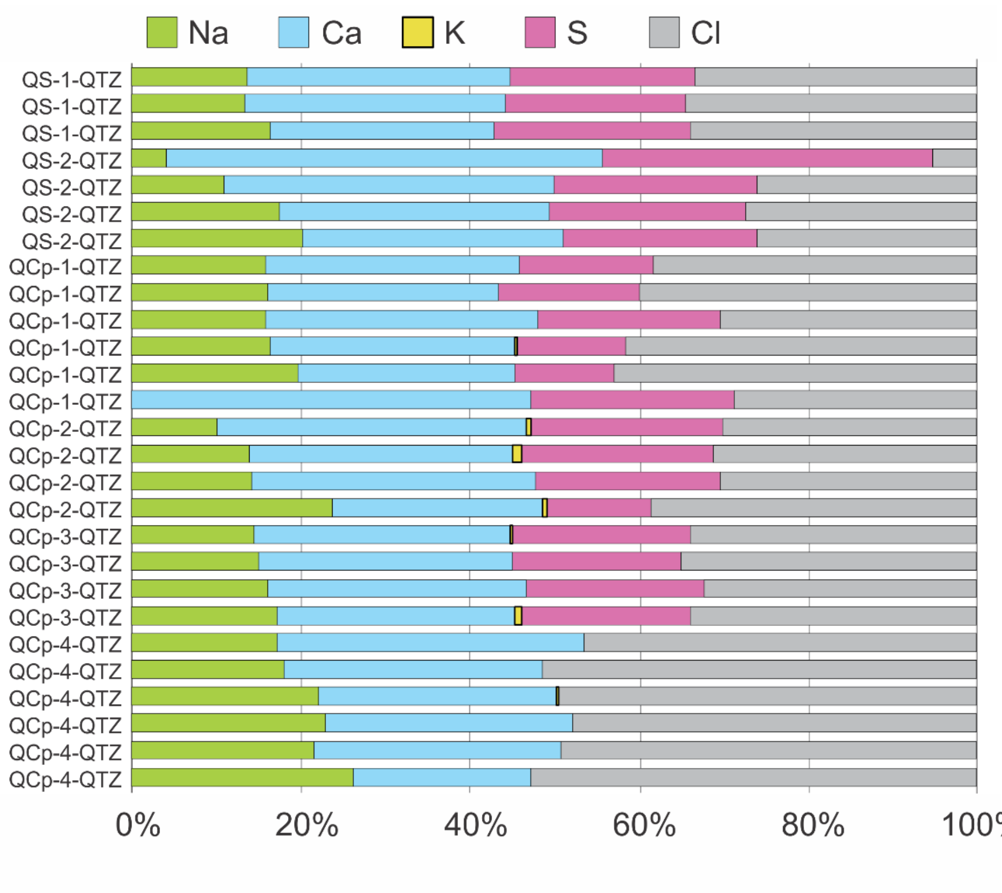

Figure 17. (A) Graphical presentation of relative proportions of Na, Ca, K, S, and Cl (in wt. %) measured in evaporate mounds from decrepitated fluid inclusions in quartz. The data are obtained by surface scanning of the evaporate mounds using a SEM.

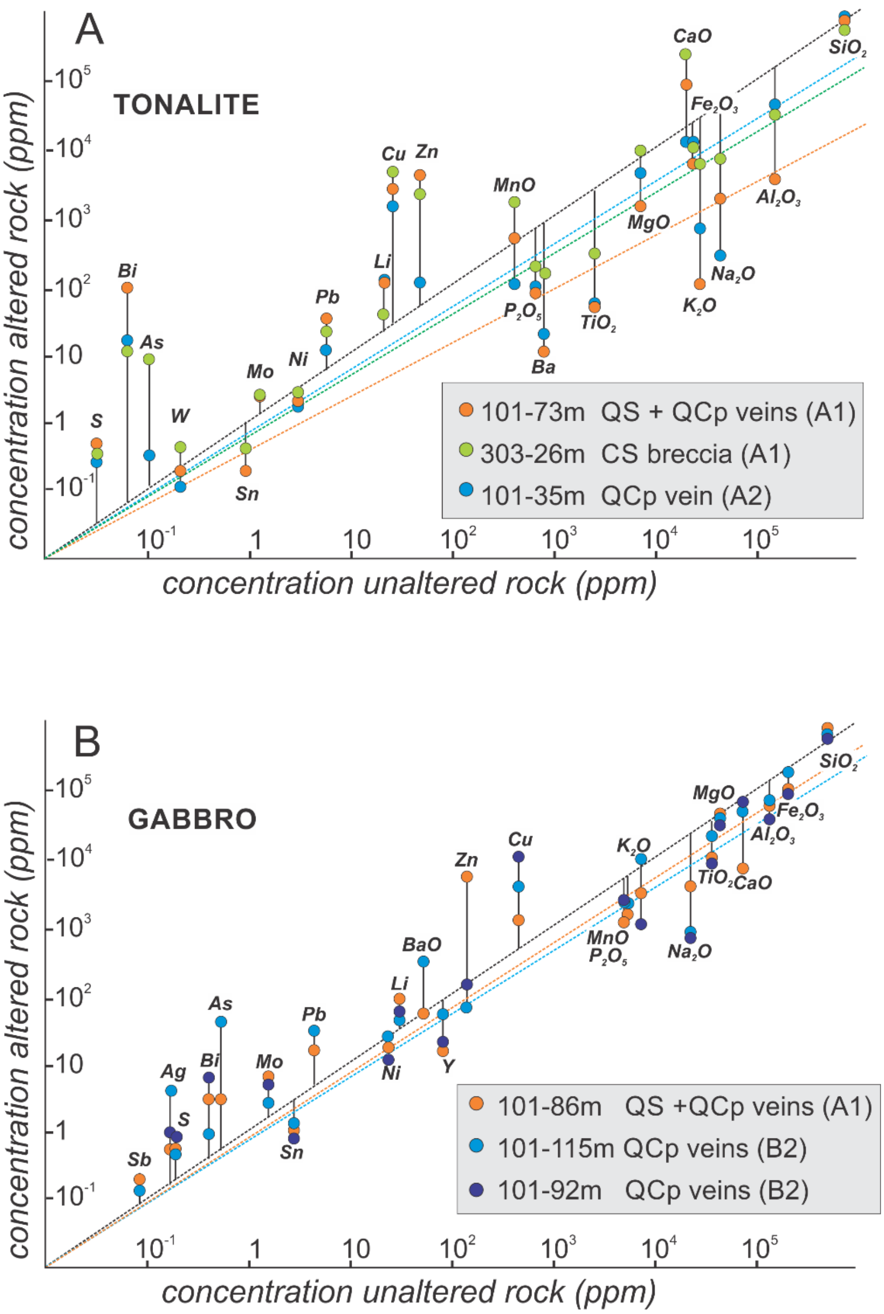

Figure 18. Isocon diagrams (after Grant, 1986) showing gains and losses of elements during fault-related hydrothermal alteration and mineralization. Applied geochemical whole rock data are from Store Norske Gull, drill core sections, of unaltered tonalite gneiss and gabbro, and altered host rocks, including veins and cataclasites in the core zones A1 and A2. For linear element correlations we used average line (Grant 1986) and additional, coloured line drawn between concentrations of presumed immobile Al_2O_3, TiO_2 and Zr. (A) Isocon diagram for altered tonalite gneiss in core and damage zones, domains A1, A2, and B1. (B) Isocon diagram for altered gabbro dike in domains A1 and B2. Note similar alteration trends for elements in both rock types (see main text for further details).

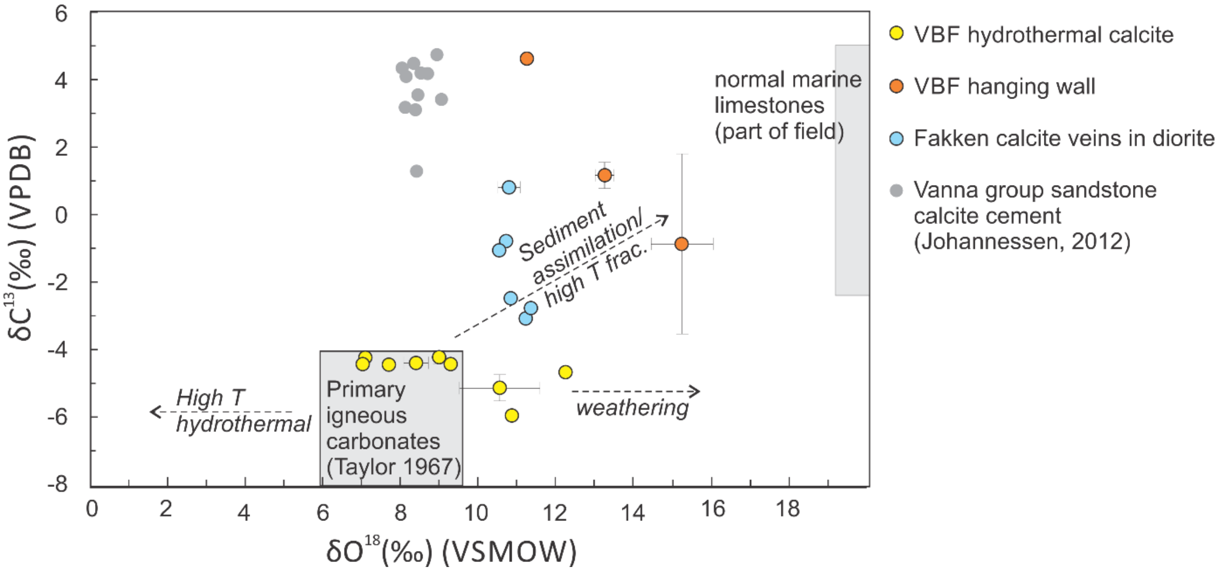

Figure 19. $\delta^{13}C$ and $\delta^{18}O$ diagram showing stable isotope composition of hydrothermal calcite from the VBF, Skipsfjord Nappe rock in hanging wall to the VBF, veins in intrusive diorite of the Vanna Group, and calcite cement from meta-sandstones in Vanna Group. Note that hydrothermal calcite from VBF overlap with primary igneous carbonates (Taylor, 1967).

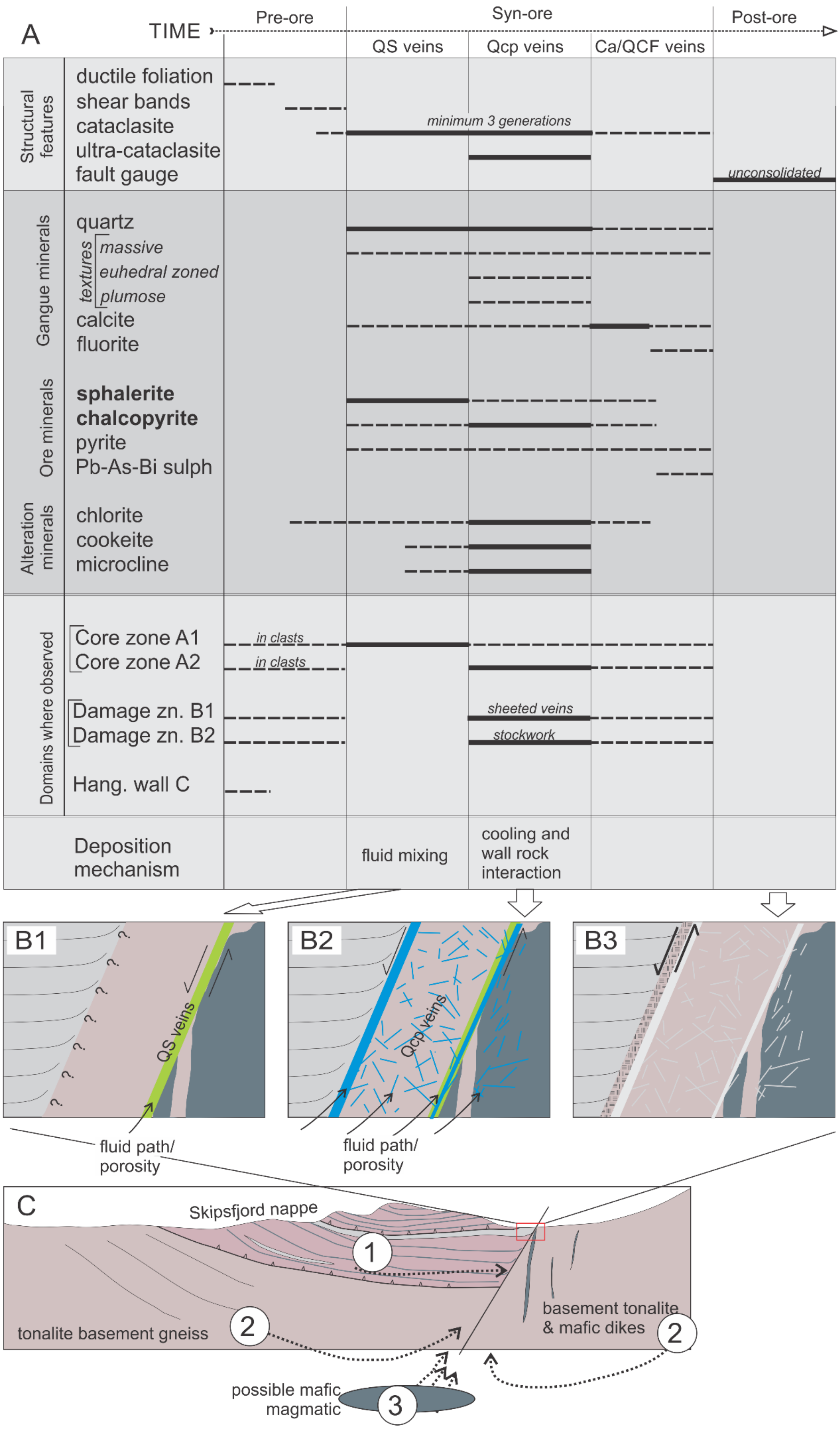

A
TIME
Pre-ore
Syn-ore
Post-ore
QS veins
Qcp veins
Ca/QCF veins
Structural features
ductile foliation
shear bands
cataclasite
ultra-cataclasite
fault gauge
minimum 3 generations
unconsolidated
Gangue minerals
quartz
textures
massive
euhedral zoned
plumose
calcite
fluorite
Ore minerals
sphalerite
chalcopyrite
pyrite
Pb-As-Bi sulph
Alteration minerals
chlorite
cookeite
microcline
Domains where observed
Core zone A1
Core zone A2
Damage zn. B1
Damage zn. B2
Hang. wall C
in clasts
in clasts
sheeted veins
stockwork
Deposition mechanism
fluid mixing
cooling and wall rock interaction
B1
B2
B3
QS veins
Qcp veins
fluid path/ porosity
fluid path/ porosity
C
Skipsfjord nappe
1
2
2
3
tonalite basement gneiss
basement tonalite & mafic dikes
possible mafic magmatic

Figure 20. Tentative para-genetic evolution model for the VBF and its Cu-Zn mineralization: (A) Summary of interpreted ore and gangue mineral growth in fault rocks and veins relative to the ore-forming events (pre-, syn-, post-), as seen within textural domains of the VBF. (B) Schematic illustration of the movement and mineralization history of the VBF, creating porosity and permeability contrasts that may have controlled the injection of QS and QCp veins, and final, post-ore movement (fault gouge). B1) The early movement caused fracturing, cataclasis and increased permeability in the core zone (domain A1), which acted as fluid conduit for later injections and cataclasis. B2) Reduced permeability forced later injections of QCp and Ca-veins into the damage zone and core zone (domain A2). B3) the final post-ore fault movement generated unconsolidated fault gouge in core zone A2. (C) Schematic representation of possible hydrothermal fluid sources of the mineralized VBF, including; the basinal brines from the cover-basement sequence represented by the meta-sedimentary Skipsfjord Nappe rocks and its lower contact with basement tonalite gneisses (1), the tonalite basement gneisses and enclosed mafic dikes (2), and a possible mafic intrusion (dike swarm) and/or deep magmatic source (3).

Table captions

Table 1. Chemical compositions of secondary chlorite formed in halos of injected QCp hydrothermal veins in core zone cataclasites of the VBF, associated with mineralization. Formula is calculated on the basis of 14 oxygens. Mdn±σ = median value plus/minus one standard deviation

** formation temperature calculated using the geothermometer of Cathelineau (1988).*

Sample - depth (m)	n	Material analysed	domain	Chlorite type	SiO_2 (%) ±σ	Al_2O_3 (%) ±σ	FeO (%) ±σ	MnO (%) ±σ	MgO (%) ±σ	Total ±σ	Temp (°C)*	Average structural formula
V6 - surface	8	cataclasite	A2	Clinochlore	27.4 ± 0.9	19.4 ± 0.7	22.9 ± 1.1	0.6 ± 0.1	14.5 ± 0.7	84.7 ± 2.1	**280°C**	$(Mg_{2.33}Fe_{2.06}Al_{1.40}Mn_{0.05})(Si_{2.94}Al_{1.06})O_{10}(OH)_8$
101-70.5	8	cataclasite	A1	Chamosite	28.9 ± 0.7	19.4 ± 0.6	28.3 ± 1.2	0.7 ± 0.1	15.7 ± 0.8	93.0 ± 1.0	**295°C**	$(Mg_{2.35}Fe_{2.37}Al_{1.18}Mn_{0.03})(Si_{2.89}Al_{1.11})O_{10}(OH)_8$
101-93	10	Mg-rich core cataclasite	A1	Clinochlore	27.5 ± 0.6	18.5 ± 0.6	19.4 ± 1.2	0.1 ± 0.1	18.3 ± 0.9	84.0 ± 1.4	**285°C**	$(Mg_{2.61}Fe_{2.00}Al_{1.26}Mn_{0.01})(Si_{2.93}Al_{1.07})O_{10}(OH)_8$
101-93	8	Fe-rich rim cataclasite	A1	Chamosite/ Clinochlore	25.7 ± 0.4	18.6 ± 0.3	24.9 ± 0.4	0.4 ± 0.2	13.8 ± 0.6	83.4 ± 1.1	**305°C**	$(Mg_{2.28}Fe_{2.31}Al_{1.30}Mn_{0.03})(Si_{2.86}Al_{1.14})O_{10}(OH)_8$

Table 2. Summary of fluid inclusion microthermometry from quartz, sphalerite and calcite in hydrothermal veins. Abbreviations; SPH = sphalerite; QTZ = quartz; CA = Calcite, Mdn±σ = median value plus/minus one standard deviation, n= number of fluid inclusion analyses

** melted at eutectic (-52°C)*

*** DNF - Did not freeze at -130°C for 5 minutes*

**** calculated wt. % $NaCl+CaCl_2$ (Steele-MacInnis et al., 2011)*

Host mineral	Vein type	Incl. type	P/PS	Microthermometric data: T_{im} (°C)		T_s (°C)		T_h (°C)		Salinity ($NaCl+CaCl_2$)***		Ratio ($NaCl/CaCl_2$)		n
				Range	Mdn±σ	Range	Mdn±σ	Range	Mdn±σ	Range	Mdn±σ	Range	Mdn±σ	
SPH	QS	1	P	-46.9 to -38.1	-43.1 ± 3.2	90 - 98	95 ± 3	164 to 197	179 ± 15.0	32.8 to 34.2	33.5 ± 0.5	0.27 to 0.34	0.29 ± 0.03	4
SPH	QS	1	P	-52*	-	96 - 104	100 ± 3	190 to 218	200 ± 10.2	34.9 to 35.2	35.1 ± 0.1	0.25 to 0.26	0.26 ± 0.01	4
SPH	QS	2a	P	-53.6 to -36.2	-42.8 ± 5.6	-	-	155 to 186	164 ± 11.0	27.3 to 31.4	29.3 ± 1.4	0.06*	-	7
QTZ	QS	1	P	-52.3 to -39.9	-44.2 ± 4.1	86 - 135	106 ± 15	97 to 199	177 ± 32.3	32.9 to 36.3	34.2 ± 1.0	0.29 to 0.36	0.31 ± 0.02	9
QTZ	QS	1	P	-52*	-	70 - 137	120 ± 19	70 to 198	171 ± 38.9	34.1 to 36.4	35.8 ± 0.7	0.21 to 0.32	0.29 ± 0.03	15
QTZ	QS	2b	P	-52.0 to -30.0	-46.7 ± 5.9	-	-	125 to 205	155 ± 29.5	25.0 to 31.4	30.2 ± 1.7	0.06*	-	10
QTZ	QS	3	PS	-48.2 to -40.3	-45.9 ± 2.6	-	-	19 to 36	22 ± 6.5	28.6 to 30.6	30.0 ± 0.7	0.06*	-	6
QTZ	QCP	1	P	-43.5 to -37.5	-41.9 ± 2.5	87 - 117	96 ± 13	146 to 167	161 ± 8.8	32.6 to 34.4	33.1 ± 0.8	0.29 to 0.34	0.33 ± 0.02	3
QTZ	QCP	1	P	-52*	-	115 - 151	121 ± 10	128 to 239	170 ± 30.3	35.6 to 36.9	35.8 ± 0.4	0.28 to 0.34	0.29 ± 0.02	15
QTZ	QCP	2b	P	-54.4 to -23.9	-44.9 ± 6.0	-	-	35 to 218	127 ± 41.6	22.5 to 31.4	29.8 ± 1.7	0.06*	-	51
QTZ	QCP	2b	P	DNF**	-	-	-	156 to 220	179 ± 20.5	-	-	-	-	15
CAL	CA	1	P	-47.5 to -43	-45.3 ± 2.3	75 - 130	103 ± 28	146 to 175	161 ± 14.4	33.0 to 35.5	24.1 ± 1.3	0.27 to 0.33	0.30 ± 0.03	2
CAL	CA	2a	P	-19.8 to -18.3	-19.7 ± 0.7	-	-	94 to 126	116 ± 13.4	19.8 to 20.6	20.5 ± 0.4	0.06*	0.06 ± 0.00	3
CAL	CA	2a	p	-50.3 to -23.5	-44.8 ± 8.3	-	-	146 to 189	161 ± 11.7	22.3 to 31.0	29.8 ± 2.6	0.06*	-	14

References

Armitage, P.E.B. & Bergh, S.G. 2005: Structural development of the Mjelde-Skorelvvatn Zone on Kvaløya, Troms: a metasupracrustal shear belt in the Precambrian West Troms Basement Complex, North Norway. *Norwegian Journal of Geology* 85, 117-133.

Augland, L.E., Andresen, A., Gasser, D. & Steltenpohl, M.G. 2014: Early Ordovician to Silurian evolution of exotic terranes in the Scandinavian Caledonides of the Ofoten-Troms area - terrane characterization and correlation based on new U-Pb zircon ages and Lu-Hf isotopes, *In*: Corfu, F., Gasser, D., Chew, D.M. (Eds.), *New perspectives on the Caledonides of Scandinavia and related areas.* The Geological Society of London, London, pp. 655-678.

Banks, D.A., Davies, G.R., Yardley, B.W.D., McCaig, A.M. & Grant, N.T. 1991: The chemistry of brines from an Alpine thrust system in the Central Pyrenees: An application of fluid inclusion analysis to the study of fluid behaviour in orogenesis. *Geochimica et Cosmochimica acta* 55, 1021-1030.

Bergh, S.G., Kullerud, K., Armitage, P.E.B., Zwaan, K.B., Corfu, F., Ravna, E.J.K. & Myhre, P.I. 2010: Neoarchean to Svecofennian tectono-magmatic evolution of the West Troms Basement Complex, North Norway. *Norwegian Journal of Geology* 90, 21-48.

Bergh, S.G., Kullerud, K., Corfu, F., Armitage, P.E.B., Davidsen, B., Johansen, H.W., Pettersen, T. & Knudsen, S. 2007: Low-grade sedimentary rocks on Vanna, North Norway: a new occurrence of a Palaeoproterozoic (2.4-2.2 Ga) cover succession in northern Fennoscandia. *Norwegian Journal of Geology* 87, 301-318.

Binns, R.E., Chroston, P.N. & Matthews, D.W. 1980: Low-grade sediments on Precambrian Gneiss on Vanna, Troms, Northern Norway. *Offprint NGU* 359, 61-72.

Blystad, P., Brekke, H., B., F.R., Larsen, B.T., Skogseid, J. & B., T. 1995: Structural elements of the Norwegian continental shelf. Part II: the Norwegian Sea Region. *Norwegian Petroleum Directorate Bulletin* 8, 1-45.

Bodnar, R.J. & Vityk, M.O. 1994: Interpretation of microthermometric data for H_2O-NaCl fluid inclusions, *In*: De Vivo, B., Frezzotti, M.L. (Eds.), *Fluid inclusions in minerals, methods and applications*. Virginia Tech, Blacksburg, VA, pp. 117-130.

Boiron, M.-C., Cathelineau, M. & Richard, A. 2010: Fluid flow and metal deposition near basement/cover unconformity: lessons and analogies from Pb-Zn-F-Ba systems for the understanding of Proterozoic U deposits. *Geofluids* 10, 270-292.

Braathen, A. & Davidsen, B. 2000: Structure and stratigraphy of the Palaeoproterozoic Karasjok Greenstone Belt, north Norway - regional implications. *Norsk Geologisk Tidsskrift* 80, 33-50.

Bucher, K. & Stober, I. 2010: Fluids in the upper continental crust. *Geofluids* 10, 241-253.

Burisch, M., Marks, M.A.W., Nowak, M. & Markl, G. 2016: The effect of temperature and cataclastic deformation on the composition of upper crustal fluids - an experimental approach. *Chemical Geology* 433, 24-35.

Cathelineau, M. 1988: Cation site occupancy in chlorites and illites as a function of temperature. *Clay Minerals* 23, 471-485.

Chu, H., Chi, G. & Chou, I-M. 2016: Freezing and melting behaviors of H2O-NaCl-CaCl2 solutions in fused silica capillaries and glass-sandwiched films: implications for fluid inclusion studies. *Geofluids* 16, 518-532.

Corbett, G.J. & Leach, T.M. 1998: Southwest Pacific Rim gold-copper systems; structure, alteration, and mineralization, *Special Publications. Society of Economic Geology*, p. 236.

Corfu, F., Armitage, P.E.B., Kullerud, K. & Bergh, S.G. 2003: Preliminary U-Pb geochronology in the West Troms Basement Complex, north Norway: Archean and Palaeoproterozoic events and younger overprints. *NGU Bulletin* 441, 61-72.

Dallmeyer, R.D. 1992: $^{40}Ar/^{39}Ar$ mineral ages within the Western Gneiss Terrane, Troms: evidence of polyphase Proterozoic tectonothermal activity (Svecokarelian and Sveconorwegian). *Precambrian Research* 57, 195-206.

Davids, C., Benowitz, J.A., Layer, P.W. & Bergh, S.G. 2018: Direct $^{40}Ar/^{39}Ar$ K-feldspar dating of Late Permian-Early Triassic brittle faulting in northern Norway. *Terra Nova* 30, 263-269.

Davids, C., Wemmer, K., Zwingmann, H., Kohlmann, F., Jacobs, J. & Bergh, S.G. 2013: K-Ar illite and apatite fission track constraints on brittle faulting and the evolution of the northern Norwegian passive margin. *Tectonophysics* 608, 196-211.

Dong, G., Morrison, G. & Jaireth, S. 1995: Quartz textures in epithermal veins, Queensland - classification, origin, and implication. *Economic Geology* 90, 1841-1856.

Dubois, M., Monnin, C., Castelain, T., Coquinot, Y., Gouy, S., Gauthier, A. & Goffè, B. 2010: Investigations of the H_2O-NaCl-LiCl system: a synthethic fluid inclusion study and thermodynamic modeling from -50° to +100°C and up to 12 mol/kg. *Economic Geology* 105, 10.

Faleide, J.-I., Tsikalas, F., Breivik, A.J., Mjelde, R., Ritzmann, O., Engen, Ø., Wilson, J. & Eldholm, O. 2008: Structure and evolution of the continental margin off Norway and the Barents Sea. *Episodes* 31, 82-91.

Forslund, T. 1988: *Post-kaledonske forkastninger i Vest-Troms: med vekt på Straumsbukta-Kvaløyslettaforkastningen, Kvaløya*. MSc thesis. UiT the arctic University of Tromsø, Tromsø, p. 160.

Fournier, R.O. & Potter, R.W. 1982: An equation correlating the solubility of quartz in water from 25° to 900°C at pressures up to 10,000 bars. *Geochimica et Cosmochimica acta* 46, 1969-1973.

Franklin, J.M., Lydon, J.W. & Sangster, D.F. 1981: Volcanic-associated massive sulfide deposits, *In*: Skinner, B.J. (Ed.), *Economic Geology 75th Anniversary Volume*, pp. 485-627.

Gabrielsen, R.H., B., F.R., Jensen, L.N., Kalheim, J.E. & Riis, F. 1990: Structural elements of the Norwegian continental shelf - Part I: the Barents Sea Region. *Norwegian Petroleum Directorate Bulletin* 6.

Gabrielsen, R.H. & Braathen, A. 2014: Models of fracture lineaments - joint swarms, fracture corridors and faults in crystalline rocks, and their genetic relations. *Tectonophysics* 628, 26-45.

Galley, A.G., Hannington, M. & Jonasson, I. 2007: Volcanogenic massive sulphide deposits, *In*: Goodfellow, W.D. (Ed.), *Mineral deposits of Canada: a synthesis of major deposit-types, district metallogeny, the evolution of geological provinces, and exploration method*. Geological Association of Canada, Mineral deposits division, pp. 141-161.

Grant, J.A. 1986: The isocon diagram - a simple solution to Gresens' equation for metasomatic alteration. *Economic Geology* 81, 1976-1981.

Griffin, B. J., Joy, D. C. & Michael, J. R. 2010: A comparison of a luminescence –based VPSE and an electron based GSED for SE and CL imaging in variable pressure SEM with conventional SE imaging. *Microscopy and Microanalysis* 16, 624-625.

Haaland, L.C. 2018: *Geometry and kinematic evolution of ductile shear zones in the Ersfjord Granite (1.79 Ga), West Troms Basement Complex: a Svecofennian accretionary thrust system*. MSc thesis, Department of Geosciences. UiT the arctic University of Norway, Tromsø, p. 79.

Hansen, J.-A., Bergh, S.G. & Henningsen, T. 2012: Mesozoic rifting and basin evolution on the Lofoten and Vesterålen margin, North Norway; time constraints and regional implications. *Norwegian Journal of Geology* 91, 203-228.

Hemley, J.J. & Cygan, C.L. 1992: Hydrothermal ore-forming processes in the light of studies in rock-buffered systems: iron-copper-zinc-lead sulfide solubility relations. *Economic Geology* 87, 1-22.

Hubbert, M.K. & Rubey, W.W. 1959: Role of fluid pressure in mechanics of overthrust faulting. *Bulletin of the Geological Society of America* 70, 115-166.

Indrevær, K., Bergh, S.G., Koehl, J.-B., Hansen, J.-A., Schermer, E.R. & Ingebrigtsen, A. 2013: Post-Caledonian brittle fault zones on the hyperextended SW Barents Sea margin: New insights into onshore and offshore margin architecture. *Norwegian Journal of Geology* 93, 167-189.

Indrevær, K., Stunitz, H. & Bergh, S.G. 2014: On Palaeozoic-Mesozoic brittle normal faults along the SW Barents Sea margin: fault processes and implications for basement permeability and margin evolution. *Journal of the Geological Society of London* 171, 831-846.

Ingebritsen, S.E. & Manning, C.E. 2010: Permeability of the continental crust: dynamic variations inferred from seismicity and metamorphism. *Geofluids* 10, 193-206.

Johannessen, H. 2012: *Tinnvatnformasjonen i Vannas proterozoiske lagrekke: Sedimentære facies og avsetningsmiljø*. MSc thesis, Department of Geology. University of Tromsø, Tromsø, p. 105.

Johansen, H. 1987*: Forholdet mellom det prekambriske underlaget og overliggende sedimentære bergarter sør-øst på Vanna, Troms*. Cand. scient thesis, Institutt for biologi og geologi. Universitetet i Tromsø, Tromsø, p. 136.

Kesler, S.E., Appold, M.S., Martini, A.M., Walter, L.M., Huston, T.J. & Kyle, J.R. 1995: Na-Cl-Br systematics of mineralizing brines in Mississippi Valley-type deposits. *Geology* 23, 641-644.

Kirstein, L.A., Davies, G.R. & Heeremans, M. 2006: The petrogenesis of Carboniferous–Permian dyke and sill intrusions across northern Europe. *Contributions to Mineralogy and Petrology* 152, 721-742.

Koehl, J.-B., Bergh, S.G., Henningsen, T. & Faleide, J.-I. 2018a: Middle to Late Devonian-Carboniferous collapse basins on the Finnmark Platform and in the southwesternmost Nordkapp basin, SW Barents Sea. *Solid Earth* 9, 341-362.

Koehl, J.-B., Bergh, S.G., Osmundsen, P.T., Redfield, T.F., Indrevær, K., Lea, H. & Bergø, E. 2018b: Late Devonian-Carboniferous faulting in NW Finmark and controlling fabrics. *Manuscript submitted to Norwegian Journal of Geology*.

Koistinen, T., Stephens, M.B., Bogatchev, V., Nordgulen, Ø., Wennerström, M. & Korhonen, J. 2001: Geological map of the Fennoscandian Shield, scale 1:2 000 000. *Geological surveys of Finland, Norway, Sweden, and the north-west department of ministry of Natural Resources of Russia.*

Kontak, D.J. 2004: Analysis of evaporate mounds as a complement to fluid-inclusion thermometric data: case studies from granitic environments in Nova Scotia and Peru. *The Canadian Mineralogist* 42, 1315-1330.

Kontak, D.J., Kyser, K., Gize, A. & Marshall, D. 2006: Structurally controlled vein barite mineralization in the Maritimes Basin of eastern Canada: geologic setting, stable isotopes, and fluid inclusions. *Economic Geology* 101, 407-430.

Kucha, H. & Pawlikoswki, M. 1986: Two-brine model of the genesis of strata-bound Zechstain deposits (Kupferschiefer type), Poland. *Mineralium Deposita* 21, 70-80.

Kullerud, K., Skjerlie, K.P., Corfu, F. & de la Rosa, J.D. 2006: The 2.40 Ga Ringvassøy mafic dykes, West Troms Basement Complex, Norway: The concluding act of early Palaeoproterozoic continental breakup. *Precambrian Research* 150, 183-200.

Kullerud, K., Zozulya, D., Bergh, S.G., Hansen, H. & Ravna, E.J.K. 2011: Geochemistry and tectonic setting of a lamproite dyke in Kvaløya, North Norway. *Lithos* 126, 278-189.

Lippard, S.J. & Prestvik, T. 1997: Carboniferous dolerite dykes on Magerøy; new age determinations and tectonic significance. *Norsk Geologisk Tidsskrift* 77, 159-163.

Meinert, L.D., Dipple, G.M. & Nicolescu, S. 2005: World skarn deposits, *In*: Hedenquist, J.W., Thompson, J.F.H., Goldfarb, R.J., Richards, J.P. (Eds.), *One hundred anniversary volume*. Society of Economic Geology, Littleton, pp. 299-336.

Monsen, K. 2014: *Hydrothermal Cu-Zn mineralization at Vanna, West Troms Basement Complex*. MSc thesis, Department of Geology. UiT the arctic University of Norway, Tromsø, p. 109.

Mosar, J. 2003: Scandinavias North Atlantic passive margin. *Journal of geophysical research* 108, 2360-2377.

Mosar, J., Eide, E.A., Osmundsen, P.T., Sommaruga, A. & Torsvik, T. 2002: Greenland-Norway separation: a geodynamic model for the North Atlantic. *Norwegian Journal of Geology* 82, 281-298.

Myhre, P.I., Corfu, F. & Bergh, S.G. 2011: Palaeoproterozoic (2.0-1.95 Ga) pre-orogenic supracrustal sequences in the West Troms Basement Complex, North Norway. *Precambrian Research* 186, 89-100.

Myhre, P.I., Corfu, F., Bergh, S.G. & Kullerud, K. 2013: U-Pb geochronology along an Archean geotransect in the West Troms Basement Complex, North Norway. *Norwegian Journal of Geology* 93, 1-24.

Nasuti, A., Roberts, D. & Gernigon, L. 2015: Multiphase mafic dykes in the Caledonides of northern Finnmark revealed by a new high-resolution aeromagnetic dataset. *Norwegian Journal of Geology* 95, 285-298.

Ojala, J.V., Hansen, H. & Ahola, H. 2013: Cu-Zn mineralisation at Vannareid, West Troms Basement Complex: a new Palaeoproterozoic VMS occurrence in the northern Fennoscandian Shield. *Abstracts and proceedings, 12th Biennial SGA Meeting*, p. 2.

Olesen, O., Lundin, E., Nordgulen, Ø., Osmundsen, P.T., Skilbrei, J.R., Smethurst, M.A., Solli, A., Bugge, T. & Fichler, C. 2002: Bridging the gap between the onshore and offshore geology in Nordland, northern Norway. *Norwegian Journal of Geology* 82, 243-262.

Olesen, O., Torsvik, T.H., Tveten, E., Zwaan, K.B., Løseth, H. & Henningsen, T. 1997: Basement structure of the continental margin in the Lofoten-Lopphavet area, northern Norway: Constraints from potential field data, on-land structural mapping and palaeomagnetic data. *Norwegian Journal of Geology* 77, 15-30.

Opheim, J.A. & Andresen, A. 1989: Basement-cover relationships on northern Vanna, Troms, Norway. *Norsk Geologisk Tidsskrift* 69, 67-81.

Oszczepalski, S. 1999: Origin of the Kupferschiefer polymetallic mineralization in Poland. *Mineralium Deposita* 34, 599-613.

Perelló, J., Clifford, J.A., Creaser, R.A. & A., V.V. 2015: An example of synorogenic sediment-hosted copper mineralization: geologic and geochronologic evidence from the Paleoproterozoic Nussir Deposit, Finnmark, arctic Norway. *Economic Geology* 110, 677-689.

Rice, A.H.N. 1990: A discussion: Basement-cover relationships on northern Vanna, Troms, Norway. *Norsk Geologisk Tidsskrift* 70, 179-186.

Rice, A.H.N. 2014: Restoration of the External Caledonides, Finnmark, North Norway. *Geological Society of London Special Publication* 390, 271-299.

Rimstidt, D., J. 1997: Gangue mineral transport and deposition, *In*: Barnes, H.L. (Ed.), *Geochemistry of hydrothermal ore deposits*, 3. ed. John Wiley & Sons, Inc, pp. 487-515.

Roberts, D. 2011: Age of the Hamningberg dolerite dyke, Varanger Peninsula, Finnmark: Devonian rather than Vendian - a revised interpretation. *Norges Geologiske Undersøkelse Bulletin* 451, 32-36.

Roberts, D. & Lippard, S.J. 2005: Inferred Mesozoic faulting in Finnmark: current status and offshore links. *NGU Bulletin* 443, 55-60.

Roberts, D., Torsvik, T., Andersen, T.B. & Rehnström, E.F. 2003: The Early Carboniferous Magerøy dykes, northern Norway; palaeomagnetism and palaeogeography. *Geological Magazine* 140, 443-451.

Roedder, E. 1984: *Fluid inclusions*. U S geological Survey, Blacksburg, Virginia, p. 644.

Rye, R.O. & Ohmoto, H. 1974: Sulfur and Carbon isotopes and ore genesis: a review. *Economic Geology* 69, 825-843.

Savard, M.M. & Kontak, D.J. 1995: $\delta^{13}C$-$\delta^{18}O$-$^{87}Sr/^{86}Sr$ covariations in ore-stage calcites at and around the Gays River Zn-Pb deposit (Nova Scotia, Canada) - evidence for fluid mixing. *Economic Geology* 93, 181-196.

Schmid, S.M. & Handy, M.R. 1991: Towards a genetic classification of fault rocks: geological usage and tectonophysical implications, *In*: Muller, D.W., McKenzie, J.A., Weissert, H. (Eds.), *Controversies in modern geology*. Academic press, London, pp. 339-361.

Seward, T.M. & Barnes, H.L. 1997: Metal transport by hydrothermal ore fluids, *In*: Barnes, H.L. (Ed.), *Geochemistry of hydrothermal ore deposits*, 3. ed. John Wiley & Sons, Inc, pp. 435-486.

Sheperd, T.J. 1985: *A practical guide to fluid inclusions*. Blackie &Son Ltd, p. 235.

Sibson, R.H. 1977: Fault rocks and fault mechanisms. *Journal of the Geological Society of London* 133, 191-216.

Sibson, R.H., Moore, J.M. & Rankin, A.H. 1975: Seismic pumping - a hydrothermal fluid transport mechanism. *Journal of the Geological Society of London* 131, 653-659.

Simmons, S.F., White, N.C. & John, D.A. 2005: Geological characteristics of epithermal precious and base metal deposits, *In*: Hedenquist, J.W., Thompson, J.F.H., Goldfarb, R.J., Richards, J.P. (Eds.), *One hundred year anniversary volume*. Society of Economic Geology, Littleton, pp. 485-522.

Smelror, M., Petrov, O., Larssen, G.B. & Werner, S. 2009: *Geological history of the Barents Sea*. Geological Survey of Norway, p. 135.

Steele-MacInnis, M., Bodnar, R.J. & Naden, J. 2011: Numerical model to determine the composition of H_2O-NaCl-$CaCl_2$ fluid inclusions based on microthermometric and microanalytical data. *Geochimica et Cosmochimica acta* 75, 21-40.

Taylor, H.P., Frechen, J. & Degens, E.T. 1967: Oxygen and carbon isotope studies of carbonatites from the Laacher See District, West Germany and the Alnö District, Sweden. *Geochimica et Cosmochimica acta* 31, 407-430.

Thorstensen, L. 2011: *Land-sokkel korrelasjon av tektoniske elementer i ytre del av Senja og Kvaløya i Troms*. MSc thesis, Department of Geology. University of Tromsø, Tromsø, p. 117.

Vanko, D. A., Bodnar, R. J. & Sterner, S. M. 1988: Synthetic fluid inclusions: VIII. Vapor-saturated halite solubility in part of the system NaClCaC12-H20, with application to fluid inclusions from oceanic hydrothermal. *Geochimica et Cosmochimica acta* 52, 2451-2456.

Vaughan, D.J. & Craig, J.R. 1997: Sulphide ore stabilities, morphologies, and intergrowth textures, *In*: Barnes, H.L. (Ed.), *Geochemistry of hydrothermal ore deposits*, 3. ed. John Wiley & Sons, Inc, pp. 367-434.

Vidal, O., De Andrade, V., Lewin, E., Munoz, M., Parra, T. & Pascarelli, S. 2006: P-T-deformation-Fe^{3+}/Fe^{2+} mapping at the thin section scale and comparison with XANES mapping: application to a garnet-bearing metapelite from the Sambagawa metamorphic belt (Japan). *Journal of Metamorphic Geology* 24, 669-683.

Walter, B., Burisch, M. & Markl, G. 2016: Long-term chemical evolution and modification of continental basement brines - a field study from the Schwarzwald, SW Germany. *Geofluids* 16, 604-624.

Wise, D.U., Dunn, D.E., Engelder, J.T., Geiser, P.A., Hatcher, R.D., Kish, S.A., Odom, A.L. & Schamel, S. 1984: Fault-related rocks: Suggestions for terminology. *Geology* 12, 391-394.

Yardley, B.W.D. 2005: Metal concentrations in crustal fluids and their relationship to ore formation. *Economic Geology* 100, 613-632.

Zhong, R., Brugger, J., Chen, Y. & Li, W. 2015: Contrasting regimes of Cu, Zn and Pb transport in ore-forming hydrothermal fluids. *Chemical Geology* 395, 154-164.